

Thermochronology and provenance of the Yakutat terrane, southern Alaska based on
fission-track and U/Pb analysis of detrital zircon

A THESIS

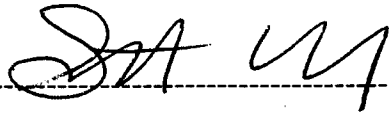
Presented to the Faculty of the
University at Albany, State University of New York

In partial fulfillment of the requirements for the degree of
Master of Science

Stephanie Ellen Perry

2006

I understand that my thesis will become a part of the permanent collection of the State University of New York at Albany libraries. My signature below authorizes the release of my thesis to any reader upon request.

A handwritten signature in black ink, appearing to read 'SAU', is positioned above a horizontal dashed line.

Stephanie Ellen Perry, Author

© Copyright by Stephanie Ellen Perry

August 1, 2006

All Rights Reserved

Thermochronology and provenance of the Yakutat terrane, southern Alaska based on
fission-track and U/Pb analysis of detrital zircon

Abstract of

A THESIS

Presented to the Faculty of the
University at Albany, State University of New York

In partial fulfillment of the requirements for the degree of
Master of Science

College of Arts & Sciences
Department of Earth and Atmospheric Sciences

Stephanie Ellen Perry

2006

ABSTRACT

Northward transport of the Yakutat terrane along the Transition and Queen Charlotte-Fairweather transform faults led to Neogene collision of the Yakutat terrane with the southern continental Alaska margin. Northward translation resulted in a stratigraphy that records the erosion of thermotectonic terranes along its path. The strata of the Yakutat terrane includes the Lower Oligocene to Lower Eocene Kulthieth Formation, the Upper Eocene to Lower Miocene Poul Creek Formation and the Miocene-Pleistocene Yakataga Formation. Detrital zircon fission-track (DZFT) ages from stratigraphically coordinated samples collected in the Northern Robinson Mountains yield provenance information of the units that can shed light on their transport history. For all dated samples 50 grains were counted and morphology/color noted and grain ages were deconvolved into component populations. The Kulthieth Formation has three primary cooling age populations at ~70-97 Ma, 38-58 Ma and 28-31 Ma. The Poul Creek Formation has three primary cooling age populations at ~61-67 Ma, 39-42 Ma and 24-33 Ma. The Yakataga Formation has three primary cooling age populations at ~68-77 Ma, 30-35 Ma and 15-21 Ma. The DZFT grains were then analyzed by LA-ICPMS to determine U/Pb crystallization ages. For the Yakataga Formation three crystallization peak age populations resulted: ~52 Ma, ~71 Ma and ~155 Ma. For the Poul Creek Formation four crystallization peak ages resulted: ~59 Ma, ~71 Ma, ~94 Ma, and ~147 Ma. Three grains yielded U/Pb ages of ~318 Ma, ~365 Ma, ~1864.71 Ma. Analysis of the Kulthieth Formation resulted in three U/Pb crystallization age populations of ~59 Ma, ~94 Ma, and ~159 Ma.

Paelocene to Eocene deposition of the Yakutat terrane stratigraphy records a long-lived, non-volcanic source terrain that crystallized from ~50-220 Ma and cooled from ~48-110 Ma. Miocene cooling episodes in the Kulthieth and the Poul Creek Formations likely records deposition associated with plutons located in the northern Coast Plutonic Complex and the Kuiu-Etoilin belt in the North American Cordillera. Late Miocene deposition of the Yakataga Formation records a provenance signal of crystallization from ~50-53 Ma and cooled from ~17-20 Ma. Late Miocene deposition is likely associated with the Chugach accretionary complex and superimposed Sanak-Baranof Plutonic Belt (~50-58 Ma).

The uniform provenance of the Kulthieth and Poul Creek Formations, the over all grain-age distribution, and the distinct lack of volcanic zircons favors northern reconstructions (i. e. Palfker et al., 1994) for the original position of the Yakutat terrane. Southern options (i. e. Bruns, 1982), can be ruled out mainly due to the lack of volcanic grains that would be expected in the stratigraphy during continuous transport of the terrane along route.

DEDICATION

To my family, Dad, Mom and Nicole. The completion of this thesis would not have been possible without you. Your constant, unwavering support, loving home, and kind words led to the building of my self-confidence needed to complete this task. Thanks for listening to my constant “geology talk” over the years and for acting interested even when you did not know what I was talking about. To everyone else in my life, thank you for all the constant support and generosity throughout the years. Your kindness will never be overlooked or forgotten. To Jessie, thank you.

ACKNOWLEDGEMENTS

I would like to express my deepest thanks to Professor John I. Garver for the use of his lab and facilities, his guidance, inspiration, professionalism and friendship over the past five years. In hopes of collaboration in the future and good times to come in life. Thanks to Professor William S. F. Kidd for his guidance through the SUNY Albany system. Also, thanks to all of the people involved in the NSF funded STEEP Alaska project but of particular note Professor Ken Ridgway and his student Paul Landis. I will never forget your generosity and understanding during the summer 2005 field season. Thanks to Bill Neubeck for his help with the preparation of my thin sections and constant problem solving with lab equipment. Best of luck during the coming years. Lastly, thank you to Steve Reese at the Oregon State University reactor for the timely irradiation of my fission-track samples. I would also like to acknowledge George Gehrels and Victor Valencia at the University of Arizona Laserchron Center for their guidance during the U/Pb analysis and data reduction and the NSF support that they receive to run their lab as a collaborative geochronology center.

This project is part of the St. Elias Erosion/Tectonics Project or STEEP an NSF Continental Dynamics program. Financial support is gratefully acknowledged from NSF EAR-0409224. Thanks to Terry Pavlis who is the project director.

TABLE OF CONTENTS

Title Page of Abstract	i
Abstract	ii
Title Page	iv
Copyright	v
Dedication	vi
Acknowledgments	vii
Table of Contents	viii
List of Tables	xii
List of Figures	xiii
Introduction	1
Overview	7
Geologic Framework of northwestern North America	7
Idaho Batholith/Omenica Belt	7
Cascade Arc	9
Coast Plutonic Complex	10
Southern and southeastern Alaska	11
Forearc Plutonism and Volcanism	11
Geologic Basins of northwestern North America	13
Tofino Basin	13
Queen Charlotte Basin	14
Alaska Deep Sea Fan Bodies	15
Geological Background of Yakutat Terrane	18

Stratigraphy.....	20
Kulthieth Formation	21
Poul Creek Formation	25
Yakataga Formation	25
Sedimentary Petrography of Yakutat Cover Stratigraphy	30
Deformation and Structure.....	31
Exhumation from previous thermochronologic studies.....	33
Fission-Track Dating Background	37
Detrital Zircon Fission-Track Background.....	39
U/Pb Background.....	42
Sedimentary Petrography Background	44
Sandstones of the Pacific Northwest and Alaska.....	45
Vitrinite Reflectance Background	48
Vitrinite Reflectance in the Pacific Northwest and Alaska	50
Detrital Zircon Fission-track Methods	51
Detrital Zircon Fission-track.....	51
Field Methods.....	51
Laboratory Separation Procedures	51
Mineral Separation.....	51
Mounting.....	55
Etching.....	55
Irradiation.....	56
Age Determination	57

U/Pb Methods	59
Fractionation Factor	63
Age Determination	64
Sedimentary Petrography	65
Vitrinite Reflectance	66
Data	66
Detrital Zircon Fission-track	66
Kulthieth Formation	71
Poul Creek Formation	76
Yakataga Formation	76
U/Pb data	80
Kulthieth Formation	80
Poul Creek Formation	80
Yakataga Formation	96
Sedimentary Petrography	96
Kulthieth Formation	104
Poul Creek Formation	104
Yakataga Formation	110
Vitrinite Reflectance	110
Interpretation	114
Kulthieth Formation and Poul Creek Formations	114
Yakataga Formation	120
Regional Considerations	124

Conclusions	130
References	132
Appendix A	153
Appendix B	188
Appendix C	267
Appendix D	284
Appendix E	317

LIST OF TABLES

Table 1. Sample locations	54
Table 2. Summary of all detrital zircon fission-track data.....	67
Table 3. Detrital zircon fission-track peak-age populations deconvolved.....	72
Table 4. Summary of U/Pb laser ablation ICPMS analysis results.....	81
Table 5. Comparison of U/Pb single grain-ages versus DZFT grain ages.....	97
Table 6. Sedimentary petrography summary	105
Table 7. Vitrinite reflectance and thermal maturity summary	113

LIST OF FIGURES

Figure 1. Structural map of collided terranes in Alaska	2
Figure 2. DEM of the Yakutat Bay area with sample locations	5
Figure 3. Sample locations in the Northern Robinson Mountains	6
Figure 4. Terrane map of northwestern North America.....	8
Figure 5. Surveyor and Baranoff fan evolution	17
Figure 6. Kuthieth Formation field photographs of sandstones.....	22
Figure 7. Kulthieth Formation cross-bedded sandstones	24
Figure 8. Poul Creek Formation siltstones.....	26
Figure 9. Yakataga Formation dropstones	28
Figure 10. Yakataga Formation diamictite	29
Figure 11. Ion spike model	38
Figure 12. Typically etched zircon from sample 05-11	40
Figure 13. Fission-track sample preparation schematic.....	52
Figure 14. DZFT Peak-Age Model.....	60
Figure 15. LA-ICPMS set-up.....	61
Figure 16. Composite probability density plot of all DZFT results.....	70
Figure 17 [A]-[E]. Kulthieth Formation sample composite distributions	75
Figure 18 [A]-[D]. Poul Creek Formation sample composite distributions	77
Figure 19 [A]-[D]. Yakataga Formation sample composite distributions	79
Figure 20. Laser-ablated zircon	88
Figure 21. U/Pb versus DZFT results	89

Figure 22. Kulthieth Formation histogram of U/Pb vs. DZFT results.....	90
Figure 23 [A]-[B]. Kulthieth Formation U/Pb Concordia diagrams.....	91
Figure 24 [A]-[B]. Kulthieth Formation U/Pb histogram distribution	92
Figure 25 [A]-[B]. Poul Creek Formation U/Pb vs. DZFT results	93
Figure 26 [A]-[B]. Poul Creek Formation U/Pb Concordia diagrams.....	94
Figure 27 [A]-[B]. Poul Creek Formation U/Pb histogram distribution.....	95
Figure 28 [A]-[B]. Yakataga Formation U/Pb vs. DZFT results	101
Figure 29 [A]-[B]. Yakataga Formation U/Pb Concordia diagrams.....	102
Figure 30 [A]-[B]. Yakataga Formation U/Pb histogram distribution.....	103
Figure 31 [A]-[B]. Sedimentary Petrography QFL ternary diagram	106
Figure 32 [A]-[B]. Sedimentary Petrography Lithics ternary diagram.....	107
Figure 33 [A]-[B]. Kulthieth Formation photomicrograph.....	108
Figure 34 [A]-[B]. Poul Creek Formation photomicrograph	109
Figure 35 [A]-[B]. Yakataga Formation photomicrograph.....	111
Figure 36. U/Pb ages of DZFT vs. Non-DZFT dated grains	115
Figure 37. Northern Coast Plutonic Complex U/Pb comparison.....	116
Figure 38. Yakataga Formation DZFT Late Miocene U/Pb distribution.....	123
Figure 39. Forearc plutonism and thermochronotour overview	125
Figure 40. Northern vs. Southern Yakutat terrane movement history	126

INTRODUCTION

The formation of the Chugach/St. Elias mountain range in southern Alaska is a result of the accretion and subduction of foreign terranes, notably the Yakutat block, beneath the southern Alaska continental margin (Figure 1). The Yakutat terrane was transported northwestward along the Transition and Queen-Charlotte Fairweather strike-slip fault system from possibly as far south as Oregon and northwestern Washington (e. g. Bruns, 1983). The Yakutat terrane is approximately 600 km long and 200 km wide and is being underthrust (affixed to the Pacific plate) beneath the Chugach terrane or Alaskan framework at approximately 0.56 mm/yr (Fletcher and Freymueller, 1999).

The transport and accretion history of a terrane commonly can be resolved by provenance analysis. Evolving techniques such as fission-track and U/Pb analysis on single grains have proved to be powerful provenance discriminators (Carter and Moss, 1999; Rahl, Reiners, Campbell, Nicolescu, and Allen, 2003; Bernet, Brandon, Garver and Molitor, 2004a, b; Bernet and Garver, 2005; Johnston, 2005; Haeussler, Gehrels, and Karl, *in prep*). By determining the provenance histories of the stratigraphic units that comprise the Yakutat block, the sediment source(s) that the terrane has encountered throughout its transport can be determined and therefore hypotheses can be tested about movement history. Only a few detrital zircon fission-track (DZFT) studies have been conducted on the stratigraphic units of the Yakutat terrane, including from youngest to oldest: Yakataga Formation, Poul Creek Formation, and the Kulthieth Formation (Armstrong, 1988; Plafker, Naeser, Zimmerman, Lull, and Hudson, 1991; Johnston, 2005). Virtually no detrital U/Pb analysis has been done (Gehrels, Dickinson, Ross,

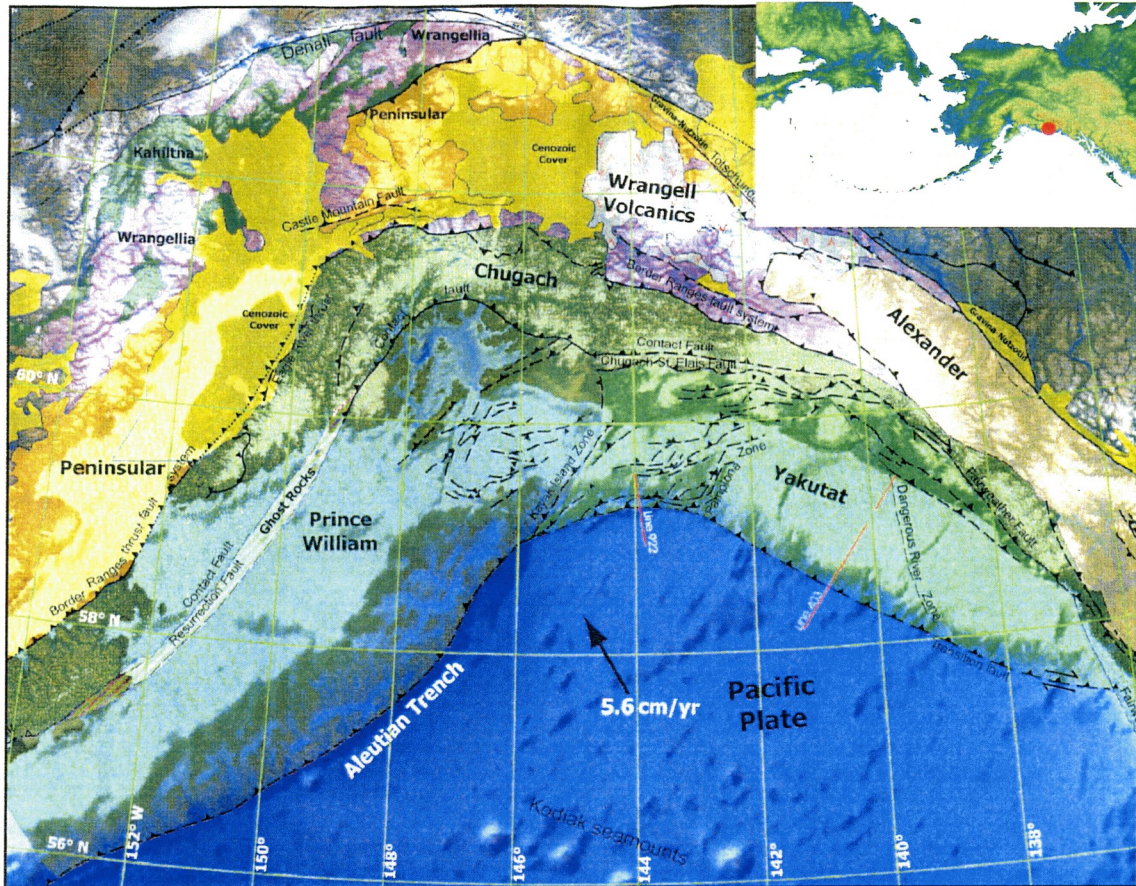


Figure 1. Tectonic terrane assemblage map of southern and southeastern Alaska (National Science Foundation Continental Dynamics Program Science Plan, 2003).

Stewart, and Howell, 1995; Carter and Moss, 1999; Rahl et al., 2003; Haeussler, Gehrels, and Karl, *in prep*).

Fission-track analysis relies on using the radioactive decay by spontaneous fission of naturally occurring ^{238}U in zircon and permits the determination of a cooling age of a single sample. Fission-track cooling ages provide a timeline for the thermal history of rocks in that when they pass below the closure temperature of $240^{\circ}\text{C} \pm 30^{\circ}\text{C}$ the radioactive clock recorded in the sample is started and zircons begin accumulating “fission-tracks”, or damage zones due to spontaneous fission events in the crystal (Brandon, Roden-Tice, and Garver, 1998; Bernet and Garver, 2005). A few samples may require multiple cooling ages as a result of multiple tectonothermal events in the source terrains through time (Brandon, Roden-Tice, and Garver, 1998; Bernet and Garver, 2005).

To better understand the entire thermal history of single zircon grains, U/Pb analysis was conducted on the same grains used to determine DZFT cooling ages. U/Pb analysis provides a crystallization age, or time of mineral crystallization (Crawford, Crawford and Gehrels, 2000; Gehrels, 2000; 2001). This powerful new technique of “double-dating” allows determination of both cooling age and formation age of a grain (Carter and Moss, 1999; Rahl et al, 2003; Garver, Reiners, Walker, Ramage and Perry, 2005). The technique relies on the quantitative decay of U and Th isotopes to end-member isotopes of Pb in a closed system (i. e. Davis, Williams and Krogh, 2003). By using a laser-ablation-inductively coupled plasma mass spectrometer (LA-ICPMS) the isotopic compositions of an individual zircon grain can be measured and used to determine a U/Pb crystallization age (Stacey and Kramers, 1975; Davis, Williams and Krogh, 2003).

A number of studies have been conducted on various plutonic, magmatic and volcanic episodes that have occurred from the southwestern coast of Oregon and Washington to the Chugach/St. Elias Range in southern/southeastern Alaska (Parrish, 1983; Plafker, 1987; Armstrong, 1988 and 1991; Crawford and Crawford, 1991; Cook, Crawford, Omar, and Crawford, 1991; Spotila, Buscher, Meigs, and Reiners, 2004). The largest and most tectonically significant element of the continental framework is the production and evolution of the Coast Plutonic Complex that extends from northwestern Washington into southeastern Alaska. Various thermochronological techniques date events occurring in and related to the uplift of the late Mesozoic to early Cenozoic Coast Plutonic Complex from ~80 to 45 Ma (Parrish, 1983; Armstrong, 1988 and 1991).

In this study, 17 samples collected from the Yakutat block stratigraphy were analyzed for DZFT and U/Pb analysis, as well as sedimentary petrography (Figure 2; Figure 3). First, zircons were investigated by DZFT analysis and cooling age populations were determined. Then U/Pb analysis was conducted on the same grains used to evaluate DZFT age populations to determine mineral crystallization ages and cooling ages for individual grains. Vitrinite reflectance on isolated kerogen was analyzed for four samples to establish the maximum temperature range experienced by the deposited rocks; three were taken from the Kulthieth Formation and one from the Poul Creek Formation. Extensive background on the techniques used as well as the methodology is explained in the text following. Finally, data are presented and interpreted in relation to age constraints on stratigraphic formations as well as possible determinations of provenance, and the significance for the transport and thermal history of the Yakutat block.

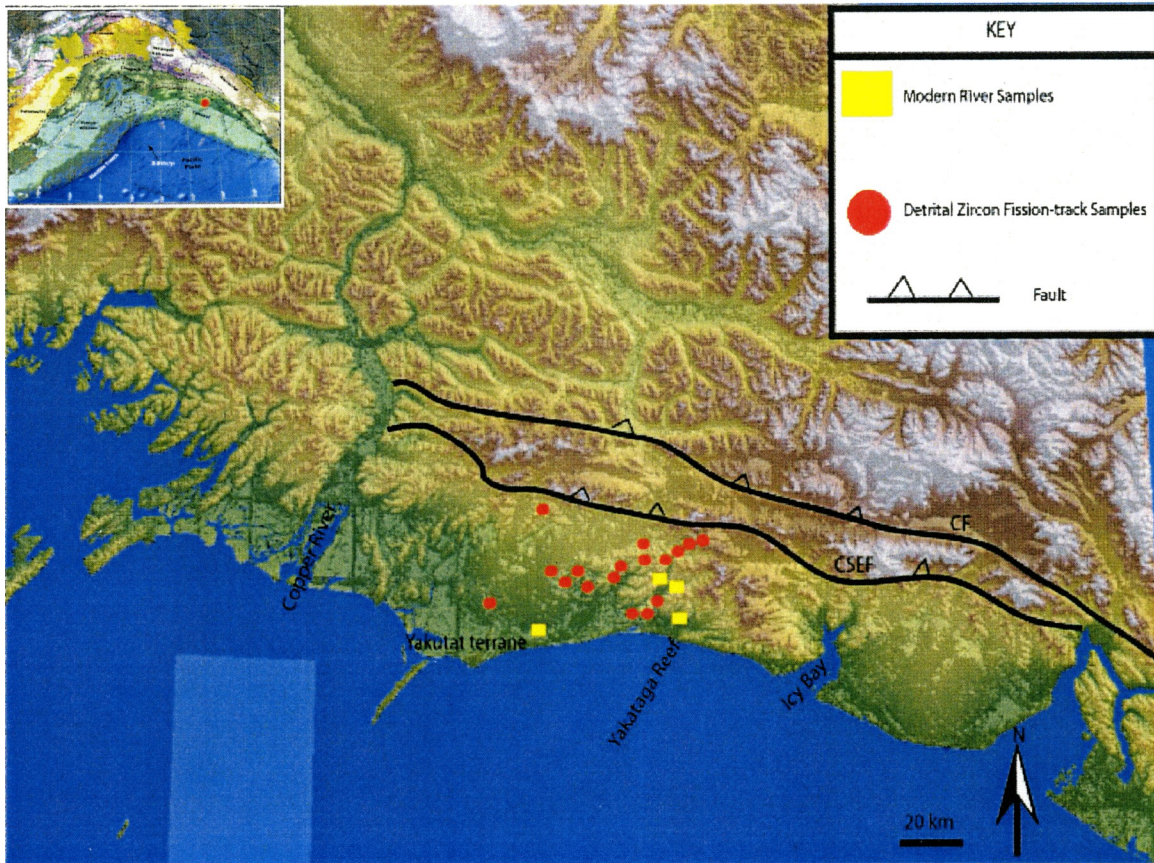


Figure 2. DEM showing sample locations of the Yakutat Bay area, southern Alaska. Box shows location of Figure 4.

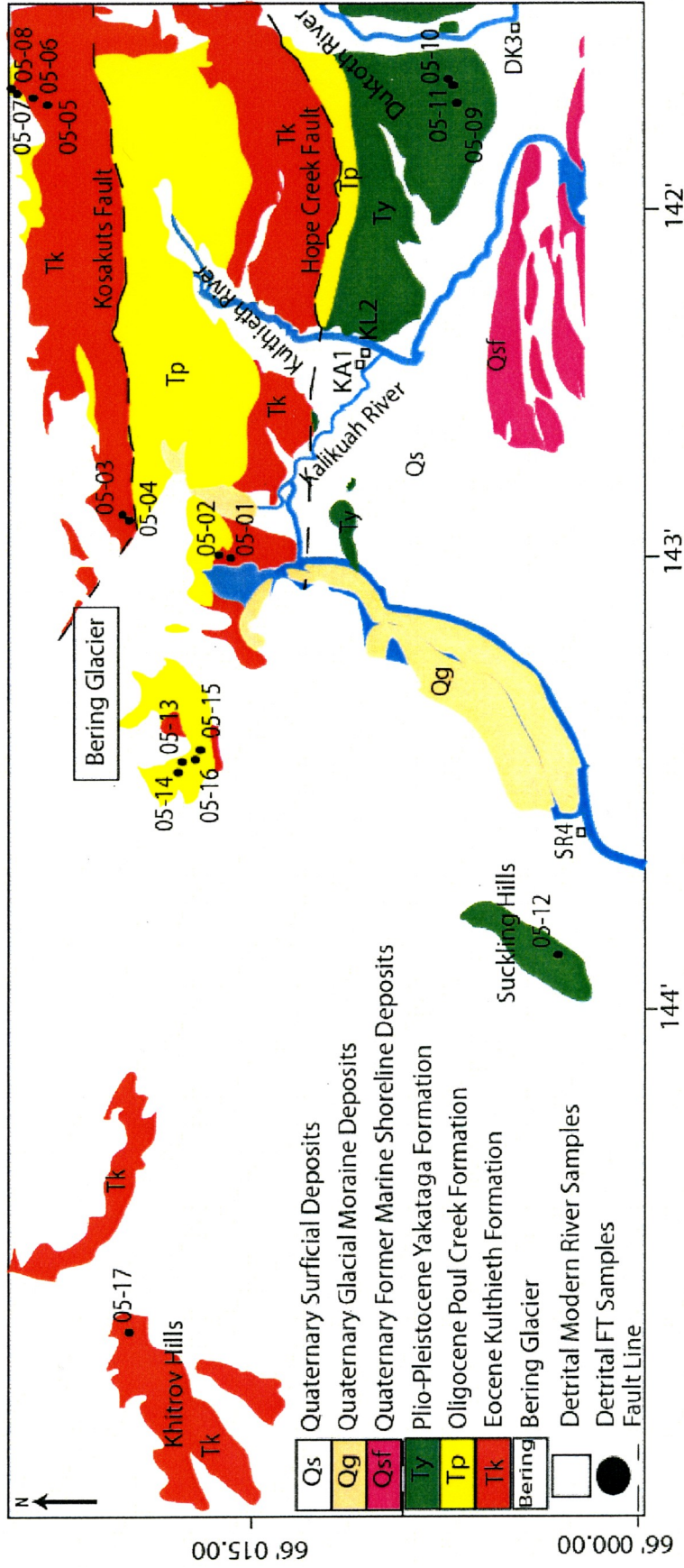


Figure 3. Sample location map of the Northern Robinson Mountains (modified from Miller, 1957; Miller, 1971).

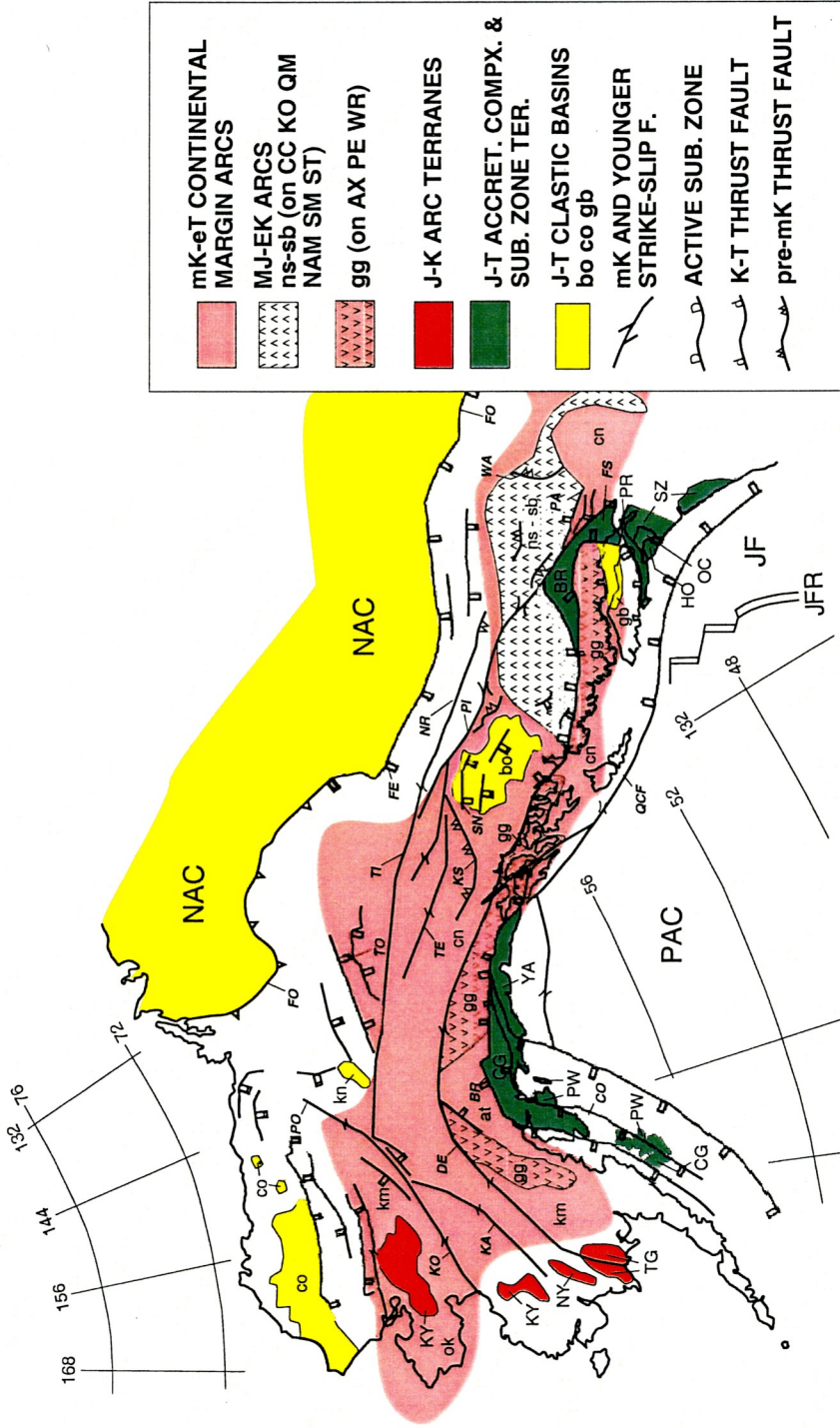
OVERVIEW

Geologic Framework of northwestern North America

The following is a brief description of the tectonic units of the continental framework of northwestern North America that have served as source terrains to offshore geologic units from the Mesozoic to the Recent (Figure 4). This framework is essential to understanding the movement history of the Yakutat terrane based on thermochronological ages determined throughout the stratigraphy.

Idaho Batholith/Oregonic Belt

The Mesozoic to Cenozoic Idaho Batholith is a large (~40,000 km²) complex with multiple intrusive phases (Hyndman, 1983). The batholith is comprised of two lobes: the southern Atlanta lobe which was intruded between ~100-75 Ma; and the northern Bitterroot lobe which was intruded between ~80-70 Ma (Armstrong, Taubeneck, and Hales, 1977). Zircon fission-track cooling ages of the plutons range from ~83 to 35 Ma with a period of Eocene plutonism and widespread thermal resetting that occurred from ~49 to 37 Ma (Taylor and Magaritz, 1978; Criss and Taylor, 1983; Criss and Champion, 1984; Sweetkind and Blackwell, 1989). The current drainage of the batholithic rocks is directed out of the Snake River drainage basin, which joins the Columbia River which empties south of the Olympic Peninsula. It is likely that this drainage did not have the capability to deposit sediment north of the Olympic Peninsula or south of Vancouver



TECTONIC FEATURES OF THE CONSOLIDATING CANADIAN AND ALASKAN TECTONIC COLLAGE

Figure 4. Map of consolidated terranes from southern British Columbia to Alaskan. Juan De Fuca Ridge (JFR), Juan De Fuca plate (JF), North American Craton (NAC), Pacific Ocean (PAC), Yakutat Terrane (YA), Prince William Terrane (PW), Chugach Terrane (CG) (Nokleberg et al., 2005).

Island any earlier than ~80 Ma because of the topographic high of the Coast Plutonic Complex which creates the drainage divide between the interior and exterior United States and Canadian drainage systems (Frisbie, 1995).

The Late Triassic to Early Jurassic Omneica Belt is a metamorphic and plutonic belt that is bound to the east by the Mackenzie and Rocky Mountains Belt and to the west by the Coast Plutonic Belt. The Omneica Belt consists of the Yukon, Quesnel and Cache Creek terranes and has experienced four major episodes of uplift, denudation and metamorphism (Anderson, 1988; Armstrong, 1988). The earliest metamorphic event affecting the belt occurred in the Late Triassic to Early Jurassic (220-180 Ma) and there was another during the Middle Jurassic with regional metamorphism occurring from ~180-160 Ma (Armstrong, 1988; Frisbie, 1995). Cooling ages associated with this Middle Jurassic metamorphic event range from ~150-130 Ma (Armstrong, 1988). A wide-spread mid-Cretaceous event (~100 Ma) affected the belt from north to south and was followed by Cenozoic plutonism (~58-44 Ma) in the core of the southern portion of the belt (Armstrong, 1988).

Cascade Arc

The Cascade arc is a continental volcanic arc built on pre-Tertiary basement rock of the Coast Range terrane, North Cascades terranes, and the Coast Plutonic Complex (Garver and Brandon, 1994a, b). Zircon fission-track cooling ages indicate that the arc has been active from ~36 Ma to the present. Development of the arc is associated with the subduction of the Juan De Fuca plate beneath the northwestern U. S. continental

margin. Throughout the evolution of the arc, volcanic and volcanic clastic sediment (Upper Eocene Puget Group and Zemorrian Blakeley Formation) were deposited on the western flank (Brandon and Vance, 1992). Activity of the arc diminished from ~17 to 7 Ma based on zircon fission-track cooling ages (Parrish, 1983; Brandon and Vance, 1992; Garver and Brandon, 1994).

Coast Plutonic Complex

The geological framework of British Columbia is dominated by the Mesozoic to Cenozoic Coast Plutonic Complex (CPC) and associated metamorphic and plutonic belts. The Coast Plutonic Belt currently represents a drainage divide that blocks sediment from interior British Columbia from directly reaching Pacific basins (Armstrong, 1988; 1991). The Coast Plutonic Belt is comprised of a basement made up of the Alexander and Wrangell terrane bodies, which accreted during the Late Mesozoic time (Armstrong, 1988; 1991).

Extensive age determinations of the entire Canadian Cordillera have resulted in well-recognized magmatic events (Armstrong, 1988). The thermal and magmatic history of the Coast Plutonic Complex suggests times of high magmatism activity at ~100-95 Ma, ~75 Ma, ~65-55 Ma (Armstrong, 1988 and 1991; Parrish, 1983). The uplift, denudation, and sedimentation of the Coast Plutonic Complex are recorded in stratigraphic units in the nearby Queen Charlotte Basin (Bruns, 1983; Plafker, 1987; Plafker, Moore and Winkler, 1994). The Coast Plutonic Complex is considered a sizable

provenance source for numerous formations in varying terranes that have collided into the southern Alaskan continental margin (Plafker, 1987; Armstrong, 1988).

Southern and southeastern Alaska

Southern and southeastern Alaska has had numerous and continuous terrane accretion throughout its geological history, acting as the final accretion site for far-traveled terranes such as the Wrangellia, Alexander, Prince William, Chugach and, recently, the Yakutat. Of particular note are the Cenozoic sequence of rocks that are actively being exhumed, eroded, and shed onto the Gulf of Alaska margin from the Chugach/ St. Elias mountain range located in the Chugach terrane (Plafker, 1987). Geological history of the actively subducting Yakutat terrane is discussed in further detail below.

Forearc Plutonism and Volcanism

Forearc plutonism along the northwest Pacific margin has been continuous from ~62 to 11 Ma (Madsen, Thorkelson, Friedman, and Marshall, 2006). Because these rocks lie outboard of the Coast Plutonic Complex, they are of primary significance as possible source rocks for offshore basins. Events can be divided into volcanic and plutonic episodes based on location and age. Along the margin from Washington to Alaska three major volcanic and plutonic events occurred beginning with the Coast Range Basalt Province of Oregon and Washington dated by detrital U/Pb and K/Ar ages as ~58-50 Ma

(Madsen et al., 2006). Then the Cascade Arc (~42 Ma-present) including the Gray's River volcanics, Goble volcanics, Tillamook and Yachats basalts were most active during the Late Eocene (Ar/Ar and K/Ar ~46-33 Ma) (Madsen et al., 2006). Plutonism from Oregon to Washington was continuous from ~60-35 Ma. Forearc plutonism has been widespread and begins with the development of the Sanak-Baranof Belt (~61-48 Ma) from the Aleutian Islands southward to the Kuiu-Etoilin Belt including islands such as Admiralty Island, Zarembo Island, Burnett Inlet, and Prince Rupert (Lindline, Crawford and Crawford, 2004; Madsen et al., 2006). Events also include the Walker Creek intrusions (U/Pb ~50.7-50.9 Ma), the Clayoquot intrusions (U/Pb ~51.2-48.8 Ma), and the Mt. Washington intrusions (U/Pb ~41-35 Ma) (Madsen et al., 2006).

On Vancouver Island the Flores volcanics represent forearc volcanism from ~51.2-50 Ma (Madsen et al., 2006). The Masset volcanics located on the Queen Charlotte Islands are dated from the Late Eocene to the Late Miocene (~43-20 Ma) (Madsen et al., 2006). The Kano intrusions are ~39-27 Ma and are associated with Masset volcanism (Madsen et al., 2006). Lastly, the Admiralty Island volcanics range in age from ~35-5 Ma and are associated with Late Eocene-Oligocene near-trench intrusions dated by detrital U/Pb and Ar/Ar from ~39-29 Ma (Madsen et al., 2006).

Geologic Basins of northwestern North America

Tofino Basin

The Olympic Peninsula and flanking sedimentary basins in the upper plate such as the Tofino Basin, are geologically related to both the Coast Range terrane and the Cascade Arc (Garver and Brandon, 1994). The upper plate stratigraphy on the Peninsula consists mainly of lower Eocene basalts (basement rock) and overlying basin strata, which are Eocene to Miocene (Shouldice, 1971; Garver and Brandon, 1994).

Vancouver Island consists largely of materials accreted to the North American continental margin during the collision of the Wrangell terrane during the Mesozoic. The Mesozoic rocks of Vancouver Island form the basement to the Cenozoic Tofino Basin, which is located offshore of the western margin of the island (Shouldice, 1971; Fairchild and Cowan, 1982; Brandon, 1989b). The basin margin extends west to where it meets the Queen Charlotte Fault and south to where the basin stratigraphy extends into the Olympic Peninsula (Shouldice, 1971; Tiffin, Cameron and Murray, 1972; Garver and Brandon, 1994). This basin provides important clues as to the evolution of margin sedimentation in the Cenozoic. The basin holds an almost continuous record of Tertiary sedimentation ranging from the Late Eocene to the Pliocene (Tiffin, Cameron, and Murray, 1972). The pre-Tertiary volcanic basement rocks contain younger intrusives ranging widely in age (Shouldice, 1971). These intrusive rocks are related to four major tectonic elements that represent the Cenozoic evolution of the Pacific northwest (Garver and Brandon, 1994). The Coast Range terrane composed of Eocene basalts of the Crescent Formation and

Metchosin Formation forms the basement rock to the overlying Olympic Subduction Complex and Cascade volcanic arc (Garver and Brandon, 1994). The largely Mesozoic basement rocks are intruded by Jurassic and Eocene intrusives. The Tofino Basin and the Queen Charlotte Basin to the north have some important similarities, which suggests original continuity (Shouldice, 1971).

Queen Charlotte Basin

The basement to the Queen Charlotte Islands was accreted to the western British Columbia continental margin during the Mesozoic as part of the Insular belt, which consists mainly of rocks from the Wrangell terrane but it is debated whether or not these units also include portions of the Alexander terrane, based uncertainty the location of the boundary between the two accreted terranes (Yorath and Chase, 1981; Anderson and Reichenbach, 1989; Lewis, Dietrich, and Rohr, 1991). Regardless, the overlying and adjacent Queen Charlotte Basin preserves the sedimentary provenance history of this area from the Mesozoic to the Cenozoic. Four major stratigraphic divisions have been recorded in the basin (Lewis, Dietrich and Rohr, 1991). These three divisions that overlie the Karmutsen igneous basement include: 1) the Yakoun and Moresby Groups and Longarm Formation, deposited during the middle to late Jurassic; 2) the Cretaceous Longarm, Honna, Haida and Skidegate Formations; and 3) the Cenozoic Skonun and the Masset Formations (Lewis, Dietrich and Rohr, 1991).

A U/Pb zircon from the Karmutsen suggests a concordant crystallization age at ~309 Ma (Anderson and Reichenbach, 1991). Within the Middle to late Jurassic Yakoun

and Maude Group strata, detrital U/Pb dates of plutonic zircons have yielded ages of ~192-153 Ma (Anderson and Reichenbach, 1991; Lewis, Dietrich and Rohr, 1991). Within the Tertiary Masset and Skonun Formations, the Kano Plutonic Suite has yielded detrital U/Pb ages of ~46-27 Ma and the volcanic Masset Formation ~19-25 Ma ages (Armstrong, 1988; 1991; Anderson and Reichenbach, 1991; Lewis, Dietrich, and Rohr, 1991).

Alaska Deep Sea Fan Bodies

The offshore southern Alaska margin has long been the topic of study for geologists trying to assess oil and gas potential of the terrigenous turbidite stratigraphy of the Gulf of Alaska. Although numerous deep wells have been drilled, little correlation has been made between the dated offshore sediments and the poorly dated onshore stratigraphy of the Yakutat terrane.

The Gulf of Alaska abyssal plain is subdivided into the Aleutian, Alaska, and Tufts Abyssal Plains, which have individual Cenozoic submarine fans known as the Zodiac, Surveyor, and Baranof fans respectively (Stevenson and Embley, 1987). These fans have partly overlapped throughout their development, beginning with the Zodiac fan, which developed in the late Eocene into the Oligocene (~42-32 Ma) and was possibly still active until the Miocene (~24 Ma) (Stevenson, Scholl, and Vallier, 1983; Stevenson and Embley, 1987). Gradual shifting of the Zodiac Fan to the northeast initiated the growth of the Surveyor fan from the Oligocene to the Recent (~20-0 Ma) (Stevenson, Scholl, and Vallier, 1983; Stevenson and Embley, 1987). The Baranof fan

was deposited during the Late Miocene to the Recent (~10 Ma to 0 Ma) (Stevenson, Scholl, and Vallier, 1983; Stevenson and Embley, 1987).

Deposition of the Zodiac fan began no later than the Late Eocene and continued into the end of the Early Oligocene and possibly the Early Miocene (Stewart, 1976; Stevenson, Scholl, and Vallier, 1983). Sources of this sediment have been postulated as a granitic-metamorphic source terrain, but no definite source has been identified because of the size, extent, and mineralogy of the fan (Stewart, 1976; Stevenson, Scholl, and Vallier, 1983). Mineralogy suggests a steady sedimentation to the fan from ~40-30 Ma (Stewart, 1976; Stevenson, Scholl, and Vallier, 1983). The granitic-metamorphic composition may correspond with the Yukon-Tanana terrane whose drainage entered the fan around Cook Inlet (Stewart, 1976; Stevenson, Scholl, and Vallier, 1983).

Surveyor Fan deposition began in the Late Miocene and has continued into the Holocene (Stevenson and Embley, 1987). The lack of major well-developed drainages along the southern and southeastern Alaskan coastline suggests that provenance is most likely glacially driven as outwashed sediment crosses the Yakutat block terrane (Stevenson and Embley, 1987). Since deposition began, the fan location and channel head have moved based on Yakutat block translation northward by approximately 120-150 km (Figure 5) (Stevenson, Scholl, and Vallier, 1983; Stevenson and Embley, 1987).

Deposition of the Baranof fan began no earlier than Late Miocene time (Stevenson and Embley, 1987). The only known sediment source for the provenance of units Pliocene and younger in age within the fan are the glaciated coastal mountains of Alaska and western Canada (Stevenson and Embley, 1987). Sedimentation on the fan is thought to be the result of collision of the Yakutat terrane. Since deposition began, the

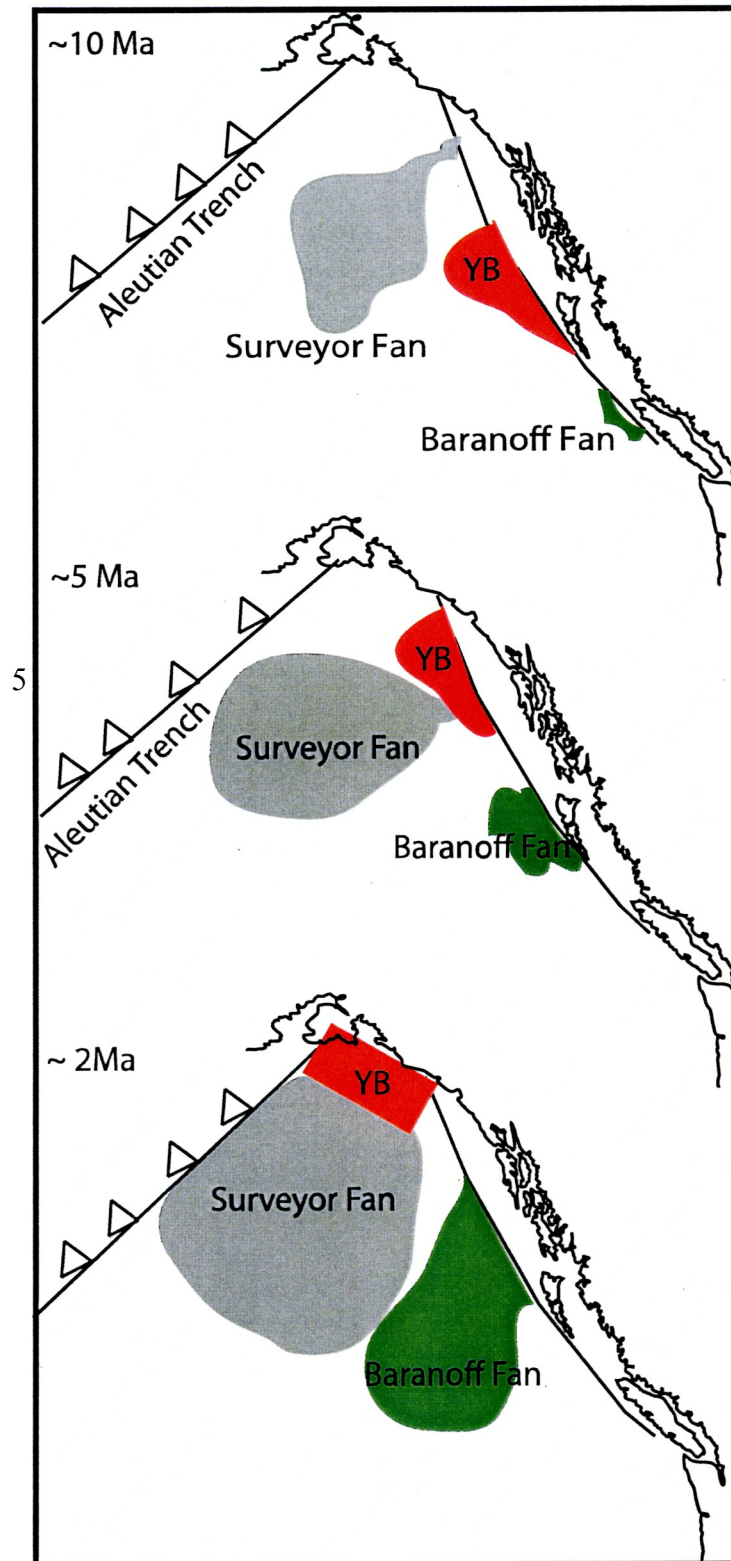


Figure 5. Alaska deep sea fan distribution as a result of the northwestward movement of the Yakutat terrane during the Mesozoic (modified from Stevenson and Embley, 1987).

fan location and channel head have moved based on the encroachment of the Yakutat block northward approximately 120-150 km (Stevenson, Scholl, and Vallier, 1983; Stevenson and Embley, 1987). Collision of the Yakutat terrane is inferred to have played a role in the switching of fan deposition direction, essentially providing a barrier from northeast transport and starving the Surveyor fan of glacially derived Pliocene sediment (Stevenson and Embley, 1987). The Baranof fan could have recorded transport of sediment into the nearby Queen Charlotte basin until northward transport of the Yakutat terrane changed the dynamics and drainage patterns of sediment into the fan (Stevenson and Embley, 1987; Yorath, 1987). The Yakutat terrane itself does not contain the Pliocene record of Baranof fan deposition but it might record the pre-Pliocene deposition beginning with Surveyor fan deposition, in the Late Eocene (Stevenson and Embley, 1987).

GEOLOGICAL BACKGROUND OF YAKUTAT TERRANE

Southern Alaska has been the site of the collision of various allochthonous terranes during the Cenozoic. Terranes such as the Prince William and Yakutat block terranes have been transported northwestward along two transcurrent faults along the continental margin (Plafker, 1987). The Yakutat block is the part of the Yakutat terrane east of the Pamplona fault zone, which is now accreted or attached to the Pacific plate (Plafker, Moore and Winkler, 1994). The transition from the transform Queen Charlotte-Fairweather fault in the east to the convergent Alaska–Aleutian subduction zone in the west has resulted from the transport and collision of the Yakutat block terrane. This

subduction zone was produced by collision, although most of the movement of the Yakutat terrane was along the British Columbia margin and has been not directly related to the Alaska-Aleutian subduction zone.

The movement history of the Yakutat terrane prior to collision is controversial. Its movement history involves the transfer along the northwest Pacific continental margin (~50 Ma to the Recent) (Bruns, 1983; Plafker, 1987). One hypothesis invokes modest transport and shortening within the terrane boundary (Plafker, 1994). A far-traveled hypothesis is based on the reconstruction of magnetic anomalies and an understanding of the development of the subduction of the Kula-Farallon spreading center (Bruns, 1983). This reconstruction places the Yakutat terrane as far south as northern California or southern Oregon at ~45 Ma (Bruns, 1983).

Although the exact transport history of the terrane is debated, it is known from geophysical, seismic, and fault studies conducted on the block that it has accreted since the Pliocene (Bruns, 1983; Fletcher and Freymueller, 1999). GPS measurements of plate velocity for the Yakutat microplate indicate plate motion on the order of approximately ~44 mm/yr to the north (Plafker et al., 1994; Fletcher and Freymueller, 1999). This rate is slower than the rate calculated for Pacific plate motion, which is ~52 mm/yr in the region (Sauber, McClusky, and King, 1997; Fletcher and Freymueller, 1999). The Dangerous River Zone (DRZ) represents the transition from continental crust in the east to oceanic plateau in the west within the basement of the Yakutat terrane (Figure 1) (Plafker, 1987).

The two terranes bounding the Yakutat block terrane are the Prince William terrane on the west and the Chugach terrane to the north (Plafker, 1987). Wrangellia is located east of the Chugach terrane. Due to the Cenozoic collision of the Chugach-Prince

William composite terrane it is possible that some sediment deposition in the Prince William terrane was derived from the Chugach terrane itself (Plafker, 1987). In this case the Chugach terrane was accreted prior to the Prince William terrane and forms a backstop for collision of foreign terranes (Plafker et al., 1994). Within the Chugach terrane, rocks are metamorphosed from zeolite to amphibolite facies, and this metamorphism is inferred to be the result of the subduction of the spreading center beneath the terrane in the Eocene (Plafker, 1987; Bruhn, Pavlis, Plafker and Serpa, 2004). Subduction of this spreading center resulted in the intrusion of dikes and plutons at approximately ~51 Ma (Plafker et al., 1994). The consequential underthrusting of approximately ~225 km of Yakutat terrane beneath the Chugach terrane has resulted in the formation of the Chugach/ St. Elias Range due to uplift and exhumation (Plafker, 1987).

Glaciation of the Chugach/St. Elias Range orogenic belt is severe and is considered to be an important driving mechanism of deformation and material flux (Meigs and Sauber, 2000; Montgomery, 2002; Spotila, Buscher, Meigs, and Reiners, 2004). This flux of material has evolved so that it now incorporates the Yakutat terrane stratigraphy (Bruns, 1983; Plafker et al., 1994).

Stratigraphy

The stratigraphy of the Yakutat terrane records the sedimentation since the Eocene, so it has a rich record of the surrounding geologic events (Plafker, 1987). The sedimentary cover is underlain by two basement types, one a poorly known ocean plateau

and the other a continental framework, which is principally the Upper Paleocene and Lower to Middle Eocene Orca Group (Plafker, 1987).

The boundary in the basement between the uplifted, exposed oceanic crust versus the continental crust of the Yakutat block is identified as the Dangerous River Zone (DRZ) (Plafker, 1987). The DRZ is a regionally high-angle structure that strikes ~N-S (Figure 1) (Plafker, 1987; Bruhn et al., 2004). Stratigraphic sequences vary across this boundary, but only deposition of sediment and the resulting stratigraphy west of this zone is analyzed and discussed in this paper. The basement rock to the west of the Orca Group is metamorphosed oceanic crust with Late Paleocene to Early Eocene fossils (Lagoe, 1983; Plafker, 1987). Lying conformably to the east and on the Orca Group are three formations that comprise the Cenozoic basin strata that have an estimated thickness of ~9,500-10,000 meters. From oldest to youngest these units include the Lower Eocene to Oligocene Kulthieth Formation, the Upper Eocene, Oligocene and possibly Lower Miocene Poul Creek Formation, and the Miocene to Pleistocene Yakataga Formations (Plafker, 1980).

Kulthieth Formation

The Lower Eocene to Oligocene Kulthieth Formation (Tk) (~57-30 Ma) is mainly a gray- to white-weathering, organic-rich sandstone that conformably overlies the Orca Group in the Northern Robinson Mountains (Figure 6 [A], [B]) (Plafker, 1987). In general, the unit consists of arkosic sandstone with interbedded medium to thick coal beds, and abundant marine fossils (Plafker, 1987). Locally the unit is deformed (Plafker,

[A]



[B]



Figure 6. [A] Interbedded massive coarse-grained sandstone and coal deposits within the Kulthieth Formation, Northern Robinson Mountains. Tent campsite on ledge is facing in the southwest direction. [B] Medium- to thick-bedded, red-weathering, gray sandstones of the Kulthieth Formation with students for scale.

1987). The formation was deposited in an environment that represents non-marine alluvial-plain, delta-plain, barrier-beach, and shallow-marine deposits. Sandstones contain abundant cross-bedding showing transport to the northwest (Figure 7 [A], [B]) (Plafker, 1987; Bruhn et al., 2004). The lower section of the Kulthieth Formation consists mainly of trough cross-bedded sandstone with interbedded coal. The middle section consists of ripple-laminated sandstone with interbedded medium-grained siltstone (Wahrhaftig, Bartsch-Winkler, and Stricker, 1994). Interbedded within these two rock types is local calcareous shale containing abundant marine mollusks and leaf fossils (Plafker, 1987). Ages of the fossil assemblages suggest deposition of the Kulthieth Formation during the Early Eocene to the Early Oligocene (~54-33 Ma) (Plafker, 1987). The upper section of the Kulthieth Formation marks a transition into massive sandstones.

Estimated thicknesses of the Kulthieth Formation, in the Yakataga area, is ~2,800 meters (Miller, 1957; Plafker 1987; Wahrhaftig, Bartsh-Winkler, and Stricker, 1994). The depositional age range for this formation is not well constrained. Recent studies of U-Th/He dating of detrital apatite (AHe) and zircon fission-track dating (ZFT) analysis have yielded several new geochronological ages (Spotila et al., 2004; Johnston, 2005). Two samples yielded a young zircon fission-track peak-age between ~26 and 30 Ma (Johnston, 2005). These ages match within error, or are slightly younger than, the estimated age range for the entire formation (Plafker, 1987; Johnston, 2005).

[A]



[B]



Figure 7. [A] Medium- to thick-bedded, coarse-grained sandstone of the Kulthieth Formation containing cross-beds. Student taking measurements for scale. [B] Thin-bedded, coarse-grained sandstone containing cross-beds of the Kulthieth Formation.

Poul Creek Formation

The Upper Eocene to Lower Miocene Poul Creek Formation (Tp) conformably overlies the Lower Eocene to Lower Oligocene Kulthieth Formation and consists mainly of highly deformed, fine-grained, glauconitic, organic-rich, red- to orange-weathering, white sandstone interbedded with water lain basaltic tuff, breccia, pillow lava and variable deposits of the Cenotaph Volcanics (Figure 8 [A], [B]) (Plafker, 1987). The Poul Creek Formation records a marine transgression during its deposition (Plafker, 1987). It is estimated to have a thickness of ~1, 900 meters and it is best exposed in the Grindle Hills of the Northern Robinson Mountains (Plafker, 1987). Age constraints for this unit are better than for the Kulthieth Formation but are still relatively poor. According to Plafker (1987), the Poul Creek Formation ranges in age from Upper Eocene to Lower Oligocene and possibly into the Lower Miocene (~40-20 Ma). Depositional age is partly constrained by detrital zircon fission-track ages that have young populations of ~34 Ma to 41 Ma (Middle Eocene to Early Oligocene) (Johnston, 2005). These ages overlap with Plafker's (1987) original estimate based on the paleontologically determined age.

Yakataga Formation

The Yakataga Formation extends from the Coast Mountains in the Prince William terrane across the Dangerous River Zone divide, overlapping onto the continental segment of the Yakutat terrane. The deposition of this unit is represented by coeval strata in the Surveyor Fan, which indicates mainly a northwestward transport direction (Gulick

[A]



[B]



Figure 8. [A] Along strike photograph of red-weathering, coarse-grained siltstone of the Poul Creek Formation. [B] Close-up of broken, red-weathering, coarse-grained siltstone of the Poul Creek Formation located in the Grindle Hills.

and Jaeger, 2003; Ridgway, unpublished). The Plio-Pleistocene Yakataga Formation (Ty) conformably overlies the Poul Creek Formation and consists of mainly glacially derived sediment with abundant dropstones and diamictite deposits. Deposition of the lower Yakataga Formation (Ty) occurred in neritic to bathyal water depths (Martin, 1993; Plafker 1987). This lower unit is recognized by its transition into thick diamictite characterized by dropstones in a bioturbated medium- to fine-grained sandstones inferred to have been derived from the Chugach and St. Elias Mountains (Figure 9 [A], [B]) (Eyles and Lagoe, 1990). The lower Yakataga Formation is also characterized by soft-sediment deposition (Figure 9 [A], [B]; Figure 10 [A], [B]) (Plafker, 1987). Glacial-related sedimentation apparently has accumulation rates of up to $\sim 800 \text{ m/Ma}^{-1}$ (Powell and Cooper, 2002) and resulted in accumulation of approximately $\sim 5,000$ meters of Yakataga strata. The thickness of the sediment increases from east to west, in some places reaching up to $\sim 6,000$ m in thickness (Bruns and Schwab, 1983; Plafker 1987). Beds thicken and coarsen upsection, and the upper part has thick debris flows as well as turbidites (Gulick and Jaeger, 2003).

Deposition of the Yakataga Formation has apparently recorded a transition in the climatic setting of the region. The depositional age of the Yakataga Formation is believed to be Plio-Pleistocene, but it is poorly dated due to the lack of fossil control. Age constraints on the unit are based on a K/Ar age of ~ 6.2 Ma on a dacitic plug that cuts the sequence on Kayak Island (Plafker, 1987). Of note is the Mid-Pliocene Warm Interval, which occurred from approximately ~ 4.5 to 2.8 Ma well within known deposition of the Yakataga Formation (Shackleton, Hall, Pate, 1995; White, Ager, Adam, Leopold, Liu, Jette, and Schweger, 1997; Lagoe and Zellers, 1996). Although they are still debated, the



Figure 9. [A] Diapiric soft-sediment formation of fine-grained sandstones in the Yakataga Formation located on Kulthieth Mountain. [B] Dropstone deposits within the Plio-Pleistocene Yakataga Formation.

[A]



[B]



Figure 10. [A] Diamicite deposit within the Yakataga Formation, Northern Robinson Mountains. [B] Overview photograph of same diamicite deposit shown in [A].

oxygen isotope records provide a constraint on the timing of the development of tidewater glaciation, which is present represented by drop-stones and ice-rafted debris (Lagoe, Eyles, Eyles and Hale, 1993).

Sedimentary Petrography of Yakutat Cover Stratigraphy

Sedimentary petrography of the Kulthieth and Poul Creek Formation of the Yakutat block terrane stratigraphy is known from a single petroleum well (Plafker, Winkler, Coonrad, and Claypool, 1980). QFL ratios (%) are provided and mean percentages plotted on a QFL ternary diagram where Q = % quartz, F = % total feldspar, and L = total rock fragments (Plafker et al., 1980). For the Kulthieth Formation quartz is ~41%, feldspars ~34%, and lithics ~25% based on 8 samples (Plafker et al., 1980). For the Poul Creek Formation quartz is ~37%, feldspars 41%, and lithics ~22% based on 10 samples. These two formations plot as lithofeldspathic sandstone, and they note the abundance of volcanic and plutonic grains on a VSM ternary diagram where V = volcanic and plutonic %, S = sedimentary %, and M = metamorphic percentage (Plafker et al., 1980). The Kulthieth and Poul Creek Formations have heavy mineral suites that consist of biotite, epidote, muscovite, amphibole, and garnet, suggesting possible greenschist to amphibolite facies metamorphic rocks in the source (Nokleberg et al., 2005).

The Kulthieth Formation is generally described as containing abundant metamorphic prehnite, carbonized plant material, mica, pyrite micronodules, and glauconite (Plafker, 1987; Plafker et al., 1994; Nokleberg et al., 2005). The overlying

Poul Creek Formation is described as containing abundant mica, glauconite, and mafic tuffaceous grains (Plafker, 1987; Plafker et al., 1994; Nokleberg et al., 2005).

Deformation and Structure

The Yakutat terrane is bound on the east by the Fairweather fault, on the north by the Chugach/St. Elias thrust fault, on the west by the Pamplona Zone, and on the south by the Kayak Island fault zone (Figure 1) (Plafker, 1987). The Chugach/St. Elias Range marks the structural backstop to the foreland basin deposits of the Yakutat terrane. Collision of the Yakutat terrane has produced a seaward-vergent thrust belt and the Yakataga Formation is the foreland deposit associated with that collision. These depositional settings vary from nonmarine to marine across the Dangerous River Zone (DRZ) and the section thickens from east to west with increasing structural deformation to the west as well (Bruhn et al., 2004). Starting from the east, the DRZ marks a major transition from the Mesozoic continental crust to the Paleogene oceanic crust of the Yakutat block terrane (Plafker, 1987).

To the west of the DRZ lies the Pamplona Zone (PZ) fold and thrust belt where deformed sedimentary units lie to the east and the fold-and-thrust belt that is associated with the Aleutian megathrust lie to the west (Plafker, 1987). Within the PZ the sedimentary stratigraphy includes the Kulthieth, the Poul Creek, and the Yakataga Formations. Here the formations are actively being thrust beneath the Chugach terrane to the north and the Prince William terrane to the west (Plafker, 1987). Westward subduction has been identified by marine reflection data that shows a magnetic anomaly

extending from beneath the Prince William terrane and which corresponds to the basal unit of the Yakutat terrane (Figure 1) (Bayer, Mattick, Plafker, and Bruns, 1978). Another key deformational feature associated with the Chugach/St. Elias thrust fault is reverse faulting and folding which have been mapped and associated with the accommodation of space in the compressional zone (Bruhn et al., 2004). Compressional structures in the fold and thrust belt trend north-northeast and are comprised of broad synclinal structures and tightly folded anticlines (Figure 1). Within the Cenozoic shortening is ~ 45%, and 25% in the sedimentary cover (Plafker, 1987). The degree of metamorphism of the Yakutat block varies in this zone with local amphibolite facies rocks in the east to prehnite facies rocks in the west.

The boundary between the Pamplona zone and the Kayak Island Zone is thought to lie beneath the Bering Glacier. The Kayak Island Zone is followed by the Copper River, which has one of the highest sediment loads of any river in the world (Bruhn et al., 2004; Plafker, 1987). The Kayak Island Zone marks a transition from the exposed Paleogene sedimentary rock to overlying Quaternary deposits supplied by the river and derived from the nearby Miles Glacier. The Kayak Island Zone also marks the location of the Chugach/ St. Elias fault, which strikes east west and has a slight northward dip (Bruhn et al., 2004).

All zones west of the DRZ are thought to represent the accommodation of strike-slip motion along the Queen Charlotte-Fairweather Fault that lies to the east (Plafker, 1987). Active deformation is accommodated by strike-slip motion and active thrusting to the west of the Yakutat terrane (Plafker, 1987). Collision of the Yakutat terrane is thought

to be influenced by the northward dip of the Chugach/ St. Elias Range Fault; this dip allows the thrusting of the Yakutat terrane to the north (Bruhn et al., 2004).

Exhumation from previous thermochronologic studies

The use of low-temperature thermochronology in understanding orogenic evolution has become a widely used technique to address the exhumation history of an evolving orogenic belt (O'Sullivan and Currie, 1996, Spotila et al., 2004). Denudation, uplift, exhumation, and depositional rates for orogens can be determined by thermochronological techniques applied to low-temperature minerals such as apatite and zircon. There has been little thermochronological work done previously on the Yakutat block. Johnston (2005) conducted a study focusing on the rocks in the Bering Glacier/Northern Robinson Mountain area using zircon and apatite fission-track dating techniques as well as U-Th/He dating of zircons. The results and implications of this study are discussed further below.

One of the earliest studies of Cenozoic exhumation in the nearby Central Alaska Range used apatite and zircon fission-track dating on rocks from three peaks in the Central Alaska Range including Mt. McKinley, Mt. Dan Beard and Mt. Huntington (Plafker, Naeser, Zimmermann, Lull, and Hudson, 1991). Timing of Cenozoic cooling showed pronounced periods of rapid exhumation in the Middle Eocene, Middle Miocene, and Middle Pliocene (Plafker et al., 1991). The more rapid estimated exhumation rates were ~1.3 mm/yr for the last ~4.2 Ma, and two mechanisms are suggested for driving the increase to ~1.3 mm/yr. One explanation for the increase in exhumation since ~4.2 Ma is

a northward regional tilting of the range, attributed to compression from oblique underthrusting of terrane along a splay of the Denali fault system (Plafker et al., 1991).

Another possible explanation is the change in relative Pacific-North American plate motion and rotation as recorded by GPS measurements and associated with the continued collision and subduction of the Yakutat block terrane (microplate) beneath the southern Alaskan margin (Plafker et al., 1991).

Closer to the collision zone, the northern St. Elias Mountains and related foothills have also been investigated (O'Sullivan, Plafker, and Murphy, 1995). Apatite fission-track (AFT) ages ranging from ~4.5-1.3 Ma give an erosional exhumation rate of approximately ~1.5-1.9 mm/yr (O'Sullivan, Plafker, and Murphy, 1995). Previous thermochronology on K/Ar (biotite) suggested a local cooling/heating event during the Pliocene (O'Sullivan, Plafker, and Murphy, 1995). It is inferred that rapid exhumation has occurred since approximately ~4 Ma and thus the authors postulate that the driving mechanism is the Yakutat block collision (O'Sullivan, Plafker, and Murphy, 1995).

An age elevation transect in the Denali area (Mt. McKinley) using apatite fission-track thermochronology showed summit ages of ~16 Ma and the youngest cooling ages and rapid exhumation at about ~6 Ma (Fitzgerald, Sorkhabi, Redfield, and Stump, 1995). This work shows a significant break in slope of apatite fission-track ages at ~6 Ma and indicates the onset of rapid exhumation (Fitzgerald et al., 1995). Exhumation rates were calculated to be ~1.5 mm/yr (Fitzgerald et al., 1995). Fitzgerald and colleagues interpret the increase in exhumation as caused by the change in plate motion and rotation with respect to the Pacific and North American plates (Fitzgerald et al., 1995). Changing plate vectors may also have affected the Yakutat terrane at ~5-6 Ma (Fitzgerald et al., 1995).

Accommodation of these subtle plate motion changes may be reflected in the increased and more severe shortening of rock as a result of compression within the fold and thrust belt in the Pamplona Zone (Bruhn et al., 2004). The conclusion is that, prior to increased exhumation in the Middle Miocene, the Central Alaska Range was tectonically and thermally stable. If this hypothesis is correct, the timing has implications for the Yakutat Collision.

In a related study, O'Sullivan and Currie (1996) used apatite fission-track dating of Mt. Logan in the hanging wall of the collisional zone to explore the implications of thermochronologic ages which suggested fluctuations in late Cenozoic exhumational rates. Three distinct clusters of cooling ages yielded exhumation rates of the St. Elias Mountains as approximately $\sim 0.3 - 0.7$ mm/yr from the Middle Eocene to the Recent based on ages ranging from $\sim 40-4$ Ma (O'Sullivan and Currie, 1996). In this elevation transect, ages decrease downward and all samples were reset with respect to the zircon fission-track closure temperature of $\sim 240^{\circ}\text{C} \pm 30$ for the system (see Brandon and Vance, 1992 and Bernet, Zattin, Garver, Brandon and Vance, 2001). Fission-track ages indicate rapid Miocene cooling that must reflect perturbation related to underthrusting of the Yakutat terrane (O'Sullivan and Currie, 1996). A break in slope of the lower section of the apatite fission-track ages represents an exhumed partial annealing zone, and the time of the break in slope suggests exhumation occurred as a result of the onset of uplift and erosion starting at ~ 5 Ma (O'Sullivan and Currie, 1996). From these data O'Sullivan and Currie (1996) concluded that three episodes of highly elevated rates of exhumation and erosion occurred during the Middle Eocene, Middle Miocene and Middle Pliocene unclear (O'Sullivan and Currie, 1996).

A recent study was conducted around the Bering Glacier/Northern Robinson Mountain area extending into the Yakutat District of southern Alaska. This study applied apatite and zircon fission-track dating and U-Th/He dating of apatite to the Cenozoic stratigraphic sequence associated with the Yakutat block collision (Spotila, Buscher, Meigs, and Reiners, 2004). Interpretation of the thermochronology was aided by a balanced cross-section that addressed shortening in the cover sequence (Johnston, 2005). Most ZFT samples yielded multiple peak ages, which suggested that almost all samples were unreset with respect to the zircon fission-track closure temperature of $\sim 240^{\circ}\text{C} \pm 30$. Minimum peak ages ranged from ~ 26 -41 Ma, with increases in age in older units (Brandon et al., 1998; Johnston, 2005). However, results from the Kulthieth Formation yielded a ZFT minimum age younger than the known stratigraphic depositional age (Early Eocene to Oligocene) for these samples. These young ranges have been attributed to resetting of radiation-damaged zircon (Johnston, 2005). Apatite fission-track and apatite U-Th/He dating yielded results that bear on orographic changes due to precipitation and glacial influences within the range (Spotila, Buscher, Meigs, and Reiners, 2004; Johnston, 2005). Apatite fission-track ages from rocks in the thrust belt range from ~ 3.4 -31.5 Ma, with ages increasing inland (Spotila et al., 2004; Johnston, 2005). Spotila and others (2004) attribute this trend, also seen in the apatite U-Th/He data, to the influence of significant precipitation and erosion closer to the Gulf of Alaska coast. As one traverses north into the backstop of the Chugach/St. Elias Range thermochronologic ages increase; this suggests slower exhumation which is inferred to reflect less precipitation and therefore less erosion of rock. Estimated exhumation rates

across the orogenic belt are ~0.5-1.5 mm/yr from the Eocene to the Recent based on all thermochronologic systems (Johnston, 2005; Spotila et al., 2004).

FISSION-TRACK DATING BACKGROUND

Minerals such as garnet, pyroxene, epidote, zircon and apatite contain naturally occurring ^{238}U that undergo spontaneous fission. Each of these fission events leaves a trail of damage that is sensitive to thermal annealing and they are therefore suitable for thermochronological studies. In 1964 at GE Electrical Company in Schenectady, New York three scientists developed a method of recording spontaneous fission events in zircon grains. Robert Fleischer, Robert Walker and Raymond Price discovered that the spontaneous fission of naturally occurring ^{238}U causes atomic disorder that results in measurable damage zones (Figure 11) (Fleischer, Price and Walker 1965; Fleischer, Price and Walker, 1975).

Before one is to understand the measurement of these damage zones and what they can tell us, it is important to understand how they occur. The formation of spontaneous fission-tracks within individual grains begins after the rock has cooled below a temperature specific to each mineral. In typical settings this cooling interval starts as the rock passes through the Partial Annealing Zone (PAZ). The PAZ for zircon ranges down from $240^{\circ}\text{C} \pm 30$ and in typical settings is located approximately 7.5-10 km beneath the Earth's crust, assuming a continental geothermal gradient of 25 to $35^{\circ}\text{C}/\text{km}$ (Brandon, Roden-Tice, and Garver 1998; Bernet et al., 2001). While in the PAZ, tracks in a zircon crystal grain are annealed or shortened. The kinetics of this annealing are a

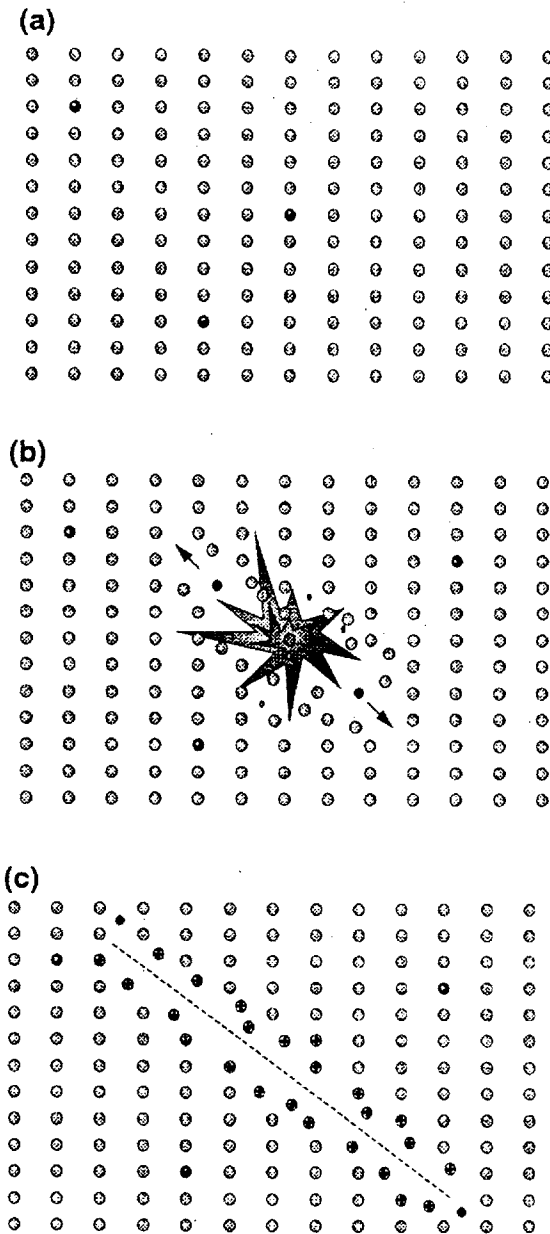


Figure 11. "Ion spike mechanism" of track formation (Fleischer et al., 1965). Charged fission fragments recoil and strip electrons along its path. This process is inferred to cause a fission track.

function of the specific grain characteristics which are mainly a function of radiation damage. As rock enters the PAZ the geological clock is “set” to zero and as it progresses through the PAZ the mineral grains begin retaining fission-tracks, recording the thermal and exhumation history of the rock (Figure 12). In other words, when the rock enters the PAZ it is effectively track-free; the tracks measured in the lab have formed during the time in between when the rock cooled sufficiently to the PAZ and when it reached the surface. The accumulation of fission-tracks, in a mineral grain with uniform uranium concentration, is constant over time because the decay rate of ^{238}U is constant; therefore the accumulation of fission-tracks within the grains of a given sample is a direct indication of the time since cooling below the closure temperature in an orogenic system. The spontaneous fission rate of ^{238}U is $7.03 \pm 0.11 \times 10^{-17} \text{ yr}^{-1}$, which is much slower than other radioactive decay rates used for thermochronological analysis such as $^{39}\text{Ar}/^{40}\text{Ar}$ dating and U+Th/He dating (Garver, 2003). As the radioactive isotopes ^{238}U , ^{235}U and ^{232}Th within the zircon decay, α -particles are ejected into the crystal lattice (and the parent atom recoils). This α -decay creates α -particle damage to the radiation crystal structure of the mineral.

DETRITAL ZIRCON FISSION-TRACK BACKGROUND

Detrital zircon fission-track (DZFT) analysis utilizes the ability of zircon to yield single-grain cooling ages after passing through a closure temperature of $240^\circ\text{C} \pm 30$ and transport this information to nearby sedimentary basins (Hurford, 1983; Brandon et al., 1998; Garver, Brandon, Roden-Tice and Kamp, 1999; Bernet et al., 2001; Bernet and

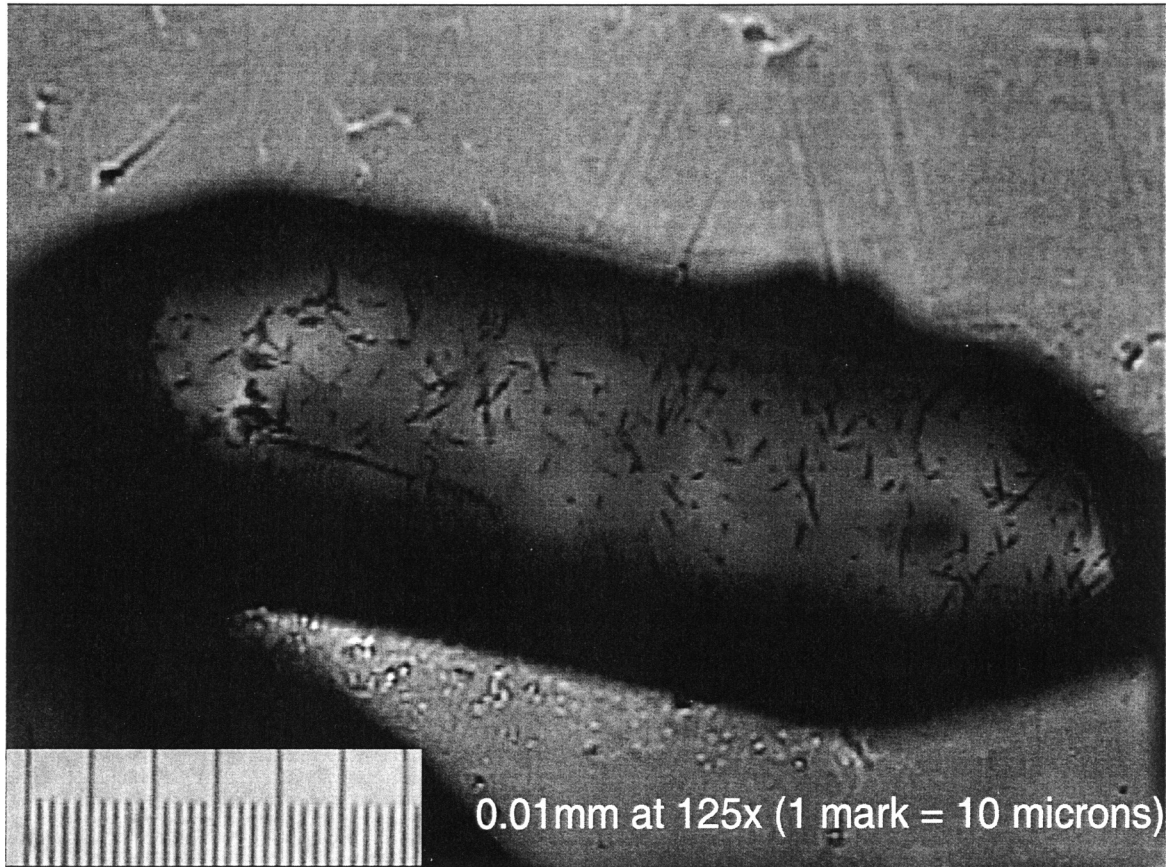


Figure 12. Composite picture of a well-etched zircon from sample 05-11.

Garver, 2005). The precision of individual grain-age determinations is relatively low and therefore representative cooling ages for a sample are determined by analysis of a suite of detrital grains (Brandon and Vance, 1992; Garver and Brandon, 1994 a, b; Bernet and Garver, 2005). The significance of DZFT analysis lies in the ability to determine the provenance of sedimentary basins, as well as provide insight into the long-term geothermal evolution of nearby orogenic belts. The system is complemented by two other geochronological techniques for zircon such as U/Pb analysis ($800^{\circ}\text{C} \pm 40$) and U+Th/He analysis ($70\text{-}90^{\circ}\text{C}$) (Dempster, 1935; Davis and Krogh, 2003; Reiners, Farley and Hickes, 2002; Ehlers and Farley, 2003; Reiners, Spell, Nicolescu and Zanetti, 2003).

The differences in detrital analysis versus standard fission-track analysis lie in field collection, sample preparation, and interpretation. Field collection involves sampling sandstones of known stratigraphic position. Sample preparation techniques are identical to the aforementioned process for fission-track analysis. Sample preparation varies in etching techniques and the quantity of zircon grains mounted in PFA Teflon®. Typically 50-100 single grain analyses are dated on a single sample mount to ensure that all major representative cooling ages are revealed in the data. Therefore approximately 200-1000 zircon grains are mounted and embedded into the PFA Teflon® to provide ample countable zircons. Usually several mounts are prepared for a single sample so that each mount can be etched for varying amounts of time (Naeser, Zeitler, Naeser, and Cervany 1987; Garver, Soloviev, Bullen and Brandon, 2000b; Bernet, Brandon, Garver and Molitor, 2004b). By preparing multiple mounts that are etched for different times, the researcher increases the probability that all representative-cooling ages will be accounted for during analysis. This technique is referred to as the *Multi-Mount technique*, but there

are other techniques used in labs that conduct DZFT analysis (Bernet and Garver, 2005). These techniques are the *Multi-Etch technique*, which involves a single mount per sample that is analyzed and re-etched multiple times to expose multiple cooling age populations, and the *Optimal Etch technique*, where a single mount is etched for an optimal amount of time ignoring all other cooling ages that may be retained within the sample (Bernet and Garver, 2005). After sample preparation and analysis cooling age populations are deconvolved. For this study BINOMFIT software was used, which uses multiple statistical analyses to group single grain ages into specific populations (Brandon, 1996). These grain-age populations can then be examined to determine if samples were thermally reset in the basin after sedimentation, or not. If these ages are unreset then inferences can be made about the thermal history of the source terrains.

U/Pb BACKGROUND

The U/Pb dating technique is routinely used to determine the crystallization ages of single zircon grains based on the radioactive decay of U and Th to end products ^{206}Pb and ^{207}Pb in a closed system (Tilton and Aldrich, 1955). Accessory minerals such as zircon contain naturally occurring ^{238}U , ^{235}U , and ^{232}Th . These radioactive isotopes decay to the stable daughter isotopes ^{206}Pb , ^{207}Pb and ^{208}Pb ; respectively. Zircon has a natural ability to retain the original amount of U isotopes and accumulated radiogenic Pb within its crystallographic structure while excluding Pb accumulation during crystallization. This fractionation has led to the development and advancement of the U/Pb dating method over time, beginning with Isotope Dilution-Ionization Mass Spectrometry (ID-

TIMS) analysis and progressing to the routine use of laser-ablation ICPMS technology (Davis, Williams, and Krogh, 2003). George Tilton and others (1955) used the ID-TIMS method to date zircon by comparing the amount of U/Pb isotope compositions measured to a known amount of “spike” isotope. The implementation of the spike-method was a groundbreaking innovation in the U/Pb decay series determinations and is still used today. By 1957 scientists discovered the increasing tendency for zircon grain ages to be discordant with increasing levels of common Pb within the crystal (Krogh, 1973; Stacey and Kramers, 1975; Davis and Krogh, 2000). The breakthrough for the U/Pb methodology came with the development of the concordia diagram, which uses isotopic ratios to plot $^{206}\text{Pb}/^{238}\text{U}$ against $^{207}\text{Pb}/^{235}\text{U}$ abundance on a curve (Wetherill, 1956a). A concordant crystallization age of a single zircon is one that falls on the locus of all points that represent concordant ages of $^{206}\text{Pb}/^{238}\text{U}$ and $^{207}\text{Pb}/^{235}\text{U}$ predicted by the age and decay rates of the two isotopes (Wetherill, 1963; Krogh, 1994). A crystallization age becomes discordant when the isotopic ratios of $^{206}\text{Pb}/^{238}\text{U}$ vs. $^{207}\text{Pb}/^{235}\text{U}$ are not both equal to the predicted values. Discordance is related to Pb loss due to diffusion out of the zircon crystal as the internal structure of the crystal varies with age of uranium gain as well as with heating events and radiation damage (Stacey and Kramers, 1975; Oberli, Bachmann, Meier, and Dungan, 2002).

As the technique advanced for both the ID-TIMS and SHRIMP systems analysis, a computer model that used a standard least squares, goodness-of-fit mean square of weighted deviations (MSWD) was developed to determine the probability of fit of a particular determined crystallization age (Ludwig, 1980). The program was designed to consider the possibility of Pb-loss and common Pb contamination. These variables are

considered through statistical analysis using the reduction software Isoplot program (Ludwig, 1998a; 1998b; 2001; 2003). Recently, routine use of laser ablation-inductively coupled plasma mass spectrometer (LA-ICPMS) analysis on zircon has produced accurate U/Pb crystallization age results (Kapp and Gehrels, 1998; Gehrels, 2000). Using a known standard reproducibility of the standard crystallization age provides confidence in the LA-ICPMS analysis of U, Th and Pb ratios contained in a single zircon. ID-TIMS results versus LA-ICPMS results have been compared to ensure the accuracy and reproducibility of both systems in analyzing U/Pb ratios (Gehrels, 2000; 2001). Advancements continue in an effort to reduce both operator and instrumentation error and more accurately correct for such problems as Pb loss, isotope fractionation and common Pb contamination.

SEDIMENTARY PETROGRAPHY BACKGROUND

Sedimentary petrography analysis is commonly employed as a means of identifying potential source terrains for the deposition of sandstones in sedimentary basins. Robert Folk (1974) also outlined the use of sedimentary petrology analysis for detrital source indicators by describing all of the characteristics and analyses that could or should be conducted on strata collected with the intent of detrital source terrain identification. Basu and colleagues (1975) demonstrated that the maturity of sands representing a sample as well as grain size are useful in evaluating whether strata experience input from the same source terrains or not. The maturity of sands within the sample are distinctive and can provide source terrain indications such as volcanic or

plutonic, based on mineral structure and sand grain size and maturity (Blatt and Christie, 1963). Basu and others (1975) conducted analysis on the undulatory extinction and polycrystalline behavior of detrital quartz with the intent of interpreting these data to determine provenance of the samples. Samples were collected from various locations throughout the United States and the percentages of polycrystalline (2-3 subgrains) versus nonundulatory versus polycrystalline (>3 subgrains) versus undulatory quartz were plotted against each other on a diamond ternary diagram (Basu et al., 1975).

Sandstones of the Pacific Northwest and Alaska

Little research has been done on petrofacies analysis of sandstones in southeastern Alaska, but some studies discuss the sedimentary petrography of units in the area from the northern margin of British Columbia to the northwestern margin of Washington (Snively, Niem, MacLeod, Pearl and Rau, 1980; Heller, Tabor, O'Neil, Pevear, Shafiquillah, and Winslow, 1992; Garver and Brandon, 1994). Most abundant research has been conducted on the Queen Charlotte Basin located off the western margin of southern British Columbia. Most data suggests that strata in the Pacific Northwest originated from volcanic-plutonic terrains such as the Cascades, the Idaho Batholith and the Coast Plutonic Complex (Garver and Brandon, 1994). Although sandstones are compositionally similar, provenance of Pacific Northwest basin strata originates from one of five sources including the Coast Plutonic Complex of southwestern Washington, the Omineca Belt of southeastern British Columbia and northwestern Washington, the Coast Ranges of western Oregon and Washington and the Idaho Batholith (Dickinson, 1988;

Garver and Brandon, 1994). The Coast Plutonic Complex represents a Late Mesozoic to Early Cenozoic batholithic source, the Coast Range terrane a Lower Eocene basaltic source, the Olympic subduction complex a Cenozoic sandstone, mudstone and pillow basalt source, and the Cascade volcanic arc a Tertiary volcanic source (Garver and Brandon, 1994).

Two studies addressing the use of sedimentary provenance analysis were conducted on sandstones from the Tofino Basin, the Olympic Peninsula, and the Olympic Mountains in Washington. Petrofacies distinctions are clear in different formations for the Tofino basin (Garver and Brandon, 1994). The Adwell, Lyre, and Hoko River Formations are classified as a lithic petrofacies based on the abundance of basaltic and phyllitic detritus and the dominant presence of chert, polycrystalline quartz, and volcanic lithic fragments. Based on these characteristics, sedimentary provenance suggests sediment input from the British Columbia Coast Ranges and southern Vancouver Island (Ainsfield, 1972; Marcott, 1984; De Chant, 1989; Garver and Brandon, 1994). The Makah Formation, including the Baada Point and Dtokoah Point members, are defined as being a lithic feldspathic petrofacies because of the abundance of quartz and feldspar (Snively and others, 1980; Garver and Brandon, 1994). The first petrofacies identified in the Tofino Basin strata sequence are a micaceous feldspathic petrofacies. This includes the Klachopis Point and Third Beach Members and the Falls Creek Unit of the Makah Formation, Pysht Formation, and Clallam Formation. Analysis of these units provides evidence for the unroofing of material atop a plutonic basement because of the change upsection from a lithic rich petrofacies to a micaceous rich petrofacies (Garver and Brandon, 1994). The sedimentary petrography analysis was combined with detrital zircon

fission-track analysis to better establish the provenance of these strata in the Tofino basin. By using zircon fission-track data from bedrock in the Coast Plutonic Complex, Parrish (1988) and Garver and Brandon (1994), constructed a model cooling age distribution for material shed off of the Coast Plutonic Complex. It was inferred from combined petrofacies and zircon fission-track analysis that the main source for sediment shed into the Tofino Basin from the Oligocene to the Miocene was from the northern Coast Plutonic Complex of British Columbia. The lack of volcanic grains within the samples suggests a Coast Plutonic Complex source because these rocks are north of the Cascade Arc (Garver and Brandon, 1994).

A similar study on isotopic provenance of sandstones in the Olympic Mountains as well as analysis of two samples collected from the Yakutat terrane stratigraphy of southeastern Alaska was conducted by Heller and others (1992). One hypothesis tested was that the sedimentary petrography of strata of the Yakutat terrane is equivalent to the strata deposited in the Tye basin off the coast of northwestern Washington (Heller et al., 1992). The authors' note that the Kulthieth Formation located in southeastern Alaska is typically characterized as a micaceous arkosic sandstone (Heller et al., 1992). In combination with sedimentary petrographic analysis, Rb/Sr and K/Ar analyses were performed on white mica from whole-rock samples (Heller et al., 1992). The sandstones in the Tye basin and within the Olympic Mountains are remarkably similar therefore requiring a secondary analysis of samples to define differences between the sandstone units. Of interest is the Rb/Sr levels and K/Ar ages of the Western Olympic Lithic assemblage versus the Yakutat terrane samples. $^{87}\text{Rb}/^{86}\text{Sr}$ levels range from ~4.87-7.92 ppm for the Western Olympic Lithic, assemblage and ~6.45-7.27 ppm for the Yakutat

terrane (Heller et al., 1992). K/Ar ages for detrital mica in the Western Olympic Lithic assemblage range from ~86-94 Ma and ~84-93 Ma for the Yakutat terrane (Heller et al., 1992). These results are remarkably similar. The suggested provenance for these units for both the Western Olympic Lithic assemblage and the Yakutat terrane is that they were derived from the Omenica Crystalline Belt of southern British Columbia (Heller et al., 1992). A southern source was ruled out because of the dissimilarity in Rb/Sr levels and K/Ar ages with formations such as the Tye Formation and Herren unit (Heller et al., 1992).

VITINRITE REFLECTANCE BACKGROUND

Vitrinite reflectance is the study of the thermal history of rocks containing organic matter that has been heated over geological time. The technique is generally used to determine the thermal maturity of rocks to assess their hydrocarbon potential and therefore potential for oil production and entrapment. The temperature sensitivity for the vitrinite reflectance system ranges from ~60-200°C (Bostick, 1979). Within this temperature range pronounced subdivisions are made based on stages of thermal maturity correlated with increasing temperature. The minimum temperature threshold or the point at which organic contents such as peat and lignite become dehydrated is ~60°C (Khorasani and Michelson, 1994; Sweeney and Burnham, 1990). Between ~60-120°C vitrinite reflectance values of ~0.5-0.6% represent the heating and dehydrating of organic material resulting in the production of oil (Cook and Muchison, 1977; Bostick, 1979). From ~ 120-150°C gas is produced and typically is represented by vitrinite reflectance

values of ~0.85-1.1% (Sweeney and Burnham, 1990; Cook and Sherwood, 1991). As rocks are heated beyond ~150°C they are referred to as post mature, meaning they no longer have any potential for producing oil. As temperatures reach ~200°C ($R_o\%$ ~2.0 or greater) the remaining organic compounds within the rocks are reduced to graphite and methane (Burnham and Sweeney, 1989).

The thermal history and maturity of rocks that have been buried and later exhumed is measured by the reflectance or reflectivity (R_o) of a polished, unweathered surface of the rock being examined with normal incident white light (Bostick, 1979). Two measures of reflectivity can be conducted each with different methods. If the thermal maturity of a rock is reported as $R_v \text{ max}\%$ then the rock was analyzed under cross-polarized light on a Petrographic microscope (Bostick, 1979). The two highest values of reflectance determined from analysis of difference planes of the rock positioned at varying angles are averaged together to result in the $R_v \text{ max}\%$ value (Cook and Murchison, 1977). The $R_o\%$ value of reflectance is measured in non-polarized light under a normal incident beam light source and represents the reflectance off the light source off macerals contained in the rock (Bostick, 1979). Typically 30-100 measurements are made per sample, but the quantity of measurements is dependant upon the amount of vitrinite in a sample (Cook and Sherwood, 1991). Vitrinite reflectance values commonly are complimented by total alteration index analysis (TAI). TAI is determined by matching the color of the rocks being analyzed to a universally accepted color scheme, indicating thermal maturity based on color (Dean and Turner, 1995).

Vitrinite Reflectance in the Pacific Northwest and Alaska

Vitrinite reflectance has been widely studied within sediments of the Queen Charlotte Basin, Vancouver Island, and the Yakutat terrane of southern Alaska. Of particular note is a compilation of data published on the Thermal Maturity Map of Alaska (Johnsson and Howell, 1996). This map includes vitrinite reflectance values gathered across southern Alaska, including samples from the Northern Robinson Mountains east of the Bering Glacier where stratigraphy consists of the Yakataga, Poul Creek and the Kulthieth Formations. The compilation indicates that typical values in this area are ~2.5% or greater closest to the Chugach/St. Elias fault (200°C or above) (Johnsson and Howell, 1996). South of the fault and towards the southern coast values decrease to ~0.40% within the glacially derived Miocene to Recent Yakataga Formation (Johnsson and Howell, 1996).

A study conducted by Plafker and colleagues (1980) analyzed the vitrinite reflectance ($R_o\%$) and TAI of samples collected from drill holes offshore of Yakutat Bay in southern Alaska. Individual units were described and correlated with Yakutat terrane stratigraphy including the Poul Creek and Kulthieth Formations. Samples from this offshore site have $R_o\%$ of ~0.32 to 0.60%, indicating submature to immature thermal histories (Plafker et al., 1980). West of the Yakutat Seavally offshore of the Pamplona Zone $R_o\%$ values range from ~0.60 to 2.16%, indicating mature to overmature conditions (Plafker et al., 1980) and in the higher range are hot enough to anneal and reset zircon fission-tracks.

DETRITAL ZIRCON FISSION-TRACK METHODS

Field Methods

All samples collected (05-01 to 05-17) were from fresh, accessible bedrock locations consisting of fine- to coarse-grained sandstone, and one sample of conglomerate (sample 05-09). About 4-7 kg of rock was collected at each location. Four samples of sand (river sediment) were collected from large-scale glaciated drainages. Approximately 14-20 kg of loose, unsorted sand was collected from each sample location to obtain a modern river detrital fission-track provenance.

Laboratory Separation Methods

Mineral Separation

In this study 16 new detrital zircon fission-track ages were determined from samples collected throughout the Yakataga, the Poul Creek and the Kulthieth Formations located in the Northern Robinson Mountains. In the lab, zircons were separated for analysis using standard procedures for the external detector method (Naeser, 1987; 1979). The external detector method refers to the process of covering a zircon mount with a piece of low-uranium mica, which records the amount of parent ^{235}U concentration during neutron irradiation (Figure 13). The mica records the number of induced fission-tracks using a process known as neutron irradiation (Naeser, 1979).

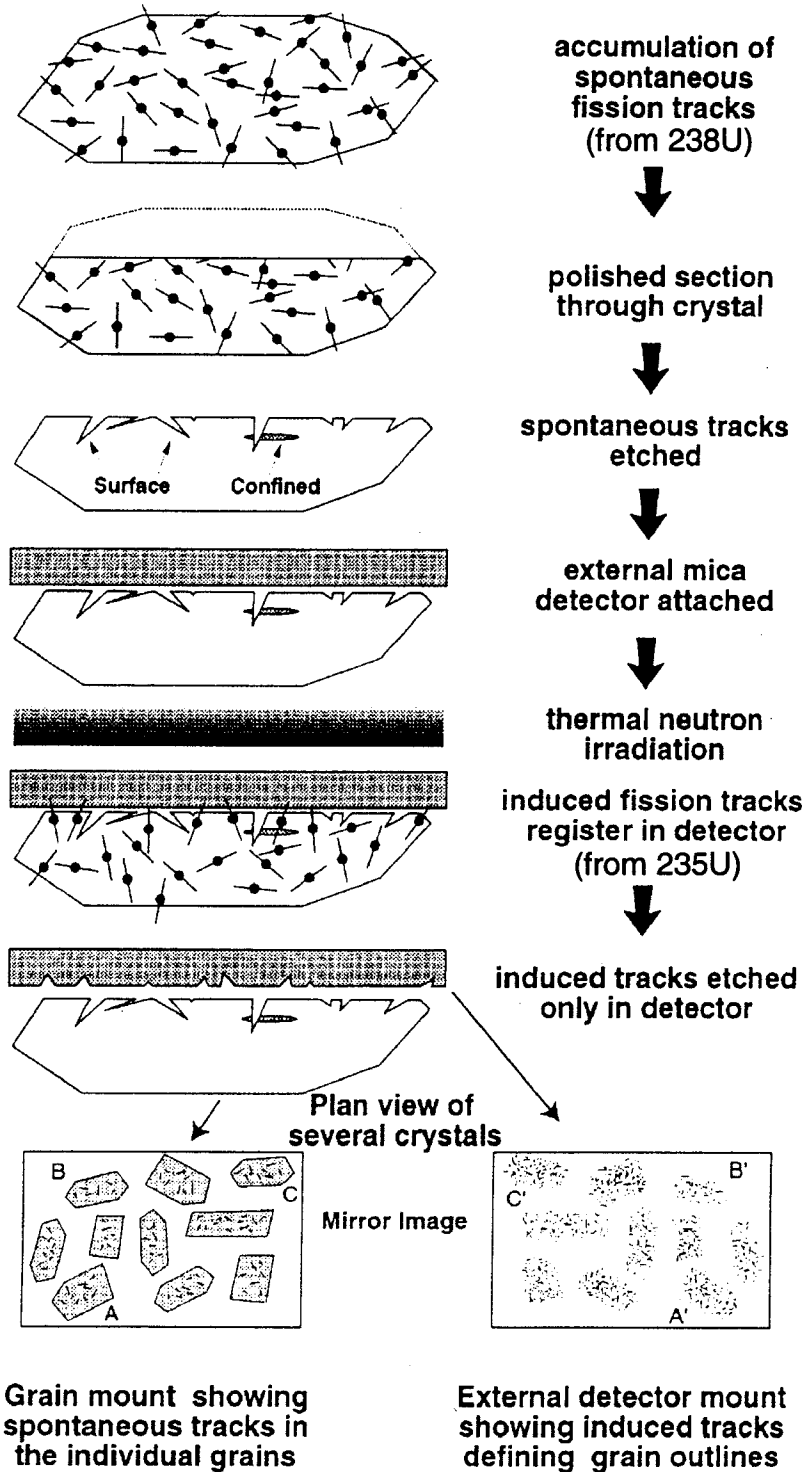


Figure 13. Schematic showing the etching and external detector methods used to etch and reveal fission tracks (see text for discussion).

For modern river samples, the loose sand was sieved through sizes 600 μm , 300 μm , 250 μm and 65 μm . The grains with a sieve size less than 250 μm and greater than 63 μm were then processed with the same steps used to process the pulverized rock of all other samples collected.

Rock samples were first crushed. The crushed rock was then pulverized and individual grains were then processed on a Rogers Table. The Rogers Table separates heavy minerals from light minerals based on grain density. The heaviest minerals collected on the Rogers Table were later separated using heavy liquids. The minerals are submersed in Tetrabromoethane, which is used to separate minerals with a density greater than 2.95 g/cm^3 which sink. The densest mineral fraction ($\rho > 2.95 \text{ g/cm}^3$) were then run through a Franz Magnetic Separator. Remaining non-magnetic grains are submersed in methlene iodide, where grains with lower specific gravity float (residual grains including apatite) and grains with higher specific gravity than the liquid sink to the bottom (zircon grains).

Samples 05-02, 05-05, 05-14, 05-15 and SR 4 did not have sufficient zircon for analysis (Table 1). Sample 05-02 was collected from a carbonate-rich bed and therefore had low to no concentration of zircon (Bernet and Garver, 2005). Sample 05-05 was collected from a unit containing interbedded shale and therefore may have been too fine-grained to yield significant zircon. Samples 05-14 and 05-15 were collected from very fine-grained rock yielding no zircon and sample SR 4 was collected from the Seal River, a major drainage originating from the Bering Glacier. It is possible that not enough loose sediment was collected from the riverbed to yield enough zircon but the separate was also epidote-rich and contained some gold.

Table 1. Sample information including stratigraphic formation, geographic information, location, rock unit, zircon yield (quantity), zircon size and shape, and zircon color quality.

Sample	Stratigraphic Formation	Geographic Location	Elevation (ft)	Latitude (°N)	Longitude (°W)	Zircon Yield	Zircon Color
05-01a	Kulthieth Formation	Donald Ridge	2166	60° 15.45	143° 04.90	high	colorless
05-01b	Kulthieth Formation	Donald Ridge	2167	60° 15.46	143° 04.91	high	colorless
05-03a	Kulthieth Formation	North of Donald Ridge	2097	60° 19.19	143° 07.05	low	colorless/some dark pink
05-03b	Kulthieth Formation	North of Donald Ridge	2098	60° 19.20	143° 07.06	low	colorless/some dark pink
05-04a	Kulthieth Formation	North of Donald Ridge	1878	60° 19.05	143° 07.16	low-average	colorless
05-04b	Kulthieth Formation	North of Donald Ridge	1879	60° 19.06	143° 07.17	low-average	colorless
05-06a	Kulthieth Formation	Northern Robinson Mountains	4031	60° 20.739	142° 36.956	low	honey
05-07a	Poul Creek Formation	Northern Robinson Mountains	4533	60° 20.784	142° 37.257	low-average	slightly honey
05-07b	Poul Creek Formation	Northern Robinson Mountains	4534	60° 20.785	142° 37.258	low-average	slightly honey
05-08a	Poul Creek Formation	Northern Robinson Mountains	4536	60° 20.786	142° 37.281	average	honey
05-08b	Poul Creek Formation	Northern Robinson Mountains	4537	60° 20.787	142° 37.282	average	honey
05-09a	Yakataga Formation	Kulthieth Mountain	2690	60° 10.035	142° 38.482	low	honey
05-10a	Yakataga Formation	Kulthieth Mountain	2639	60° 10.125	142° 37.766	average	colorless
05-10b	Yakataga Formation	Kulthieth Mountain	2640	60° 10.126	142° 37.767	average	colorless
05-11a	Yakataga Formation	Kulthieth Mountain	2652	60° 10.126	142° 37.769	low	colorless
05-11b	Yakataga Formation	Kulthieth Mountain	2653	60° 10.127	142° 37.770	low	colorless
05-12a	Yakataga Formation	Suckling Hills	920	60° 03.222	143° 47.112	average	colorless/slightly pink
05-12b	Yakataga Formation	Suckling Hills	920	60° 03.223	143° 47.113	average	colorless/slightly pink
05-13a	Poul Creek Formation	Grindle Hills	2013	60° 16.950	143° 19.274	low	honey
05-16a	Poul Creek Formation	Grindle Hills	2014	60° 16.951	143° 19.275	average	colorless/slightly honey
05-16b	Poul Creek Formation	Grindle Hills	1858	60° 16.804	143° 19.033	average	colorless/slightly honey
05-17a	Kulthieth Formation	Khistrov Hills	4128	60° 44.343	143° 25.145	average	colorless/some dark pink
05-17b	Kulthieth Formation	Khistrov Hills	4129	60° 44.344	143° 25.146	average	colorless/some dark pink
KA 1a	Kaliakh River	Kaliakh River	49	60° 11.561	142° 53.950	average	colorless
KA 1b	Kaliakh River	Kaliakh River	49	60° 11.562	142° 53.951	average	colorless
KL 2a	Kulthieth River	Kulthieth River	71	60° 11.710	142° 53.405	average	mixed
KL 2b	Kulthieth River	Kulthieth River	71	60° 11.711	142° 53.406	average	mixed
DK 3a	Duktoth River	Duktoth River	86	60° 07.748	142° 32.847	low	colorless

No Zircon Yield

Sample	Stratigraphic Formation	Geographic Location	Elevation (ft)	Latitude (°N)	Longitude (°W)	Zircon Yield	Reason
05-02	Kulthieth Formation	Donald Ridge	1961	60 15.575	143° 04.844	none	Carbonate-Rich
05-05	Kulthieth Formation	Northern Robinson Mountains	3144	60 20.509	142° 36.881	none	Contained interbedded shale
05-14	Poul Creek Formation	Grindle Hills	2166	60 17.020	143° 19.284	none	Too fine grained
05-15	Poul Creek Formation	Grindle Hills	1622	60 16.868	143° 18.908	none	Too fine grained
SR 4	Seal River	Seal River	8	60 06.892	143° 27.784	none	Epidote-rich, Low zircon yield

Mounting

Approximately 200-1000 zircon grains were mounted in a single 2x2 cm² square of PFA Teflon™ at about 330°C using the glass sandwich technique (Garver and Kamp 2002; Garver, 2003; Bernet and Garver, 2005). Each of these Teflon™ zircon mounts were then polished first using 600 grit sandpaper, then 9 μm diamond paste, and finally 1 μm diamond paste in order to expose a scratch-free interior face of each grain. Once the grain mount is polished it is ready to be etched.

Etching

Etching refers to the process in which the damaged tracks are made visible for counting.¹ Each polished zircon mount is placed or etched in a KOH: NaOH eutectic solution at 228°C (Garver and Kamp, 2002; Garver, 2003) for a specific amount of time. For detrital suites, etch time varies based on the sample characteristics (mainly age range). Typically a long and short etch are done on two different mounts per sample collected to ensure the full range of zircon fission-track ages are countable. For the Kulthieth and Poul Creek samples collected, the long etch times were approximately 18 hours while the short etch time was approximately 15 hours. For the Yakataga Formation samples the long etch was approximately 20 hours while the short etch was approximately 15 hours (Appendix A). The length of etching time determines the length

¹ Though in early literature Fleischer refers to tracks as “etches”, the term ‘etching’ is now used to refer to the above mentioned process.

of the tracks visible in the crystal lattice of the grain (Garver, 2003). The younger population in a sample requires a longer etch time because these grains typically have little radiation damage, a condition which records etching.

Irradiation

A piece of low-uranium mica is then attached to the grain side of etched mounts to serve as an external detector during irradiation (Figure 13). This step allows the calculation of the uranium content of a zircon based on the density of induced tracks as measured with a glass dosimeter. These induced tracks are a function of both the neutron flux and ^{235}U concentration. The purpose of the glass dosimeter is to record the neutron flux during the irradiation process.

Samples were sent to the nuclear reactor at Oregon State University and irradiated with a flux of $2 \times 10^{15} \text{ n/cm}^2$. The unknown samples were packaged in with uranium glass dosimeters and age standards (Fish Canyon Tuff ~26 Ma, and Buluk Member Tuff ~16 Ma) of known age. These standards provide a relationship between track density and neutron dose, and this is the basis for the zeta method. The irradiation package consists of grain mounts stacked on top of each other with glass dosimeters located on the bottom, middle, and top in order to measure variation in neutron flux or 'fluence', and is used to interpolate the neutron flux for each position. The neutron flux is highest closest to the bottom of the stack and lowest at the top of the stack. The slow-neutron bombardment of the samples result in the attached mica recording induced fission-track events based on the amount of ^{235}U in the zircon grains.

After irradiation, the mica detectors are etched in 48% HF for 18 minutes at room temperature and attached to a glass slide with corresponding grain mounts. A Kinetek automated stage is used to precisely align the grains with their corresponding mica detector and fission tracks are counted on an Olympus BH2 microscope at 1250x (100x dry objective; 10x oculars; 1.25 tube factor) using reflected and transmitted light on both the Teflon mount and mica.

In general 50-100 grains are counted per sample for detrital zircon fission-track analysis. Counted grains have a uniform track density and countable density of induced tracks on the mica. Counting the glass dosimeters on the top and bottom of the packages and interpolating between these positions determines the neutron fluence flux (Appendix A; Appendix B).

Age Determination

A personal calibration (Zeta factor) must be determined by repeatedly measuring known-age standards to correct for individual counter error and variability (Hurford and Green, 1983; Fleischer, 2004). The Zeta factor is calculated using a computer program (Zetafactor) and it is based on the individual's record of counting the age standards. The zeta factor used in this study was 363.8 ± 6.5 (total standard error) based on 24 separate analyses of the Fish Canyon, Buluk Member and Peach Springs Formation tuffs from a number of different irradiations (Appendix A). For unknowns, about 50 grains per sample were counted. Each grain yields an age based on the relationship of induced track density (ρ_i), spontaneous track density (ρ_s), and uranium concentration (ρ_d). Counting of detrital

zircon fission-track suites requires unique attention to each individual grain counted. Grains with any imperfections such as strong zonation, cracks, inclusions or uneven surfaces were rejected. Individual grains that were under-etched or over-etched were also rejected. Counted grains containing well-etched fission tracks were counted regardless of shape, size, color or clarity. For all samples a minimum of six squares in the fixed area 100 x 100 square grid were counted (1 square = $6.1 \times 10^{-5} \text{ cm}^2$). For every grain counted, the shape, color, and size were noted. Every grain was categorized into one of three shapes: euhedral, semi-rounded, and rounded. Color was noted with varying degrees of honey distinguished between slightly honey, honey, and dark honey. No pink/rose or black grains were observed. The dimensions of every grain were determined by using a digitizing tablet synchronized with the field of view in the microscope. All color observations and grain measurements were made using transmitted light at a power of 10x objective, 10x oculars, with a tube factor of 1.25x (125x total magnification) (Appendix C).

The program Zeta-age is used to calculate the sample ages based on the Zeta factor, the sample fluence, the relative standard error for the fluence monitor, the uranium concentration of the monitor standard, the counter square size, the spontaneous track density, the induced track density, and the number of squares counted (Galbraith, 1988; Galbraith and Green, 1990; Galbraith and Laslett, 1997; Brandon, 1996). The program peak-fits the individual grain ages, which results in a single age for the sample with error plus or minus two sigma (Galbraith, 1988; Galbraith and Green, 1990; Galbraith and Laslett, 1993; Brandon and Vance, 1992; Brandon, 1996).

For each sample there is a distribution of ages based on the individual grains counted; i.e. ages and relative precision varies from grain to grain. The Zeta-age program sums and distributes the individual ages, creating a peak-fitted curve where the peak indicates the cooling age of the sample (Galbraith, 1988; Galbraith and Green, 1990; Galbraith and Laslett, 1993). If a sample produces more than one peak-age the ages are deconvolved using the best-fit binomial peak program BINOMFIT (Brandon and Vance, 1992; Brandon, 1992; 1996). If the sample fails χ^2 (i.e. is below 5%) the sample is probably represented by more than one peak-age because the individual grain ages are over-dispersed (Appendix D). Multiple peak ages within a sample result from different source regions with different thermal histories (Figure 14).

U/Pb METHODS

Samples were dated using U/Pb analysis: 1) detrital zircon fission-track dated grains and; 2) non-detrital zircon fission-track dated grains in the same samples. DZFT samples 05-01, 05-04, 05-07, 05-13, 05-10, and 05-11 were analyzed with a Micromass Isoprobe (GVI Isoprobe) multicollector inductively coupled plasma mass spectrometer (ICPMS), using a DUV193 Excimer laser ablation system (New Wave Instruments) at the University of Arizona Laserchron Center, Tucson (Figure 15) (<http://www.geo.arizona.edu/alc/>). This laser operates at a wavelength of 193 nm with an output energy of ~40 mJ yielding approximately 8 laser pulses per second. The same grains used to determine detrital zircon fission-track cooling ages were used to determine

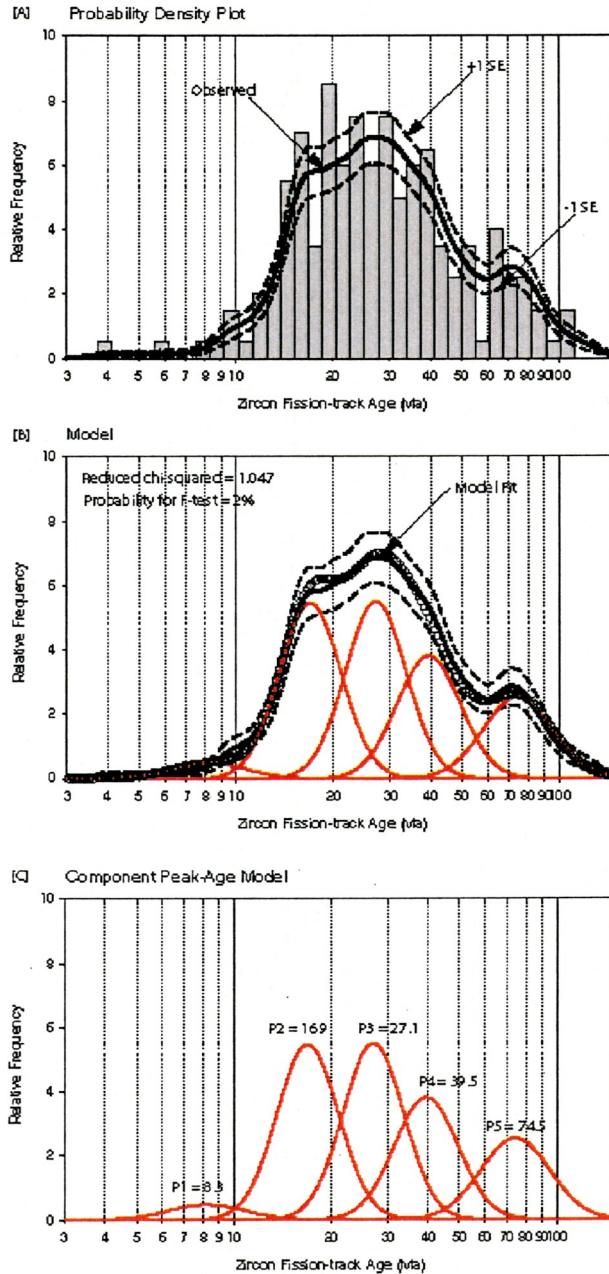


Figure 14. Step-wise schematic illustrating the process for determining DZFT component peak-age populations. [A] Histogram Probability Density Plot based on individual grain age determinations. [B] A model is developed by deconvolving the histogram probability density plot using the BINOMFIT software program into individual component grain-age populations (Brandon, 1996). [C] A representative component peak-age model is finalized.

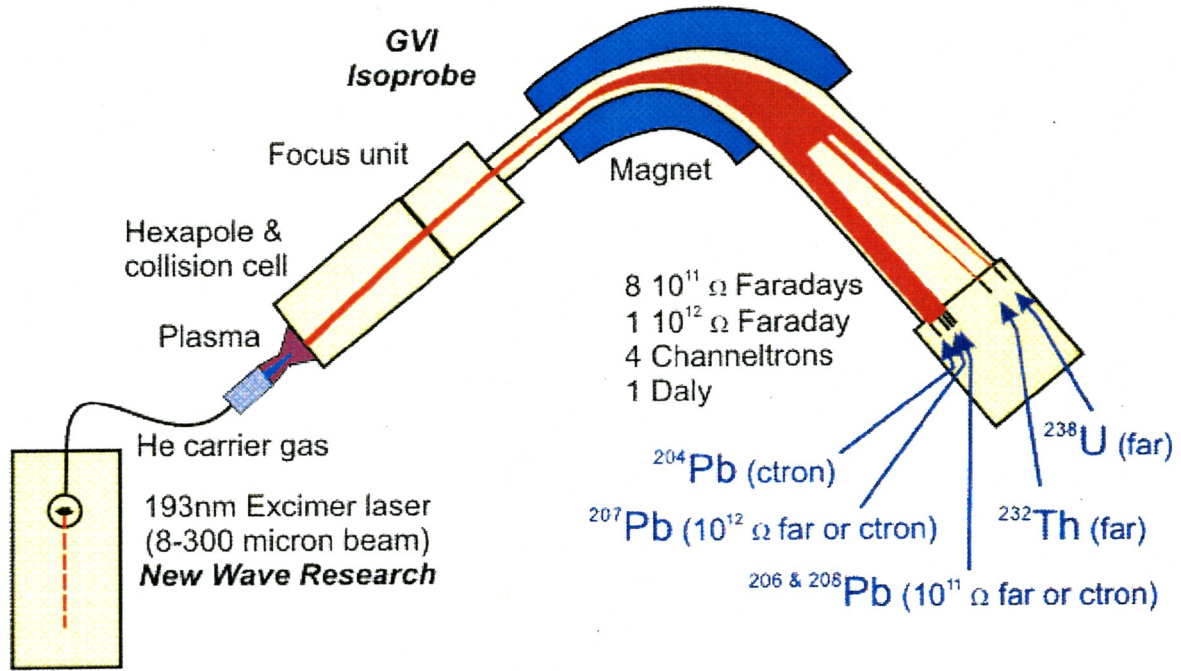


Figure 15. Schematic of the U/Pb dating LA-ICPMS extraction line used in the Laserchron Lab at the University of Arizona (<http://www.geo.arizona.edu/alc/>).

the U/Pb crystallization ages of 05-01, 05-04, 05-07, 05-13, 05-10, and 05-11. In addition, 50 random grains from samples 05-01, 05-13, and 05-11 were dated. A laser beam diameter of 35 μm was used yielding ablation pits $\sim 15 \mu\text{m}$ deep on all grains except the 50 random grains dated in sample 05-13. The size of the zircons in sample 05-13 was smaller than the laser-beam diameter of 35 μm , therefore the diameter was reduced to 25 μm and the data was corrected for fractionation. DZFT grains containing fractures and inclusions were ablated away from the imperfections to obtain an accurate age of the grain, but all grains were ablated on the interior portion of the zircon crystal for consistency. The random grains analyzed were dated regardless of the size or shape of the grains, although grains that contained fractures and/or inclusions were avoided. For every five unknown grains analyzed a standard was measured to correct for interelement fractionation (Gehrels, unpublished data, 2004). The standards used were large fragments of zircon from Sri Lanka with a known age of 564 \pm 4 m.y. (2 sigma error) (ID-TIMS) (Gehrels, unpublished data, 2004). For each laser ablation analysis the operator controlled the timing of the firing of the laser as well as the shut off mechanism. For the times before, in-between, and after firing and shut-off of the laser, the laser automatically went through the following three steps: 1) one twenty second integration on peaks with the laser off to acquire background measurements; 2) twenty one-second pulsating integrations with the laser firing; 3) a thirty second delay before the laser was ready for the next analysis to purge the Argon line of the previous sample. Every second during the firing of the laser an isotopic measurement of the zircon crystal. The determined age of the crystal is calculated by averaging all eighteen measurements and correcting for interelemental fractionation.

Once ablated the U, Th, and Pb isotopes were carried in Argon gas into the plasma source of the mass spectrometer equipped with a flight tube. The plasma mass spectrometer contains nine adjustable Faraday collectors (eight use a $10e^{11}$ ohm resistor and one uses a $10e^{12}$ ohm resistor) and four low-side Channletrons, which function as the ion counters (Gehrels, unpublished data, 2004). All measurements were made in static mode using Faraday detectors ($10e^{11}$ ohm resistor) for ^{238}U , ^{232}Th , and $^{208-206}\text{Pb}$ and ($10e^{12}$ ohm resistor) ^{207}Pb . An ion-counting channel was used to measure the amount of naturally occurring ^{204}Pb in the zircon. Contaminant common Pb from within the lab was corrected for assuming a previously measured initial Pb composition ($^{206}\text{Pb}/^{204}\text{Pb}$ ratio +/- 1.0 and $^{207}\text{Pb}/^{204}\text{Pb}$ ratio +/- 0.3) (Stacey and Kramers, 1975). To accurately measure the ^{204}Pb the amount of ^{204}Hg present in the argon gas plasma source must be measured and corrected for. This is accomplished by measuring the levels of ^{204}Hg intensity as the laser is firing and subtracting these values from the 20 seconds of background ^{204}Hg levels measured prior to firing (Gehrels, unpublished data, 2004).

The U and Th concentrations for each sample were determined by analyzing fragments of SRM 610 trace element glass with ~450 ppm. These measurements were then inserted into the Isoplot Excel Spreadsheet program and the U and Th concentration crystallization ages were automatically corrected for the inputted parameters (Ludwig, 2003).

Fractionation Factor

There are three important ways in which the fractionation of Pb/U and Pb/Th need to be accounted and corrected for during analysis. The first is the fractionation of isotopes

Pb/U and Pb/Th, which occurs within the laser pit during ablation. The rate of carrier flow gas across the surface of the sample is the most sensitive location to measure fractionation; therefore a balance between signal intensity and stability must be accomplished. The carrier gas flow rate in this study was 0.45 ml/minute generating a sensitivity of 0.9 for the Pb/U isotopes. A fractionation correction (factor) was determined by the analysis of known standards with a maximum fractionation percent of ~3% for $^{206}\text{Pb}/^{207}\text{Pb}$. Error on the fractionation factor is ~1% (2 sigma) for $^{206}\text{Pb}/^{238}\text{U}$. The second is the fractionation of isotopes as the depth of ablation increases throughout analysis of a single grain. In general the Pb/U and Pb/Th ratios increase by ~5% during a single analysis. This fractionation is corrected for by applying a sliding-window depth-related fractionation factor for the unknown grains. The third is the variation in flow rate and/or pattern of the argon carrier gas across the surface of the grains embedded in PFA Teflon® due to imperfections in the Teflon® surface. This factor was more difficult to reduce because the sample can not be altered in order to control the variation.

Age Determination

All data were loaded into the ZIRCONagecalc program in the Microsoft Excel based program Isoplot (Ludwig, 2003). Correction for U and Th concentrations based on the measurement of SRM 610 trace element glass was manually entered into the program. For the purposes of this study all discordant and concordant age data, as well as samples with high error and common ^{204}Pb concentration, were included in the crystallization age determinations by increasing the data filtering cutoff percent from ~10% to ~30%.

Relative age probability curves were automatically constructed by calculating a normal distribution for each analysis based on reported age and uncertainty, summing the probability plots of all acceptable analyses into a single curve, and then by dividing the normalized data in the area underneath a curve by the total number of analyses. All fractionation factors are automatically accounted for.

SEDIMENTARY PETROGRAPHY

Petrographic analyses were conducted on thin sections using a 200 point-count method (Blatt and Christie, 1963; Conolly, 1965). Thin sections were stained for easier identification of feldspars. An amaranth solution was used to stain for Ca-feldspar and a sodium cobaltinitrite solution was used to stain for K-feldspar. All point counts were performed using the Swift Automatic Point Counter Model F with an x-axis interval of 1mm between each counted grain. Traverses across the thin section were performed with a y-axis interval of 1.3mm between rows so counted grains were not recounted.

Notes were taken on distinguishing characteristics of the metamorphic minerals present, the matrix type, and the overall types, size and sorting of the grains represented in the thin sections. Minerals were divided into six main categories, including quartz, feldspar, lithics (volcanic, sedimentary and metamorphic), matrix and other accessory minerals. These six categories were subdivided based on different characteristics and types of the minerals present. Quartz grains were identified according to monocrystalline, polycrystalline, undulatory and/or chert types. Feldspars included plagioclase (Ca and Na-feldspar) and K-feldspar. Volcanic lithics included felsites, microlite, lathwork, and

other indistinguishable volcanic grains. Metamorphic lithics were broken down into foliated and non-foliated grains and sedimentary lithics included clay-rich, sandstone and carbonate grains. The matrix present was identified as either crushed grains or phyllosilicate or other. Other accessory minerals included titanite, epidote, sphene, hornblende, glauconite, actinolite, apatite, zircon and garnet. Types and quantity of mica including chlorite, muscovite and biotite were noted separately.

VITRINITE REFLECTANCE

Whole rock portions, approximately 30 x 40 cm in size, for samples 05-01, 05-03, 05-04, and 05-07 were sent to Humble Geochemical Services for analysis of isolated kerogen. Samples 05-01, 05-03 and 05-04 were selected from the Kulthieth Formation based on the samples retaining a young DZFT cooling age and sample 05-07 from the Poul Creek Formation was selected based on the same criteria. These samples were analyzed for percent source material, color, Thermal Alteration Index (TAI), preservation, palynofacies, and vitrinite. One sample, 05-04, was analyzed for Total Organic Carbon (TOC) content.

DATA

Detrital Zircon Fission-Track

All samples yielded pooled detrital zircon fission-track ages ranging from 25.1 Ma (+0.9, -1.0) to 39.4 Ma (+1.7, -1.8) (Table 2; Figure 16; Appendix B). All samples

Table 2. Summary of detrital zircon fission-track data

Sample	Elevation	ρ_s	N_s	ρ_i	N_i	ρ_d	N_d	n	χ^2	Age	-1 σ	+1 σ	U \pm 2se	
<u>Yakataga Formation (Plio-Pleistocene)</u>														
05-09	2690	Zircon	5.29 x 10 ⁶	2355	7.35 x 10 ⁶	3271	2.212 x 10 ⁵	1371	50	00.0	28.9	-1.1	+1.1	408.8 \pm 22.3
05-10	2639	Zircon	4.62 x 10 ⁶	2245	6.98 x 10 ⁶	3390	2.188 x 10 ⁵	1360	50	00.0	26.3	-1.0	+1.0	392.5 \pm 21.6
05-11	2652	Zircon	5.52 x 10 ⁶	2485	8.70 x 10 ⁶	3917	2.176 x 10 ⁵	1345	50	00.0	25.1	-0.9	+1.0	491.8 \pm 26.6
05-12	920	Zircon	5.37 x 10 ⁶	2616	6.78 x 10 ⁶	3305	2.152 x 10 ⁵	1330	50	00.0	30.9	-1.2	+1.2	387.5 \pm 22.1
<u>Poul Creek Formation (Upper Eocene to Upper Miocene)</u>														
05-07	4533	Zircon	4.67 x 10 ⁶	1986	4.94 x 10 ⁶	2100	2.235 x 10 ⁵	1382	50	00.0	38.3	-1.5	+1.6	272.0 \pm 16.2
05-08	4536	Zircon	4.60 x 10 ⁶	1668	4.49 x 10 ⁶	1625	2.057 x 10 ⁵	1271	50	39.8	38.3	-1.8	+1.8	268.2 \pm 19.4
05-13	2013	Zircon	5.48 x 10 ⁶	1918	6.49 x 10 ⁶	2275	2.117 x 10 ⁵	1315	50	00.0	32.4	-1.4	+1.4	377.3 \pm 23.9
05-16	1858	Zircon	5.37 x 10 ⁶	1826	5.20 x 10 ⁶	1768	2.105 x 10 ⁵	1301	50	00.0	39.4	-1.7	+1.8	303.6 \pm 20.6

Kulthieth Formation (Lower Eocene to Lower Oligocene)

05-01	2166	Zircon	4.67×10^6	1772	5.66×10^6	2148	2.318×10^5	1434	50	00.0	34.7	-1.4	+1.5	300.2 \pm 17.2
05-03	2097	Zircon	5.12×10^6	1807	5.55×10^6	1960	2.295×10^5	1419	50	00.0	38.4	-1.6	+1.6	297.6 \pm 17.6
05-04	1878	Zircon	5.37×10^6	1834	5.85×10^6	1999	2.271×10^5	1404	50	00.6	37.8	-1.5	+1.6	316.9 \pm 18.8
05-06	4031	Zircon	5.37×10^6	2149	6.03×10^6	2414	2.247×10^5	1393	50	00.0	36.3	-1.4	+1.5	330.1 \pm 18.8
05-17	4128	Zircon	6.01×10^6	1676	7.00×10^6	1954	2.081×10^5	1286	50	01.9	32.4	-1.4	+1.5	413.8 \pm 28.0

Modern River

KA-1	49	Zircon	5.21×10^6	2211	5.89×10^6	2501	2.425×10^5	1500	50	00.0	38.9	-1.5	+1.5	299.0 \pm 16.2
KL-2	71	Zircon	6.18×10^6	2444	7.23×10^6	2859	2.401×10^5	1485	50	00.0	37.2	-1.4	+1.4	370.2 \pm 19.4
DK-3	86	Zircon	5.59×10^6	2508	6.23×10^6	2797	3.245×10^5	1474	50	00.0	38.7	-1.4	+1.5	322.3 \pm 17.0

Note: Elevations are given in meters, ρ_s is the density (cm^3) of spontaneous tracks and N_s is the number of spontaneous tracks counted; ρ_i is the density (cm^3) of induced tracks; and ρ_d is the density (cm^2) of tracks on the fluence monitor (CN5); n is the number of grains counted; and χ^2 is the Chi-squared probability (%). Fission track ages ($\pm 1\sigma$) were determined using the Zeta method, and ages were calculated using the computer program and equations in Brandon (1992). All ages with $\chi^2 > 5\%$ are reported as pooled ages, otherwise, χ^2 are shown. For zircon,

a Zeta factor of 358.59 ± 5.12 (± 1 se - SEP) is based on determinations from both the Fish Canyon Tuff and the Buluk Tuff zircon. Glass monitors (CN5 for zircon), placed at the top and bottom of the irradiation package were used to determine the fluence gradient. All samples were counted at 1250x using a dry 100x objective (10x oculars and 1.25x tube factor) on an Olympus BMAX 60 microscope fitted with an automated stage and a digitizing tablet.

Approximate peak ages shown on the composite DZFT diagram

	Peak 1	Peak 2	Peak 3	Peak 4
Yakataga Formation	17.1	26.3	39.3	72.3
Poul Creek Formation	N/a	28.9	41.1	62.6
Kulthieth Formation	N/a	27.8	38.5	63.5

Detrital Zircon Fission-Track Results

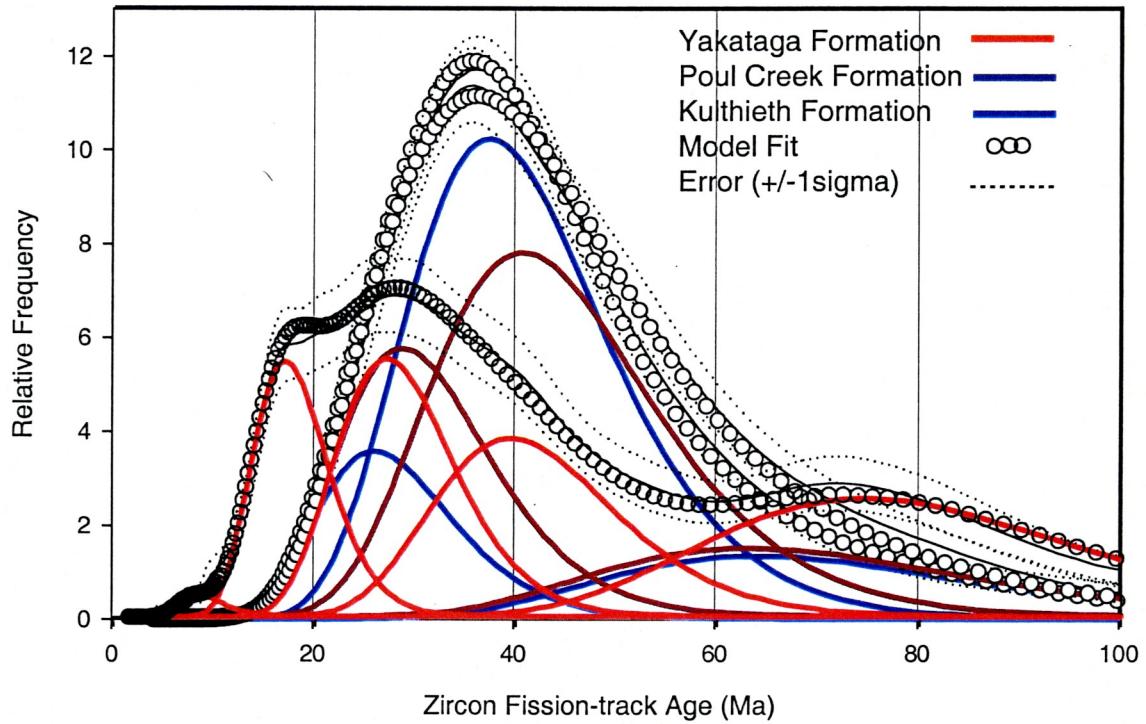


Figure 16. Composite plot showing all DZFT results for the Kulthieth, the Poul Creek, and the Yakataga Formations. Results are based on 5 samples from the Kulthieth Formation, and 4 samples each from the Poul Creek and Yakataga Formations.

with the exception of sample 05-08 failed χ^2 , therefore each sample consists of multiple populations of grain ages, which is typical for detrital suites (Bernet and Garver, 2005). These ages were deconvolved into multiple component age populations using the binomial peak-fitting technique (Brandon et al., 1998). All samples have a significant primary peak (Peak 1) ranging in age from 29.8 Ma (+3.0, -3.3) to 57.6 Ma (+13.5, -17.6) (Table 2). Sample 05-08 passed χ^2 but still has two resolvable peak-ages consisting of 37.5 Ma (+3.7, -4.1) (Peak 1), and 65.8 Ma (+32.7, -64.8) (Peak 2) (Table 3). Data are summarized based on technique used and the formation from which the samples were collected. Zircon grain characteristics, including color, size, shape, and other attributes are shown for each sample in Appendix C and Appendix E.

Kulthieth Formation

Samples 05-01, 05-03, 05-04, 05-06 and 05-17 were collected from the Kulthieth Formation at varying locations within the unit as well as geographically. Sample 05-01 was collected from Donald Ridge and yielded two peaks: 31.4 Ma (-3.0, +3.3) and 54.7 Ma (-10.2, +12.6) (Figure 17 [A]). Sample 05-03 was collected north of Donald Ridge and has three peak ages: 28.1 Ma (-4.7, +5.7), 43.5 Ma (-6.0, +7.0) and 97.0 Ma (-28.9, +41.1) (Figure 17 [B]). Samples 05-04 and 05-06 are from the Northern Robinson Mountains. Sample 05-04 has two peak ages: 30.8 Ma (-6.0, +7.4) and 44.1 Ma (-6.8, +8.0) and sample 05-06 has three peak ages: 22.3 Ma (-5.1, +6.6), 37.5 Ma (-3.6, +4.0) and 80.2 Ma (-25.5, +37.3) (Figure 17 [C]; Figure 17 [D]). Sample 05-17 was collected

Table 3. Summary of component populations for individual samples collected through the Yakutat terrane stratigraphy.

Sample	Unit	Age	n	Peak 1	Peak 2	Peak 3	Peak 4
<u>Yakataga Formation (Plio-Pleistocene)</u>							
05-09*	<i>Kulthieth Mth</i>	Plio-Pleistocene	50	16.9 -1.8/+2.1 39.3%	-	32.4 -4.9/+5.7 30.2%	67.8 -8.4/+9.6 30.4%
05-10	<i>Kulthieth Mth</i>	Plio-Pleistocene	50	15.8 -1.7/+1.9 43.5%	-	32.8 -4.1/+4.7 39.4%	72.5 -11.6/+13.7 17.1%
05-11	<i>Kulthieth Mth</i>	Plio-Pleistocene	50	15.1 -1.6/+1.8 37.4%	-	29.8 -3.0/+3.3 48.8%	71.9 -12.6/+15.3 13.7%
05-12	<i>Suckling Hills</i>	Plio-Pleistocene	50	-	21.3 -3.0/+3.4 38.7%	34.8 -4.6/+5.3 49.4%	76.8 -16.2/+20.5 11.9%
<u>Poul Creek Formation (Upper Eocene to Upper Miocene)</u>							
05-07	<i>Robinson Mtns</i>	U Eocene- U Mio	50	-	29.0 -5.8/+7.3 39.2%	42.0 -9.9/+13.0 49.8%	67.2 -21.6/+31.7 11.0%
05-08	<i>Robinson Mtns</i>	U Eocene- L Mio.	50	-	-	37.5 -3.7/+4.1	65.8 -32.7/+64.8

05-13*	Grindle Hills	U Eocene- U Mio	50	-	-	96.0%	4.0%
				24.4	38.9	-	-
				-4.1/+4.9	-4.9/+5.6	-	-
				35.8%	64.2%	-	-
05-16	Grindle Hills	U Eocene- U Mio	50	-	32.6	54.7	
				-	-4.5/+5.3	-10.2/+12.6	
				-	58.6%	41.4%	
<u>Kulthieth Formation (Lower Eocene to Lower Oligocene)</u>							
05-01	Donald Ridge	L Eocene- L Oligo.	50	-	31.4	57.6	
				-	-3.0/+3.3	-13.5/+17.6	
				-	78.4%	21.6%	
05-03	Robinson Mtns	L Eocene- L Oligo.	50	-	28.1	43.5	97.0
				-	-4.7/+5.7	-6.0/+7.0	-28.9/+41.1
				-	34.2%	59.2%	6.6%
05-04	Robinson Mtns	L Eocene- L Oligo.	50	-	30.8	44.1	-
				-	-6.0/+7.4	-6.8/+8.0	-
				-	41.1%	58.9%	-
05-06*	Robinson Mtns	L Eocene- L Oligo.	50	-	22.3	37.5	80.2
				-	-5.1/+6.6	-3.6/+4.0	-25.5/+37.3
				-	12.6%	82.2%	5.2%
05-17	Khitrov Hills	L Eocene- L Oligo.	50	-	30.1	45.3	-
				-	-3.4/+3.9	-11.5/+15.3	-
				-	79.8%	20.2%	-

Modern Rivers

KA 1	<i>Kalikuah River</i>	Modern	50	-	30.7	-	52.3
				-	-3.7/+4.2	-	-7.1/+8.2
				-	50.3%	-	21.6%
KL 2	<i>Kulthieth River</i>	Modern	50	-	32.2	-	56.4
				-	-2.9/+3.2	-	-9.0/+10.8
				-	64.7%	-	35.3%
DK 3	<i>Duktoth River</i>	Modern	50	19.5	34.8	46.7	-
				-4.4/+5.7	-6.3/+7.7	-6.6/+7.7	-
				8.8%	36.6%	54.6%	-

* one mount only

Note: Elevations are given in meters, ρ_s is the density (cm^2) of spontaneous tracks and N_s is the number of spontaneous tracks counted; ρ_i is the density (cm^2) of induced tracks; and ρ_d is the density (cm^2) of tracks on the fluence monitor (CN5); n is the number of grains counted. Binomial peak fitted components determined from routine outlines in Brandon (1992). For all samples that pass χ^2 , the χ^2 age is given as P1.

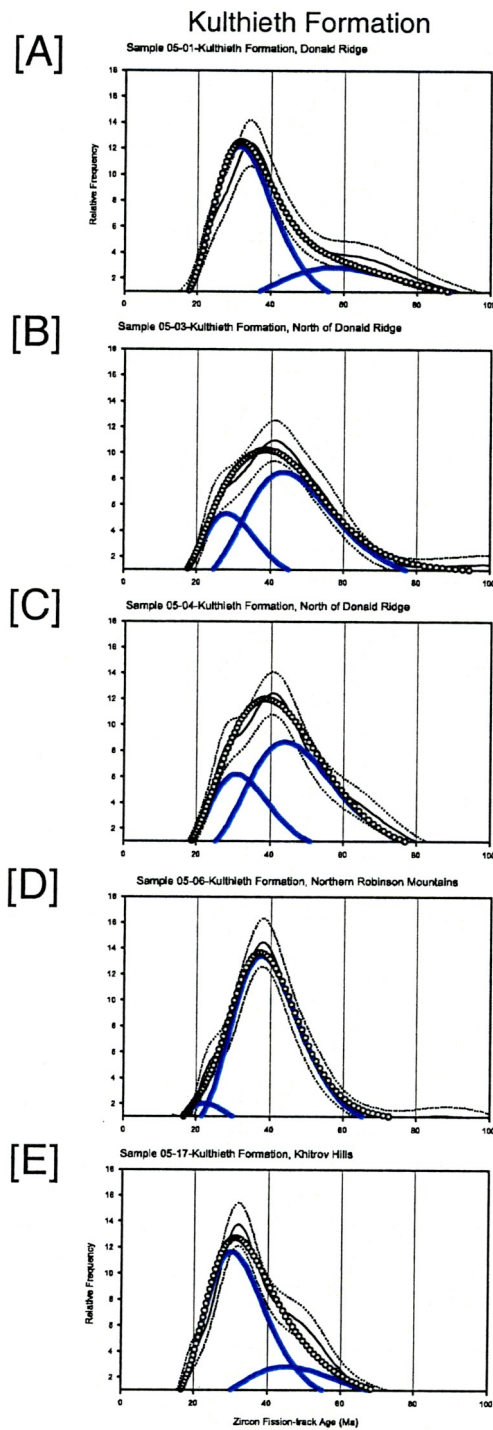


Figure 17 [A]-[E]. Observed composite probability plots (± 2 SE) and fitted peaks plotted with zircon fission-track age (Ma) versus relative frequency for samples collected throughout the Kulthieth Formation. Decomposition of grain-age populations is performed using the BINOMFIT software (Brandon, 1996).

from the Khitrov Hills and yielded two peak ages of 30.1 Ma (-3.4, +3.9) and 45.3 Ma (-11.5 +15.3) (Figure 17 [E]).

In addition to individual plots, all data from each formation were combined, deconvolved, and plotted against each other. The peak ages representing the overall defining cooling age populations from each formation are shown.

Poul Creek Formation

Sample 05-07, and 05-08 were collected from the Northern Robinson Mountains at different elevations. Sample 05-07 yielded three peak ages: 29.0 Ma (-5.8, +7.3), 42.0 Ma (-9.9, +13.0), and 67.2 Ma (-21.6, +31.7) (Figure 18 [A]). Sample 05-08 which passed χ^2 yielded two peak ages of 37.5 Ma (-3.7, +4.1), and 65.8 Ma (-32.7, +64.8) (Figure 18 [B]). Samples 05-13 and 05-16 were collected in the Grindle Hills at varying elevations and each yielded two peak ages. Sample 05-13 has two peaks: 24.4 Ma (-4.1, +4.9), and 38.9 Ma (-4.9, +5.6) and Sample 05-16 has two peak ages: 32.6 Ma (-4.5, +5.3), and 54.7 Ma (-10.2, +12.6) (Figure 18 [C]; Figure 18 [D]).

Yakataga Formation

Samples 05-09, 05-10, 05-11, and 05-12 were collected from the Yakataga Formation on Kulthieth Mountain located in the Northern Robinson Mountains and the Suckling Hills. Samples 05-09, 05-10, and 05-11 were collected on Kulthieth Mountain

Poul Creek Formation

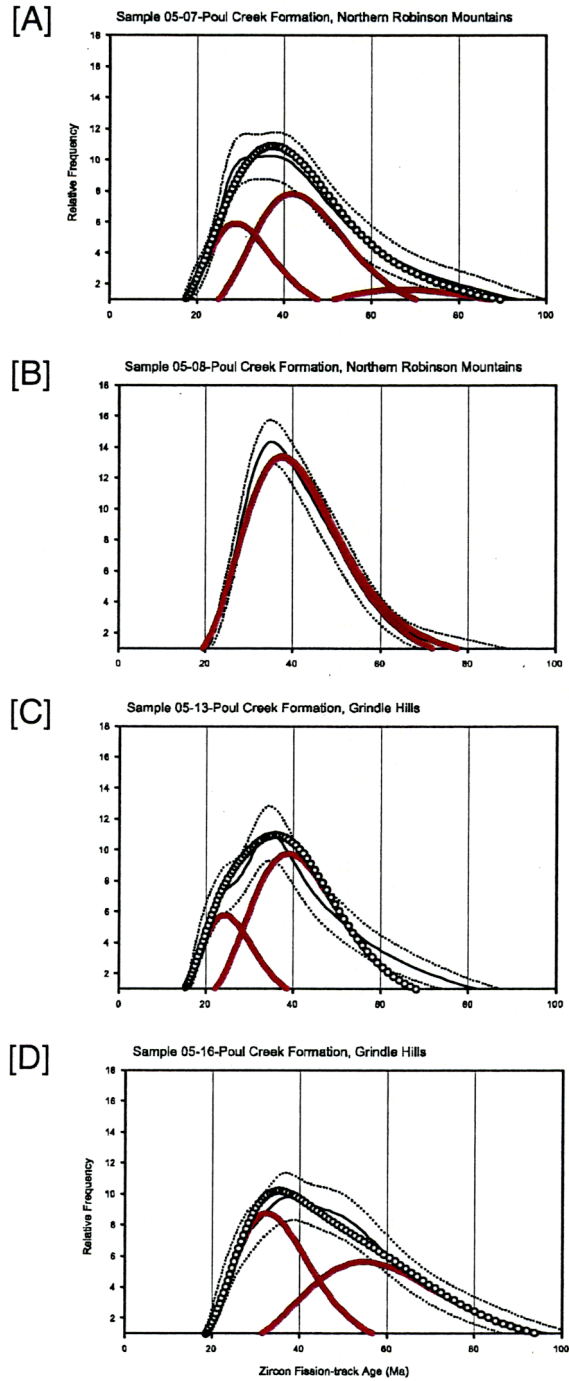


Figure 18 [A]-[D]. Observed composite probability plots (± 2 SE) and fitted peaks plotted with zircon fission-track age (Ma) versus relative frequency for samples collected throughout the Poul Creek Formation. Decomposition of grain-age populations is performed using the BINOMFIT software (Brandon, 1996).

from varying elevations. All samples yielded three cooling age populations. Sample 05-09 yielded ages of 16.9 Ma (-1.8, +2.1), 32.4 Ma (-4.9, +5.7), and 67.8 Ma (-8.4, +9.6) (Table 3) (Figure 19 [A]; Appendix D). Sample 05-10 has three populations consisting of 15.8 Ma (-1.7, +1.9), 32.8 Ma (-4.1, +4.7), and 72.5 Ma (-11.6, +13.7) (Figure 19 [B]). Sample 05-11 has three peaks: 15.1 Ma (-1.6, +1.8), 29.8 Ma (-3.0, +3.3), and 71.9 Ma (-12.6, +15.3) (Figure 19 [C]). Sample 05-12, collected from west of the Northern Robinson Mountains in the Suckling Hills, yielded three peak ages of 21.3 Ma (-3.0, +3.4), 34.8 Ma (-4.6, +5.3), and 76.8 Ma (-16.2, +20.5) (Figure 19 [D]).

Modern Rivers

Three modern river samples were collected from the Kalikuah, Kulthieth and Duktoth Rivers. These rivers do not represent main drainage patterns originating from north of the Chugach/St. Elias Range, but rather are a direct result of drainage from the Bering Glacier and Bagley Ice Field. These drain the fold and thrust belt. The Kalikuah River yielded two peak ages: 30.7 Ma (-3.7, +4.2), and 52.3 Ma (-7.1, +8.2). The Kulthieth River has two peak ages: 32.2 Ma (-2.9, +3.2), and 56.4 Ma (-9.0, +10.8) and the Duktoth River yielded three peak ages: 19.5 Ma (-4.4, +5.7), 34.8 Ma (-6.3, +7.7), and 46.7 Ma (-6.6, +7.7).

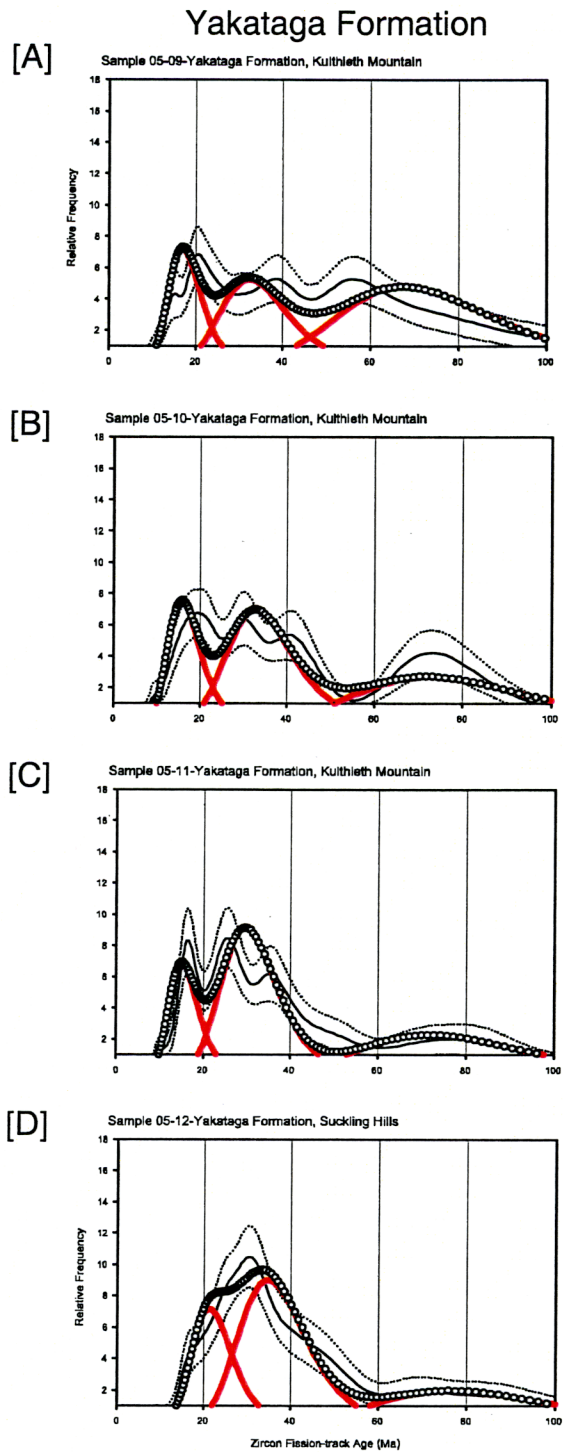


Figure 19 [A]-[D]. Observed composite probability plots (± 2 SE) and fitted peaks plotted with zircon fission-track age (Ma) versus relative frequency for samples collected throughout the Yakataga Formation. Decomposition of grain-age populations is performed using the BINOMFIT software (Brandon, 1996).

U/Pb

Kulthieth Formation

The same grains dated by detrital zircon fission-track analysis in samples 05-01 and 05-04 were analyzed using the U/Pb technique (Figure 20; Figure 21; Figure 22). In addition, 50 random grains were analyzed from sample 05-01 making 150 total analyses for the Kulthieth Formation (Table 4). Analysis resulted in three U/Pb crystallization age populations of ~59 Ma, ~94 Ma, and ~159 Ma (Figure 23 [A], [B]; Figure 24 [A], [B]). A single zircon grain age determination of ~1788 Ma was also measured. All highly discordant ages (< 5%) due to Pb loss or high common Pb content were excluded from the Concordia diagrams and are underlined in Table 4.

Poul Creek Formation

150 total analyses from the Poul Creek Formation were completed including the 100 DZFT dated-grains from samples 05-07 and 05-13 and 50 random grains from sample 05-13 (Figure 21; Figure 25 [A], [B]). Four crystallization peak ages resulted: ~59 Ma, ~71 Ma, ~94 Ma, and ~147 Ma (Table 4) (Figure 26 [A], [B]; Figure 27 [A], [B]). Three grains yielded U/Pb ages of ~318 Ma, ~364.71 Ma, ~1865 Ma. All highly discordant ages (<5%) due to Pb loss or high common Pb content were excluded from the Concordia diagrams and are underlined in Table 4.

Table 4. U-Pb (zircon) geochronologic analyses by Laser-Ablation Multicollector ICP Mass Spectrometry. Age determinations in red were discluded from concordia diagrams because of high imprecision or high common Pb values.

Analysis	U (ppm)	206Pb 204Pb	U/Th	Isotopic ratios						Apparent ages (Ma)				Best age		
				207Pb* 235U	\pm	206Pb* 238U	\pm	error (%)	206Pb* 238U	\pm	207Pb* 235U	\pm	206Pb* 207Pb*	\pm	Best age (Ma)	\pm (Ma)
<i>Yakataga Formation</i>																
0510A-1	104	12002	3.0	0.52260	4.7	0.06925	2.0	0.42	431.6	8.3	426.9	16.5	401.4	96.2	431.6	8.3
0510A-2	274	4157	4.3	0.05223	7.8	0.00817	3.1	0.40	52.4	1.6	51.7	3.9	17.8	171.0	52.4	1.6
0510A-3	279	6975	3.4	0.09318	6.3	0.01449	1.9	0.30	92.7	1.7	90.5	5.5	31.4	145.1	92.7	1.7
0510A-4	289	4508	6.3	0.05672	14.3	0.00874	2.8	0.19	56.1	1.6	56.0	7.8	51.7	336.3	56.1	1.6
0510A-5	612	6648	3.5	0.05212	7.2	0.00807	2.6	0.36	51.8	1.3	51.6	3.6	41.7	180.6	51.8	1.3
0510A-6	708	6019	1.8	0.05080	7.2	0.00797	3.8	0.54	51.2	2.0	50.3	3.5	8.2	145.8	51.2	2.0
0510A-7	325	2966	2.7	0.10155	9.5	0.01573	3.2	0.34	100.6	3.2	98.2	8.9	40.8	213.5	100.6	3.2
0510A-8	218	1718	2.1	0.05920	22.3	0.00849	3.6	0.16	54.5	2.0	58.4	12.7	221.5	514.4	54.5	2.0
0510A-9	444	5502	4.0	0.05335	11.8	0.00829	2.0	0.17	53.3	1.1	52.8	6.1	31.0	279.0	53.3	1.1
0510A-10	424	6353	3.8	0.05315	6.4	0.00823	3.7	0.59	52.9	2.0	52.6	3.3	40.1	124.0	52.9	2.0
0510A-11	94	2873	1.4	0.16123	10.0	0.02496	3.9	0.39	158.9	6.1	151.8	14.1	41.6	219.8	158.9	6.1
0510A-12	357	4782	2.0	0.16787	7.6	0.02379	5.9	0.78	151.6	8.9	157.6	11.1	248.9	109.9	151.6	8.9
0510A-13	116	1803	1.5	0.07333	19.2	0.01153	4.7	0.25	73.9	3.5	71.9	13.3	3.8	451.9	73.9	3.5
0510A-14	300	3153	1.8	0.05597	10.1	0.00876	4.1	0.41	56.2	2.3	55.3	5.4	14.8	220.7	56.2	2.3
0510A-15	96	3355	2.0	0.16870	13.5	0.02625	4.1	0.30	167.0	6.7	158.3	19.8	29.6	309.2	167.0	6.7
0510A-16	312	6386	2.5	0.09331	7.2	0.01450	1.8	0.25	92.8	1.7	90.6	6.2	32.8	186.7	92.8	1.7
0510A-17	156	2300	2.1	0.15887	14.1	0.02477	2.9	0.21	157.7	4.5	149.7	19.6	24.3	331.5	157.7	4.5
0510A-18	657	6823	3.1	0.05673	5.9	0.00826	2.7	0.47	53.0	1.4	56.0	3.2	185.5	120.9	53.0	1.4
0510A-19	41	923	2.6	0.08812	16.0	0.01370	8.4	0.53	87.7	7.3	85.8	13.2	31.0	327.7	87.7	7.3
0510A-20	181	1547	2.3	0.04267	27.3	0.00657	5.6	0.21	42.2	2.4	42.4	11.3	54.2	647.0	42.2	2.4
0510A-21	188	4049	1.5	0.11260	9.0	0.01743	2.3	0.26	111.4	2.5	108.3	9.3	41.6	209.2	111.4	2.5
0510A-22	166	4601	2.3	0.15533	9.2	0.02403	2.1	0.23	153.1	3.2	146.6	12.5	43.1	213.3	153.1	3.2
0510A-23	598	4525	3.1	0.05434	6.1	0.00846	2.2	0.36	54.3	1.2	53.7	3.2	29.2	135.9	54.3	1.2
0510A-24	112	1360	2.7	0.08084	13.1	0.01243	7.5	0.57	79.6	5.9	78.9	9.9	57.5	256.2	79.6	5.9
0510A-25	607	2720	2.1	0.05697	10.7	0.00889	5.2	0.49	57.0	2.9	56.3	5.8	23.4	224.3	57.0	2.9
0510B-1	291	3158	2.2	0.05503	11.2	0.00857	2.9	0.26	55.0	1.6	54.4	5.9	28.3	260.7	55.0	1.6
0510B-2	763	6057	2.4	0.05193	5.6	0.00814	2.8	0.50	52.3	1.4	51.4	2.8	11.4	115.8	52.3	1.4
0510B-3	676	8746	2.6	0.08809	4.8	0.01059	2.8	0.57	67.9	1.9	66.9	3.1	30.4	95.2	67.9	1.9
0510B-4	518	2711	3.6	0.05419	19.1	0.00814	5.5	0.29	52.3	2.9	53.6	9.9	112.5	433.8	52.3	2.9
0510B-5	494	6653	8.8	0.05027	11.5	0.00789	3.7	0.32	50.6	1.9	49.8	5.6	9.7	261.5	50.6	1.9
0510B-6	180	4447	1.8	0.09894	21.1	0.01418	8.4	0.40	90.7	7.5	95.8	19.3	223.6	452.7	90.7	7.5
0510B-7	219	3456	5.9	0.05325	17.7	0.00821	3.8	0.22	52.7	2.0	52.7	9.1	51.2	416.3	52.7	2.0
0510B-8	243	1412	5.7	0.05463	17.3	0.00852	5.6	0.33	54.7	3.1	54.0	9.1	24.5	394.6	54.7	3.1
0510B-9	344	2483	2.1	0.05191	9.3	0.00810	4.2	0.46	52.0	2.2	51.4	4.7	23.0	198.9	52.0	2.2
0510B-10	789	7676	1.8	0.06399	4.4	0.00998	2.1	0.47	64.0	1.3	63.0	2.7	23.0	92.9	64.0	1.3
0510B-21	76	781	3.4	0.05153	136.3	0.00903	116.8	0.86	58.0	67.4	51.0	67.9	-263.5	2035.6	58.0	67.4
0510B-22	135	1457	2.2	0.11467	18.5	0.01767	3.6	0.19	112.9	4.0	110.2	19.4	53.1	437.2	112.9	4.0
0510B-23	279	1143	2.1	0.09421	18.0	0.01250	1.9	0.10	80.1	1.5	91.4	15.8	397.8	404.6	80.1	1.5
0510B-24	130	2216	1.7	0.18607	13.5	0.02864	3.4	0.26	182.0	6.2	173.3	21.5	55.2	312.3	182.0	6.2
0510B-25	124	1902	1.9	0.15462	20.0	0.02379	2.1	0.11	151.6	3.2	146.0	27.1	56.3	477.2	151.6	3.2
0510B-11a	82	1301	2.9	0.13049	11.0	0.01882	3.9	0.35	120.2	4.6	124.5	12.9	208.5	240.2	120.2	4.6
0510B-12a	649	2068	4.5	0.05228	9.7	0.00791	2.5	0.25	50.8	1.2	51.7	4.9	94.7	222.8	50.8	1.2
0510B-13a	377	3659	5.2	0.05214	13.9	0.00821	2.4	0.17	52.7	1.3	51.6	7.0	2.3	331.2	52.7	1.3
0510B-14a	168	5221	1.7	0.16025	11.4	0.02475	3.2	0.28	157.6	5.0	150.9	16.0	47.5	261.6	157.6	5.0
0510B-15a	463	4401	3.6	0.05308	5.8	0.00830	3.1	0.53	53.3	1.6	52.5	3.0	17.4	117.6	53.3	1.6
0510B-16a	547	1863	2.5	0.06255	15.5	0.00888	3.1	0.20	57.0	1.7	61.6	9.3	243.3	352.5	57.0	1.7
0510B-17a	86	3267	2.3	0.15763	15.9	0.02481	3.4	0.21	158.0	5.3	148.6	22.1	2.0	377.5	158.0	5.3
0510B-18a	90	4193	2.9	0.20791	6.2	0.03120	3.7	0.59	198.1	7.1	191.8	10.8	115.4	117.9	198.1	7.1
0510B-19a	220	2601	4.0	0.05324	11.8	0.00814	5.2	0.44	52.3	2.7	52.7	6.1	70.9	253.4	52.3	2.7
0510B-20a	232	2342	2.0	0.04647	13.8	0.00722	5.1	0.37	46.4	2.4	46.1	6.2	34.0	307.4	46.4	2.4
0511A-1	553	6298	2.8	0.05135	7.4	0.00808	2.7	0.37	51.9	1.4	50.8	3.7	1.3	166.0	51.9	1.4
0511A-2	530	6298	5.2	0.05779	5.6	0.00892	2.1	0.37	57.3	1.2	57.0	3.1	47.5	124.8	57.3	1.2
0511A-3	614	4833	2.9	0.05389	9.7	0.00791	5.3	0.55	50.8	2.7	53.3	5.0	167.8	189.9	50.8	2.7
0511A-4	1128	15731	4.3	0.06932	5.1	0.01088	2.0	0.40	69.8	1.4	68.1	3.3	8.7	111.9	69.8	1.4
0511A-5	174	4938	2.3	0.14580	11.4	0.02249	2.4	0.21	143.4	3.4	138.2	14.7	50.2	266.0	143.4	3.4
0511A-6	379	5712	2.5	0.07578	15.2	0.01116	6.3	0.41	71.6	4.5	74.2	10.9	158.9	325.6	71.6	4.5
0511A-7	298	4159	1.9	0.07330	8.2	0.01133	2.4	0.29	72.7	1.7	71.8	5.7	44.4	187.4	72.7	1.7
0511A-8	782	5818	2.2	0.05055	6.2	0.00790	1.8	0.29	50.7	0.9	50.1	3.0	18.8	141.9	50.7	0.9
0511A-9	424	6345	2.8	0.08817	6.8	0.01362	2.3	0.34	87.2	2.0	85.8	5.5	46.5	149.0	87.2	2.0
0511A-10	760	2099	3.6	0.07044	23.9	0.00872	4.8	0.20	55.9	2.7	69.1	16.0	552.8	517.1	55.9	2.7
0511A-11	589	2445	3.2	0.08419	11.2	0.01116	2.7	0.24	71.6	2.0	82.1	8.9	399.9	245.0	71.6	2.0
0511A-12	1223	4780	4.5	0.06062	23.5	0.01149	3.0	0.13	73.6	2.2	78.7	17.8	236.7	544.8	73.6	2.2
0511A-13	755	5723	3.2	0.05280	9.0	0.00814	2.0	0.22	52.3	1.1	52.2	4.6	50.2	209.3	52.3	1.1
0511A-14	2653	17990	1.4	0.06125	2.8	0.00960	1.9	0.69	61.6	1.2	60.4	1.7	12.4	49.2	61.6	1.2
0511A-15	824	8407	2.8	0.08187	5.8	0.01288	1.2	0.21	82.5	1.0	79.9	4.5	3.7	137.3	82.5	1.0
0511A-16	201	4719	1.9	0.15294	6											

0511A-17	251	3678	1.5	0.18583	23.9	0.02535	2.8	0.12	161.4	4.5	173.1	38.1	335.5	545.6	161.4	4.5
0511A-18	1339	7676	1.9	0.05252	4.2	0.00799	1.7	0.41	51.3	0.9	52.0	2.1	82.9	91.4	51.3	0.9
0511A-19	543	12541	4.1	0.23299	9.2	0.03310	8.4	0.92	209.9	17.4	212.7	17.6	243.1	82.3	209.9	17.4
0511A-20	623	3990	3.8	0.05873	6.7	0.00840	2.9	0.43	53.9	1.5	57.9	3.8	226.9	139.4	53.9	1.5
0511A-21	446	4885	3.8	0.07420	6.7	0.01151	3.0	0.44	73.8	2.2	72.7	4.7	36.3	143.0	73.8	2.2
0511A-22	395	4807	3.4	0.10044	3.8	0.01553	2.6	0.69	99.3	2.6	97.2	3.5	44.9	65.7	99.3	2.6
0511A-23	1513	9339	3.0	0.09034	8.0	0.01322	2.5	0.32	84.6	2.1	87.8	6.7	175.1	176.9	84.6	2.1
0511A-24	584	3533	2.6	0.06338	21.4	0.00957	13.7	0.64	61.4	8.4	62.4	12.9	101.6	390.6	61.4	8.4
0511A-25	504	5544	1.7	0.09587	11.6	0.01493	2.7	0.23	95.5	2.5	93.0	10.3	27.3	271.0	95.5	2.5
0511B-1	391	2207	3.0	0.07258	18.4	0.01101	15.9	0.87	70.6	11.2	71.1	12.6	89.7	218.8	70.6	11.2
0511B-2	239	1704	2.6	0.06213	8.0	0.01069	2.1	0.26	68.6	1.4	61.2	4.8	-218.3	194.8	68.6	1.4
0511B-3	207	4200	2.1	0.16715	4.6	0.02524	1.8	0.38	160.7	2.8	156.9	6.7	100.8	101.1	160.7	2.8
0511B-4	552	900	2.7	0.18105	40.6	0.01297	19.2	0.47	83.1	15.9	169.0	63.3	1647.5	686.7	83.1	15.9
0511B-5	161	3004	3.4	0.14629	6.2	0.02519	3.1	0.50	160.4	4.9	138.6	8.0	-219.5	135.2	160.4	4.9
0511B-6	786	9834	3.5	0.22196	25.6	0.02278	21.5	0.84	145.2	30.9	203.5	47.2	947.9	284.4	145.2	30.9
0511B-7	1636	7460	2.2	0.05072	3.8	0.00761	2.1	0.54	48.9	1.0	50.2	1.9	116.5	76.4	48.9	1.0
0511B-8	560	7787	2.0	0.17003	2.9	0.02496	2.2	0.75	158.9	3.5	159.4	4.3	166.8	45.4	158.9	3.5
0511B-9	281	1432	2.6	0.05524	15.3	0.00821	4.8	0.31	52.7	2.5	54.6	8.1	139.1	54.7	52.7	2.5
0511B-10	1238	8649	3.5	0.08451	4.2	0.01331	2.7	0.64	85.2	2.3	82.4	3.3	1.1	77.3	85.2	2.3
0511B-11	248	1741	2.3	0.06568	9.3	0.01151	3.3	0.35	73.8	2.4	64.6	5.8	-264.7	222.4	73.8	2.4
0511B-12	178	1942	2.5	0.13848	53.0	0.02018	42.0	0.79	128.8	53.5	131.7	65.6	184.5	771.5	128.8	53.5
0511B-13	1426	4657	7.2	0.05677	3.6	0.00835	1.3	0.36	53.6	0.7	56.1	2.0	163.9	78.8	53.6	0.7
0511B-14	133	2341	2.2	0.15022	5.5	0.02426	2.0	0.37	154.5	3.1	142.1	7.3	-60.1	124.2	154.5	3.1
0511B-15	181	2977	1.6	0.15870	7.1	0.02411	3.9	0.55	153.6	5.9	149.6	9.9	86.0	141.5	153.6	5.9
0511B-16	1290	17148	5.9	0.12647	6.3	0.01894	6.1	0.97	120.3	7.3	120.9	7.2	132.3	36.4	120.3	7.3
0511B-17	993	4574	4.7	0.05091	4.3	0.00799	2.2	0.52	51.3	1.1	50.4	2.1	8.0	86.5	51.3	1.1
0511B-18	130	1018	4.4	0.05263	17.9	0.01214	3.9	0.22	77.8	3.0	52.1	9.1	-1017.6	523.5	77.8	3.0
0511B-19	386	480	1.2	0.01713	38.7	0.00304	15.2	0.39	19.6	3.0	17.3	6.6	-296.5	932.7	19.6	3.0
0511B-20	278	4424	2.4	0.15477	5.2	0.02358	1.7	0.33	150.3	2.5	146.1	7.1	79.4	117.3	150.3	2.5
0511B-21	509	3994	13.1	0.05439	4.6	0.00844	2.7	0.58	54.2	1.4	53.8	2.4	37.0	89.5	54.2	1.4
0511B-22	316	660	3.1	0.35187	9.3	0.02602	5.4	0.58	165.6	8.8	306.1	24.5	1587.8	141.1	165.6	8.8
0511B-23	312	705	3.8	0.09660	10.2	0.00958	3.2	0.31	65.7	1.8	64.3	8.3	995.3	198.0	65.7	1.8
0511B-24	1394	18955	3.8	0.16647	13.4	0.02522	13.3	1.00	160.5	21.2	156.3	19.4	93.4	27.9	160.5	21.2
0511B-25	145	2214	2.0	0.16358	8.2	0.02442	1.6	0.20	155.5	2.5	153.8	11.8	127.8	190.5	155.5	2.5
0511B-26	112	283	2.3	0.09070	43.7	0.00934	12.4	0.28	59.9	7.4	88.2	36.9	940.4	898.4	59.9	7.4
0511B-27	133	1159	4.9	0.08904	16.7	0.01352	4.1	0.25	86.6	3.5	85.7	13.7	60.5	387.4	86.6	3.5
0511B-28	120	808	3.5	0.03325	19.0	0.01004	8.4	0.44	64.4	5.4	33.2	6.2	-1904.1	628.2	64.4	5.4
0511B-29	683	2520	1.3	0.07581	4.7	0.01068	1.3	0.27	68.5	0.9	74.2	3.3	261.8	103.3	68.5	0.9
0511B-30	256	1161	1.8	0.03163	55.5	0.00882	4.3	0.08	56.6	2.4	31.6	17.3	-1620.8	2023.4	56.6	2.4
0511B-31	313	1338	3.7	0.04650	14.0	0.00841	2.1	0.15	54.0	1.1	46.2	6.3	-345.7	358.5	54.0	1.1
0511B-32	620	2823	4.0	0.05153	9.0	0.00830	3.0	0.34	53.3	1.6	51.0	4.5	-54.9	207.2	53.3	1.6
0511B-33	301	637	2.5	0.07527	14.3	0.00691	7.9	0.55	44.4	3.5	73.7	10.2	1172.1	237.9	44.4	3.5
0511B-34	511	6952	1.6	0.19964	3.2	0.02908	2.4	0.74	184.8	4.4	184.8	5.5	185.5	50.9	184.8	4.4
0511B-35	278	1977	2.8	0.32455	42.0	0.03650	40.1	0.96	231.1	91.0	285.4	104.8	757.6	263.5	231.1	91.0
0511B-36	274	3549	1.5	0.16057	8.5	0.02495	2.9	0.35	158.9	4.6	151.2	11.9	32.7	190.7	158.9	4.6
0511B-37	347	2597	1.6	0.11651	9.0	0.01532	6.1	0.68	98.0	6.0	111.9	9.8	418.1	148.1	98.0	6.0
0511B-38	579	3086	2.5	0.06030	5.5	0.00896	1.6	0.29	57.5	0.9	59.5	3.2	137.6	122.9	57.5	0.9
0511B-39	868	5464	3.0	0.05967	5.6	0.00951	2.3	0.40	61.0	1.4	58.9	3.2	-28.7	125.0	61.0	1.4
0511B-40	774	1115	3.5	0.08130	34.0	0.00889	3.3	0.10	57.0	1.9	79.4	26.0	817.8	727.7	57.0	1.9
0511B-41	698	4812	2.6	0.07916	5.6	0.01182	3.3	0.59	75.8	2.5	77.4	4.2	127.0	106.3	75.8	2.5
0511B-42	477	9325	2.3	0.14484	5.8	0.02305	3.5	0.80	146.9	5.1	137.3	7.5	-25.0	113.3	146.9	5.1
0511B-43	208	3246	1.6	0.14350	4.3	0.02255	3.0	0.68	143.8	4.2	136.2	5.5	5.4	76.7	143.8	4.2
0511B-44	42	747	6.3	0.12780	19.8	0.02560	8.8	0.45	163.0	14.2	122.1	22.8	-615.7	485.5	163.0	14.2
0511B-45	234	5088	3.1	0.14621	6.3	0.02304	2.3	0.36	146.8	3.3	138.6	8.2	-0.9	142.0	146.8	3.3
0511B-46	688	5675	3.3	0.07527	5.1	0.01121	2.6	0.50	71.9	1.8	73.7	3.6	132.8	103.4	71.9	1.8
0511B-47	802	6916	3.5	0.06253	4.9	0.01002	2.7	0.55	64.3	1.7	61.6	2.9	-42.4	99.9	64.3	1.7
0511B-48	332	2163	5.8	0.04597	8.9	0.00823	3.3	0.37	52.8	1.7	45.6	4.0	-318.9	212.0	52.8	1.7
0511B-49	576	1150	3.5	0.09122	12.5	0.00948	2.8	0.23	60.8	1.7	88.6	10.6	922.4	251.1	60.8	1.7
0511B-50	1027	3361	2.7	0.06227	3.0	0.00896	2.0	0.66	56.8	1.1	61.3	1.8	240.5	52.3	56.8	1.1
0511B-51	133	4200	2.2	0.35078	5.1	0.04854	3.3	0.63	305.5	9.7	305.3	13.6	303.6	90.8	305.5	9.7
0511B-52	83	1743	3.5	0.14363	13.5	0.02631	3.3	0.24	167.4	5.4	136.3	17.3	-377.2	342.3	167.4	5.4
0511B-53	763	2884	2.9	0.05858	5.2	0.00854	1.9	0.36	54.8	1.0	57.8	2.9	184.3	113.6	54.8	1.0
0511B-54	1493	12033	76.4	0.06972	5.7	0.01080	3.8	0.67	69.3	2.6	68.4	3.8	39.6	101.3	69.3	2.6
0511B-55	937	3661	2.4	0.04968	8.2	0.00822	4.1	0.50	52.7	2.2	49.2	4.0	-118.8	176.3	52.7	2.2
0511B-56	274	43929	2.1	3.85387	19.2	0.27581	19.1	0.99	1570.2	265.7	1604.1	155.8	1648.8	39.5	1648.8	39.5
0511B-57	181	1198	1.6	0.05217	31.3	0.01007	3.9	0.12	64.6	2.5	51.6	15.8	-515.4	847.4	64.6	2.5
0511B-58	150	3212	2.1	0.15128	8.6	0.02617	2.8	0.32	166.5	4.6	143.0	11.5	-230.8	205.9	166.5	4.6
0511B-59	280	4707	2.6	0.12066	5.9	0.01905	3.3	0.56	121.6	4.0	115.7	6.5	-5.1	119.1	121.6	4.0
0511B-60	948	2884	4.0	0.06502	16.8	0.00856	4.7	0.28	55.0	2.6	64.0	10.4	415.0	362.7	55.0	2.6
0511B-61	475	1481	5.9	0.08725	14.8	0.01056	4.0	0.27	67.7	2.7	84.9	12.1	601.8	310.9	67.7	2.7
0511B-62	539	3867	2.3	0.05360	8.3	0.00928	3.7	0.45	59.6	2.2	53.0	4.3	-234.0	186.5	59.6	2.2
0511B-63	668	2345	2.4	0.05493	5.9	0.00833	3.5	0.60	53.5	1.9	54.3	3.1	90.7	112.7	53.5	1.9
0511B-64	329	4434	1.5	0.16893	3.7	0.02602	2.6	0.71	165.6	4.3	158.5	5.5	53.9	62.9	165.6	4.3
0511B-65	155	605	3.2	0.09757	30.4	0.01118	6.9	0.23	71.7	4.9	94.5	27.5	718.8	643.0	71.7	4.9

0511B-66	536	4092	2.6	0.07021	4.7	0.01150	1.4	0.30	73.7	1.0	68.9	3.1	-94.1	109.3	73.7	1.0
0511B-67	438	1748	3.7	0.08340	15.4	0.01092	2.7	0.17	70.0	1.9	81.3	12.0	427.7	338.9	70.0	1.9
0511B-68	697	1877	0.8	0.07766	6.5	0.01050	3.2	0.50	67.3	2.2	75.9	4.7	355.8	127.2	67.3	2.2
0511B-69	265	33528	3.3	4.26502	22.6	0.25960	22.5	1.00	1482.7	298.7	1686.6	188.0	1950.5	31.5	1950.5	31.5
0511B-70	254	2744	3.7	0.09567	8.7	0.01512	4.6	0.53	96.8	4.5	92.8	7.7	-8.4	177.4	96.8	4.5
0511B-71	977	6240	7.7	0.08870	6.5	0.01364	5.5	0.84	87.3	4.7	86.3	5.4	58.1	85.0	87.3	4.7
0511B-72	132	1558	2.3	0.09979	9.6	0.01964	3.7	0.38	125.4	4.6	96.6	8.9	-567.3	240.0	125.4	4.6
0511B-73	490	2682	2.8	0.13520	14.9	0.01808	14.6	0.98	115.5	16.7	128.8	18.0	380.5	72.2	115.5	16.7
0511B-74	563	3840	2.0	0.09701	3.7	0.01504	2.5	0.68	96.2	2.4	94.0	3.3	37.7	65.6	96.2	2.4
0511B-75	630	2953	4.5	0.06033	5.5	0.00976	2.0	0.37	62.6	1.3	59.5	3.2	-64.1	123.8	62.6	1.3

Poul Creek Formation																
0507A-1	83	2088	1.7	0.13926	18.5	0.02164	3.8	0.21	138.0	5.3	132.4	23.0	32.7	436.3	138.0	5.3
0507A-2	310	5009	1.9	0.08377	7.7	0.01313	1.7	0.22	84.1	1.4	81.7	6.0	10.9	180.1	84.1	1.4
0507A-3	178	3623	1.1	0.20939	19.5	0.02916	4.8	0.25	185.3	8.8	193.0	34.3	289.5	435.9	185.3	8.8
0507A-4	227	3000	1.2	0.07999	31.1	0.01194	20.5	0.66	76.5	15.6	77.8	23.3	115.9	556.6	76.5	15.6
0507A-5	162	4913	2.3	0.14924	10.7	0.02347	1.9	0.17	149.5	2.7	141.2	14.1	4.1	254.7	149.5	2.7
0507A-6	214	1502	1.5	0.14371	36.5	0.02159	7.0	0.19	137.7	9.5	136.3	46.6	113.0	870.2	137.7	9.5
0507A-7	125	2253	1.7	0.08887	8.3	0.01384	4.1	0.49	88.6	3.6	86.4	6.9	26.5	172.9	88.6	3.6
0507A-8	218	2745	1.8	0.06003	26.3	0.00933	4.1	0.16	59.9	2.5	59.2	15.1	32.2	631.5	59.9	2.5
0507A-9	268	2749	2.2	0.05357	9.3	0.00638	3.4	0.36	53.8	1.8	53.0	4.8	16.2	208.5	53.8	1.8
0507A-10	74	1456	2.3	0.06430	15.2	0.01307	7.1	0.47	83.7	5.9	82.2	12.0	38.0	323.0	83.7	5.9
0507A-11	130	3686	3.1	0.14739	12.7	0.02299	2.2	0.17	146.5	3.2	139.6	16.6	24.0	300.8	146.5	3.2
0507A-12	92	2847	2.1	0.14631	16.4	0.02260	3.4	0.21	144.1	4.9	138.6	21.2	47.0	384.9	144.1	4.9
0507A-13	219	312	1.5	0.47848	24.9	0.01715	18.0	0.73	109.6	19.6	397.0	81.9	2845.4	281.1	109.6	19.6
0507A-15	329	2243	1.3	0.05610	13.7	0.00817	6.7	0.49	52.4	3.5	55.4	7.4	186.7	279.5	52.4	3.5
0507A-16	589	7766	1.6	0.07381	6.3	0.01149	3.6	0.58	73.7	2.7	72.3	4.4	28.2	122.6	73.7	2.7
0507A-17	293	5781	3.6	0.09631	5.2	0.01493	2.1	0.41	95.6	2.0	93.4	4.6	37.5	113.8	95.6	2.0
0507A-18	175	11302	2.2	0.35337	2.9	0.04987	1.6	0.55	313.7	4.9	307.3	7.7	258.2	55.8	313.7	4.9
0507A-19	157	2642	1.0	0.09379	13.6	0.01470	2.9	0.21	94.1	2.7	91.0	11.8	11.6	319.7	94.1	2.7
0507A-20	74	2264	3.6	0.10637	15.1	0.01662	5.9	0.39	106.3	6.3	102.6	14.7	19.5	334.2	106.3	6.3
0507A-21	94	1735	1.5	0.08592	11.8	0.01341	6.0	0.51	85.9	5.1	83.7	9.4	22.5	242.7	85.9	5.1
0507A-22	138	2674	2.1	0.07987	17.6	0.01233	4.3	0.25	79.0	3.4	78.0	13.2	47.5	410.7	79.0	3.4
0507A-23	116	954	2.9	0.07986	22.9	0.01108	3.8	0.16	71.0	2.6	78.0	17.2	297.3	521.2	71.0	2.6
0507A-24	124	1550	1.9	0.07009	17.0	0.00936	5.9	0.35	60.1	3.5	68.8	11.3	383.9	360.3	60.1	3.5
0507A-25	110	2250	1.8	0.10447	15.6	0.01609	2.8	0.18	102.9	2.8	100.9	15.0	53.8	369.1	102.9	2.8
0507A-13a	178	3077	1.4	0.11340	31.3	0.01669	22.3	0.71	106.7	23.6	109.1	32.4	161.1	518.2	106.7	23.6
0507B-1	399	705	1.9	0.16258	447.3	0.01240	444.1	0.99	79.4	350.9	153.0	745.3	1530.4	1092.0	79.4	350.9
0507B-2	248	3836	1.6	0.10391	12.2	0.01600	3.2	0.26	102.3	3.3	100.4	11.7	54.1	282.1	102.3	3.3
0507B-3	113	1188	4.0	0.09524	20.2	0.01490	4.1	0.20	95.4	3.9	92.4	17.9	15.9	479.7	95.4	3.9
0507B-4	107	1050	2.0	0.21403	25.7	0.02626	5.2	0.20	167.1	8.6	196.9	46.0	571.3	555.4	167.1	8.6
0507B-5	128	4017	2.2	0.12201	23.0	0.01763	6.6	0.29	112.6	7.4	116.9	25.4	204.6	517.4	112.6	7.4
0507B-6	290	10756	2.0	0.43499	2.7	0.05839	1.7	0.60	365.9	5.9	366.7	8.5	372.1	49.4	365.9	5.9
0507B-7	260	2779	3.1	0.09302	11.3	0.01444	1.5	0.13	92.4	1.4	90.3	9.8	35.0	269.5	92.4	1.4
0507B-8	297	3424	1.9	0.08478	8.9	0.01463	1.9	0.21	93.6	1.8	91.9	7.9	49.0	209.2	93.6	1.8
0507B-9	225	1397	3.0	0.05868	33.6	0.00924	4.8	0.14	59.3	2.8	57.9	18.9	0.2	821.1	59.3	2.8
0507B-10	474	3395	2.0	0.10168	16.9	0.01480	3.5	0.21	94.7	3.3	98.3	15.8	186.3	387.2	94.7	3.3
0507B-11	240	2457	2.3	0.09975	6.8	0.01544	2.6	0.38	98.8	2.5	96.5	6.3	42.1	151.5	98.8	2.5
0507B-12	117	2117	2.0	0.18037	15.4	0.02807	2.9	0.19	178.5	5.1	168.4	23.9	28.8	363.7	178.5	5.1
0507B-13	236	2947	2.2	0.14849	5.4	0.02313	1.5	0.28	147.4	2.2	140.6	7.1	26.3	124.1	147.4	2.2
0507B-14	371	2117	4.1	0.05980	19.3	0.00929	3.9	0.20	59.6	2.3	59.0	11.1	33.4	457.1	59.6	2.3
0507B-15	332	4010	1.4	0.11276	11.5	0.01752	4.8	0.42	112.0	5.3	108.5	11.8	33.0	249.9	112.0	5.3
0507B-16	349	4562	1.4	0.15021	4.2	0.02309	1.8	0.42	147.1	2.6	142.1	5.6	58.8	91.0	147.1	2.6
0507B-17	237	2543	1.5	0.15630	6.5	0.02188	2.8	0.43	139.5	3.9	147.5	9.0	277.6	134.7	139.5	3.9
0507B-18	121	1171	1.5	0.10748	24.8	0.01505	4.7	0.19	96.3	4.5	103.7	24.4	275.7	565.2	96.3	4.5
0507B-19	503	4414	2.3	0.07441	10.5	0.01167	5.2	0.50	74.8	3.9	72.9	7.4	10.2	219.6	74.8	3.9
0507B-20	146	1213	3.7	0.09574	19.8	0.01333	4.7	0.24	85.4	4.0	92.8	17.6	289.8	443.8	85.4	4.0
0507B-21	109	587	2.2	0.05389	21.4	0.00834	4.6	0.22	53.5	2.5	53.3	11.1	42.0	504.4	53.5	2.5
0507B-22	105	2834	2.0	0.19130	10.4	0.02993	3.5	0.34	190.1	6.6	177.7	17.0	16.5	236.5	190.1	6.6
0507B-23	122	823	1.8	0.06051	17.9	0.00940	4.6	0.25	60.3	2.7	59.7	10.4	34.0	417.0	60.3	2.7
0507B-24	162	2440	2.2	0.11822	13.4	0.01648	5.4	0.40	105.4	5.6	113.5	14.3	286.2	280.5	105.4	5.6
0507B-25	188	1683	1.8	0.10056	9.5	0.01473	3.2	0.33	94.3	3.0	97.3	8.8	172.0	210.2	94.3	3.0
0513B-1	194	2545	1.4	0.17283	12.4	0.02516	3.7	0.30	160.2	5.9	161.7	18.5	183.9	275.0	160.2	5.9
0513B-3	306	19036	1.3	4.85501	9.6	0.31057	9.4	0.98	1743.5	144.3	1794.5	81.2	1854.3	33.7	1854.3	33.7
0513B-4	234	680	1.2	0.06267	16.1	0.00833	3.1	0.19	53.5	1.7	61.9	9.7	401.9	355.6	53.5	1.7
0513B-5	513	3562	3.4	0.07101	5.7	0.01083	2.3	0.40	69.4	1.6	69.7	3.8	77.7	123.5	69.4	1.6
0513B-6	274	368	2.5	0.28731	12.4	0.01468	4.9	0.40	93.9	4.6	256.4	28.0	2251.5	196.5	93.9	4.6
0513B-7	250	322	2.0	0.69358	20.5	0.02844	11.8	0.58	168.3	19.6	534.9	85.5	2744.1	278.1	168.3	19.6
0513B-8	565	2449	3.5	0.19358	19.9	0.02101	12.3	0.62	134.0	16.3	179.7	32.7	832.5	326.9	134.0	16.3
0513B-9	353	1505	2.7	0.19177	9.3	0.01999	5.0	0.54	127.6	6.4	178.1	15.2	916.0	161.8	127.6	6.4
0513B-10	882	2805	16.5	0.41581	51.9	0.03976	50.8	0.98	251.3	125.2	353.1	156.0	1091.1	213.3	251.3	125.2
0513B-11	906	5336	1.1	0.07610	5.2	0.01115	1.8	0.35	71.5	1.3	74.5	3.7	172.0	113.6	71.5	1.3
0513B-12	228	306	2.2	0.33773	16.5	0.01480	11.3	0.69	94.7	10.6	295.4	42.2	2512.2	201.6	94.7	10.6
0513B-13	351	2692	2.4	0.06858	7.7	0.00935	3.1	0.41	60.0	1.9	57.8	4.3	-31.4	171.0	60.0	1.9

0513B-14	694	585	5.1	0.22677	13.9	0.01508	7.8	0.57	96.5	7.5	207.5	26.0	1783.6	209.0	96.5	7.5
0513B-15	617	366	4.4	0.38963	22.4	0.01797	15.4	0.69	114.8	17.5	333.4	63.7	2421.9	277.9	114.8	17.5
0513B-16	651	489	1.5	0.18138	31.4	0.00903	14.8	0.47	57.9	8.4	169.2	49.0	2295.9	487.7	57.9	8.4
0513B-17	274	1506	1.8	0.10192	16.6	0.01419	7.0	0.42	90.8	6.3	98.5	15.6	290.1	344.5	90.8	6.3
0513B-19	279	1548	2.1	0.06890	8.4	0.01026	3.5	0.42	65.8	2.3	67.7	5.5	133.1	179.4	65.8	2.3
0513B-20	155	359	2.6	0.27453	34.6	0.01641	14.6	0.42	104.9	15.2	246.3	75.8	1976.3	574.3	104.9	15.2
0513B-21	316	710	2.3	0.13051	87.3	0.01152	31.7	0.36	73.8	23.2	124.6	102.6	1249.3	19.3	73.8	23.2
0513B-22	313	2327	1.7	0.14110	17.2	0.02046	4.6	0.27	130.6	6.0	134.0	21.6	195.6	388.0	130.6	6.0
0513B-23	162	454	1.8	0.09544	29.8	0.00939	7.8	0.28	60.3	4.7	92.6	26.4	1033.2	593.0	60.3	4.7
0513B-24	342	440	2.2	0.26303	38.7	0.01469	29.4	0.60	94.0	27.5	237.1	77.7	2095.6	390.0	94.0	27.5
0513B-25	461	1539	1.6	0.09448	19.3	0.01124	3.3	0.17	72.0	2.3	91.7	16.9	638.4	412.3	72.0	2.3
0513B-26	397	859	5.4	0.29903	18.4	0.02339	6.4	0.15	149.1	3.6	265.6	38.5	1482.0	310.3	149.1	3.6
0513B-27	215	550	1.3	0.11892	22.6	0.00905	7.7	0.34	58.1	4.5	114.1	24.4	1534.2	404.5	58.1	4.5
0513B-28	443	1548	1.6	0.50369	10.9	0.02501	5.9	0.54	159.2	9.3	414.2	37.2	2300.3	158.9	159.2	9.3
0513B-32a	419	377	2.3	0.39981	19.7	0.01814	13.1	0.67	115.9	15.1	341.5	57.1	2454.1	248.8	115.9	15.1
0513B-31a	326	391	2.6	0.20400	17.8	0.01042	12.8	0.72	68.8	8.5	188.5	30.6	2251.6	213.8	68.8	8.5
0513B-30a	140	129	2.9	2.03335	18.0	0.04164	16.1	0.69	263.0	41.4	1126.7	123.0	3724.8	123.6	263.0	41.4
0513B-29a	244	270	1.8	0.44555	18.2	0.01877	14.0	0.77	119.9	16.6	374.2	57.1	2578.6	196.0	119.9	16.6
0513B-33	249	333	2.4	0.22171	7.4	0.01084	5.8	0.78	69.5	3.9	203.3	13.7	2327.3	83.1	69.5	3.9
0513B-34	382	589	5.1	0.39210	29.4	0.02274	11.6	0.39	144.9	16.6	335.9	84.3	2029.6	488.4	144.9	16.6
0513B-35	145	1685	3.1	0.27314	15.0	0.03266	4.8	0.32	207.2	9.7	245.2	32.8	626.9	308.8	207.2	9.7
0513B-36	571	2416	1.3	0.09694	18.5	0.01205	6.4	0.34	77.2	4.9	94.0	16.6	543.4	383.3	77.2	4.9
0513B-37	525	699	8.3	0.24177	27.6	0.01652	22.8	0.82	105.6	23.7	219.9	54.6	1734.5	291.4	105.6	23.7
0513B-38	140	1534	2.1	0.08758	11.4	0.01431	5.5	0.48	91.6	5.0	94.5	10.3	169.7	233.5	91.6	5.0
0513B-39	386	290	2.8	0.20941	35.4	0.00911	22.2	0.63	58.5	12.9	193.1	62.4	2525.0	474.4	58.5	12.9
0513B-40	433	1760	3.3	0.08326	8.1	0.01065	4.3	0.54	68.3	3.0	81.2	6.3	479.3	151.3	68.3	3.0
0513B-41	511	788	1.4	0.17308	9.6	0.01421	4.3	0.45	91.0	3.9	162.1	14.4	1389.4	165.4	91.0	3.9
0513B-42	188	1509	1.1	2.08186	14.9	0.15580	10.7	0.72	933.4	93.4	1142.8	102.7	1585.5	194.7	933.4	93.4
0513B-43	415	1578	2.4	0.07930	5.7	0.01009	3.4	0.59	64.7	2.2	77.5	4.2	492.6	101.3	64.7	2.2
0513B-44	129	526	2.0	0.51028	22.4	0.02894	9.4	0.42	183.9	17.1	418.6	77.0	2068.7	362.3	183.9	17.1
0513B-45	311	1205	2.4	0.06267	20.1	0.00843	4.5	0.22	54.1	2.4	61.7	12.1	367.8	446.0	54.1	2.4
0513B-46	113	2049	3.7	0.20390	13.3	0.03185	11.5	0.66	202.1	22.9	188.3	22.9	18.7	160.8	202.1	22.9
0513B-48	168	3001	2.1	0.14964	6.5	0.02290	2.1	0.32	146.0	3.0	141.6	8.6	69.0	145.9	146.0	3.0
0513B-49	763	5257	3.3	0.27062	24.5	0.03038	9.8	0.40	192.9	18.7	243.2	53.1	761.6	479.5	192.9	18.7
0513B-50	611	4527	3.8	0.06534	7.7	0.01000	4.2	0.55	64.1	2.7	64.3	4.8	68.8	152.8	64.1	2.7
0513B-51	252	1868	2.1	0.05821	14.0	0.00960	3.8	0.28	61.6	2.4	57.4	7.8	-111.2	331.8	61.6	2.4
0513B-52	101	2935	1.2	0.15813	10.7	0.02442	5.3	0.50	155.5	8.2	149.1	14.8	47.5	222.0	155.5	8.2
0513B-53	129	1567	1.7	0.09773	12.2	0.01476	4.3	0.35	94.5	4.0	94.7	11.1	99.5	271.8	94.5	4.0
0513B-54	124	985	2.1	0.13508	39.5	0.01345	12.0	0.30	86.1	10.3	128.6	47.8	1009.1	790.7	86.1	10.3
0513B-55	377	4018	2.2	0.05714	16.1	0.00835	7.8	0.48	53.6	4.2	56.4	8.9	177.5	331.1	53.6	4.2
0513B-56	164	2379	1.4	0.05885	21.9	0.00955	4.6	0.21	61.3	2.8	58.1	12.4	-72.0	529.7	61.3	2.8
0513B-57	114	474	2.4	0.72255	37.4	0.03130	15.0	0.40	198.7	29.4	552.2	160.7	2532.2	595.0	198.7	29.4
0513B-58	112	535	2.7	0.33223	14.3	0.02000	3.9	0.28	127.7	5.0	291.3	36.1	1963.2	245.8	127.7	5.0
0513B-59	355	3881	1.9	0.11515	7.6	0.01550	3.5	0.48	99.1	3.5	110.7	8.0	366.3	152.6	99.1	3.5
0513B-60	168	1351	2.5	0.06509	26.6	0.00920	6.9	0.26	59.1	4.1	64.0	16.5	254.0	599.6	59.1	4.1
0513B-61	317	2452	1.6	0.05519	18.3	0.00940	7.8	0.41	60.3	4.5	54.5	9.7	-191.3	420.4	60.3	4.5
0513B-62	413	4041	1.3	0.06942	6.6	0.01090	3.7	0.56	69.9	2.5	68.1	4.3	7.3	131.4	69.9	2.5
0513B-63	146	932	1.8	0.19855	22.1	0.01874	3.6	0.16	119.7	4.2	183.9	37.1	1117.5	439.7	119.7	4.2
0513B-64	251	4450	1.6	0.09292	13.9	0.01496	11.4	0.82	95.7	10.8	90.2	12.0	-53.4	192.9	95.7	10.8
0513B-65	172	730	2.0	0.05638	17.1	0.00633	6.1	0.38	40.7	2.5	55.7	9.3	760.9	338.6	40.7	2.5
0513B-66	79	2028	1.8	0.15889	15.0	0.02492	4.0	0.27	158.7	6.3	149.6	20.9	7.6	350.5	158.7	6.3
0513B-68	272	3291	2.4	0.07078	14.7	0.00993	9.2	0.62	63.7	5.8	69.4	9.8	272.9	263.3	63.7	5.8
0513B-67	118	2065	2.8	0.19520	13.9	0.02482	4.4	0.32	158.0	6.8	181.1	23.1	493.1	292.2	158.0	6.8
0513B-69	171	3852	2.6	0.19503	10.6	0.02574	2.8	0.26	163.8	4.5	180.9	17.5	410.7	228.2	163.8	4.5
0513B-70	524	2145	0.8	0.06025	7.4	0.00915	2.4	0.32	58.7	1.4	59.4	4.3	86.4	167.0	58.7	1.4
0513B-71	92	1793	1.7	0.06653	15.6	0.01216	7.1	0.46	77.9	5.5	65.4	9.8	-371.3	358.2	77.9	5.5
0513B-72	178	2456	2.1	0.05572	16.7	0.00983	5.2	0.31	63.0	3.2	55.1	8.9	-280.2	405.3	63.0	3.2
0513B-73	68	1474	1.9	0.08095	21.9	0.01406	6.9	0.32	90.0	6.2	79.0	16.7	-241.4	529.8	90.0	6.2
0513B-74	156	8036	1.4	4.48187	14.1	0.28472	11.1	0.78	1615.1	158.0	1727.6	118.0	1866.7	159.6	1615.1	159.6
0513B-75	136	616	1.3	0.14125	24.9	0.01160	7.5	0.30	74.3	5.5	134.2	31.3	1389.7	462.8	74.3	5.5
0513B-76	213	6058	1.7	0.16271	4.0	0.02389	2.4	0.60	152.2	3.6	153.1	5.7	166.6	74.6	152.2	3.6
0513B-77	78	2078	2.1	0.30822	24.6	0.03427	5.4	0.22	217.2	11.5	272.8	59.0	781.8	512.4	217.2	11.5
0513B-78	630	1832	1.2	0.05718	25.6	0.00646	3.0	0.12	41.5	1.2	56.5	14.1	749.7	546.3	41.5	1.2
0513B-79	425	7224	4.0	0.09848	10.4	0.01441	4.7	0.45	92.2	4.3	95.4	9.5	174.4	218.0	92.2	4.3
0513B-80	85	1187	1.2	0.08235	24.2	0.01141	5.5	0.23	73.1	4.0	80.3	18.7	301.2	543.3	73.1	4.0
0513B-81	198	4471	1.4	0.09532	7.4	0.01566	2.2	0.30	100.2	2.2	92.4	6.5	-103.2	173.5	100.2	2.2
0513B-82	643	871	1.7	0.14467	36.1	0.00928	28.8	0.80	59.5	17.1	137.2	46.4	1849.9	398.0	59.5	17.1
0513B-83	360	7638	1.4	0.08729	6.3	0.01428	4.5	0.72	91.4	4.1	85.0	5.1	-91.9	107.2	91.4	4.1
0513B-84	118	6354	2.7	0.21411	6.5	0.03175	3.0	0.46	201.5	5.9	197.0	11.7	143.6	135.8	201.5	5.9
0513B-85	439	2648	1.6	0.09254	12.1	0.01192	3.7	0.30	76.4	2.8	89.9	10.4	463.6	255.4	76.4	2.8
0513B-86	132	513	2.3	0.38177	33.7	0.01913	14.3	0.43	122.1	17.3	328.3	94.8	2284.8	538.5	122.1	17.3
0513B-87	117	4394	1.2	0.15724	11.7	0.02323	3.9	0.28	148.0	4.9	148.3	16.2	152.4	264.5	148.0	4.9
0513B-88	466	2851	1.0	0.17517	18.3	0.01896	12.9	0.71	121.1	15.5	163.9	27.7	837.6	271.2	121.1	15.5
0513B-89	201	2902	1.2	0.26398	21.7	0.02289	8.6	0.40	145.9	12.4	237.9	46.0	1283.9	391.1	145.9	12.4</

0513B-90	255	2748	2.3	0.04902	17.3	0.00804	3.9	0.23	51.6	2.0	48.6	8.2	-97.5	416.2	51.6	2.0
0513B-91	446	6954	5.2	0.12327	12.7	0.01661	10.9	0.86	106.2	11.5	118.0	14.2	364.2	146.0	106.2	11.5
0513B-92	270	4135	1.9	0.10444	11.8	0.01484	5.6	0.48	95.0	5.3	100.9	11.3	242.3	239.9	95.0	5.3
0513B-93	125	1148	1.4	0.03414	30.6	0.00866	6.2	0.20	55.6	3.4	34.1	10.3	-1309.6	970.7	55.6	3.4
0513B-94	88	4372	2.0	2.10371	21.2	0.15966	20.5	0.97	954.9	181.9	1150.0	146.9	1539.2	102.4	954.9	181.9
0513B-95	97	2792	1.5	0.18345	15.8	0.02591	6.9	0.43	164.9	11.2	171.0	24.9	256.3	328.9	164.9	11.2
0513B-96	91	770	1.5	0.08903	43.5	0.01447	6.4	0.15	92.6	5.9	86.6	36.1	-75.7	1097.3	92.6	5.9
0513B-97	351	3813	1.4	0.11220	13.2	0.01741	6.8	0.52	111.2	7.5	108.0	13.6	36.4	272.4	111.2	7.5
0513B-98	66	2456	2.6	0.15085	15.6	0.02442	5.2	0.34	155.5	8.1	142.7	20.7	-66.3	359.2	155.5	8.1
0513B-99	263	1017	1.1	0.32204	31.7	0.02582	10.2	0.32	164.3	16.5	283.5	78.6	1435.1	586.8	164.3	16.5
0513B-100	256	3258	4.0	0.16735	6.9	0.02165	1.8	0.26	138.1	2.4	157.1	10.1	454.5	148.4	138.1	2.4

Kulthieth Formation

0501A-1	579	5690	1.9	0.06289	5.5	0.00960	2.3	0.42	61.6	1.4	61.9	3.3	75.8	117.6	61.6	1.4
0501A-2	179	6640	3.0	0.16017	7.3	0.02454	3.0	0.41	156.3	4.6	150.9	10.2	66.4	157.9	156.3	4.6
0501A-3	213	2073	3.7	0.05915	12.3	0.00878	4.9	0.40	56.3	2.8	58.3	7.0	142.3	264.3	56.3	2.8
0501A-4	100	3977	1.8	0.16169	23.0	0.02539	2.7	0.12	161.6	4.3	152.2	32.5	7.8	555.1	161.6	4.3
0501A-5	233	2439	2.1	0.07004	13.4	0.00988	3.0	0.22	63.3	1.9	68.7	8.9	260.5	300.0	63.3	1.9
0501A-6	473	2684	1.8	0.10228	12.2	0.01438	2.4	0.20	92.1	2.2	98.9	11.5	266.5	275.8	92.1	2.2
0501A-7	100	1975	2.0	0.09766	13.4	0.01533	4.2	0.32	98.1	4.1	94.6	12.1	7.5	307.0	98.1	4.1
0501A-8	332	8126	6.3	0.06888	42.6	0.01042	40.0	0.94	56.8	26.6	67.6	27.9	96.6	349.0	56.8	26.6
0501A-9	275	3724	2.0	0.06211	15.0	0.00942	4.8	0.32	60.5	2.9	61.2	8.9	89.1	337.9	60.5	2.9
0501A-10	619	23229	2.6	0.14226	7.2	0.02212	3.5	0.48	141.0	4.9	135.1	9.1	31.4	151.2	141.0	4.9
0501A-11	92	869	2.7	0.07617	24.4	0.00991	6.4	0.26	63.6	4.1	74.5	17.5	442.2	529.9	63.6	4.1
0501A-12	197	4221	3.6	0.11004	20.1	0.01729	2.5	0.12	110.5	2.7	106.0	20.2	5.2	483.8	110.5	2.7
0501A-13	152	7020	2.4	0.52782	7.1	0.06780	2.3	0.33	422.9	9.5	430.4	24.9	470.4	148.5	422.9	9.5
0501A-14	760	7195	2.1	0.08071	6.5	0.00941	2.2	0.34	60.4	1.3	59.8	3.8	38.6	147.4	60.4	1.3
0501A-15	602	6295	5.9	0.11012	11.5	0.01581	2.8	0.24	101.1	2.8	106.1	11.6	219.0	260.2	101.1	2.8
0501A-16	477	4503	2.8	0.07778	11.4	0.01212	7.2	0.63	77.7	5.5	76.0	8.3	25.2	211.7	77.7	5.5
0501A-17	308	5373	1.8	0.09609	15.3	0.01508	1.7	0.11	96.5	1.6	93.2	13.6	8.4	367.0	96.5	1.6
0501A-18	343	3983	2.6	0.06178	8.6	0.00860	2.4	0.28	61.6	1.5	60.9	5.1	32.7	197.8	61.6	1.5
0501A-19	63	612	1.7	0.06529	23.1	0.01019	10.0	0.43	65.4	6.5	64.2	14.4	21.1	505.8	65.4	6.5
0501A-20	199	6428	3.1	0.12742	17.8	0.01756	5.6	0.31	112.2	6.2	121.8	20.4	313.3	387.1	112.2	6.2
0501A-21	107	1619	2.4	0.09529	20.8	0.01565	4.9	0.24	100.1	4.9	92.4	18.4	-102.1	500.6	100.1	4.9
0501A-22	880	9439	8.8	0.07022	17.7	0.01089	14.3	0.81	69.8	9.9	68.9	11.8	36.9	250.9	69.8	9.9
0501A-23	293	4129	1.7	0.05527	15.8	0.00864	4.0	0.25	55.5	2.2	54.6	8.4	17.2	367.8	55.5	2.2
0501A-24	214	2268	2.0	0.05766	16.0	0.00864	4.4	0.27	55.5	2.4	56.9	8.9	118.6	365.7	55.5	2.4
0501A-25	299	4495	2.7	0.07483	7.2	0.01143	2.5	0.35	73.3	1.8	73.3	5.1	73.6	160.8	73.3	1.8
0501B-1	300	1422	6.8	0.22167	18.4	0.02265	11.5	0.63	144.4	16.5	203.3	33.9	956.8	294.3	144.4	16.5
0501B-2	478	17608	1.5	0.45552	2.8	0.06048	2.6	0.93	378.5	9.5	381.1	8.8	396.9	23.1	378.5	9.5
0501B-3	152	1413	2.0	0.16719	29.8	0.01641	8.4	0.28	104.9	8.7	157.0	43.4	1038.4	590.2	104.9	8.7
0501B-4	204	1052	2.8	0.08510	23.9	0.00872	12.0	0.50	62.3	7.4	82.9	19.1	725.5	444.5	62.3	7.4
0501B-5	413	1656	2.7	0.05989	15.2	0.00864	6.7	0.44	55.5	3.7	59.2	8.7	211.4	316.5	55.5	3.7
0501B-6	255	5409	2.4	0.22909	24.8	0.02950	3.2	0.13	187.4	5.9	209.4	46.9	464.8	551.4	187.4	5.9
0501B-7	183	5938	2.2	0.40071	4.0	0.05392	1.4	0.36	338.5	4.7	342.2	11.6	366.9	83.7	338.5	4.7
0501B-8	293	1102	1.5	0.09981	23.2	0.01039	4.9	0.21	66.6	3.2	96.6	21.4	918.7	473.2	66.6	3.2
0501B-9	381	1505	2.0	0.05682	11.1	0.00860	3.5	0.31	55.2	1.9	56.1	6.1	95.3	249.8	55.2	1.9
0501B-10	194	945	2.0	0.07103	19.8	0.00844	6.5	0.33	54.2	3.5	69.7	13.3	639.7	404.1	54.2	3.5
0501B-11	279	915	2.2	0.09648	32.4	0.00955	4.8	0.15	61.3	3.0	93.5	28.9	1022.0	664.9	61.3	3.0
0501B-12	105	677	1.8	0.08589	34.0	0.00918	13.5	0.40	58.9	7.9	83.5	27.3	860.1	663.4	58.9	7.9
0501B-13	1343	2206	1.3	0.07278	10.8	0.00976	9.5	0.88	62.6	5.9	71.3	7.4	375.1	116.2	62.6	5.9
0501B-14	367	647	1.7	0.30934	38.5	0.01858	18.1	0.47	118.7	21.3	273.7	92.7	1967.7	626.3	118.7	21.3
0501B-15	310	2848	1.8	0.07445	12.4	0.01244	2.5	0.20	79.7	2.0	72.9	8.7	-144.4	302.7	79.7	2.0
0501B-16	174	2117	1.9	0.09793	14.7	0.01482	3.2	0.22	94.8	3.0	94.9	13.3	95.8	340.1	94.8	3.0
0501B-17	186	1937	1.6	0.08655	9.6	0.01472	3.3	0.35	94.2	3.1	84.3	7.8	-187.9	226.7	94.2	3.1
0501B-18	186	2074	1.3	0.08531	9.7	0.01382	5.0	0.52	88.5	4.4	83.1	7.7	-67.4	202.0	88.5	4.4
0501B-19	450	2386	2.3	0.06064	11.7	0.00873	3.7	0.32	56.0	2.1	59.8	6.8	212.9	258.0	56.0	2.1
0501B-20	84	506	1.9	0.16625	68.7	0.01691	27.8	0.40	108.1	29.8	156.2	99.8	965.9	1440.2	108.1	29.8
0501B-21	157	2611	2.2	0.24735	27.8	0.02667	6.5	0.23	169.7	10.9	224.4	56.0	845.8	572.1	169.7	10.9
0501B-22	158	1202	2.1	0.04479	26.3	0.00905	4.6	0.17	58.1	2.6	44.5	11.5	-637.8	719.9	58.1	2.6
0501B-23	259	2857	2.3	0.08389	6.6	0.01262	2.8	0.42	80.9	2.2	81.8	5.2	109.0	141.3	80.9	2.2
0501B-24	191	1255	2.6	0.60155	12.6	0.05169	4.5	0.36	324.9	14.3	478.2	48.0	1301.8	229.0	324.9	14.3
0501B-25	298	2115	2.7	0.05414	8.6	0.00890	3.5	0.41	57.1	2.0	53.5	4.5	-105.0	193.2	57.1	2.0
0501B-26	580	2324	1.0	0.06317	8.5	0.00894	3.3	0.38	57.4	1.9	62.2	5.1	250.8	180.2	57.4	1.9
0501B-27	199	2549	2.2	0.19036	8.9	0.02686	3.2	0.36	170.9	5.3	176.9	14.4	258.5	190.5	170.9	5.3
0501B-28	141	1888	2.8	0.19954	18.1	0.02649	4.1	0.22	168.5	6.8	184.7	30.6	397.2	399.0	168.5	6.8
0501B-29	467	1560	2.0	0.06160	13.3	0.00802	3.1	0.23	51.5	1.6	60.7	7.8	441.9	288.7	51.5	1.6
0501B-30	143	6649	2.1	0.40681	3.8	0.05545	2.9	0.77	347.9	9.9	346.6	11.2	337.9	54.7	347.9	9.9
0501B-31	200	4213	2.5	0.21217	4.9	0.03127	2.7	0.55	198.5	5.2	195.4	8.7	157.5	95.3	198.5	5.2
0501B-32	281	4620	1.3	0.14206	7.7	0.02237	5.4	0.70	142.6	7.6	134.9	9.7	0.6	132.7	142.6	7.6
0501B-33	341	871	1.5	0.08645	9.8	0.00864	3.7	0.38	55.5	2.1	84.2	7.9	1000.6	184.7	55.5	2.1
0501B-34	497	9438	1.5	0.18291	5.4	0.02738	5.1	0.94	174.1	8.8	170.6	8.6	121.7	42.7	174.1	8.8
0501B-35	685	4452	1.9	0.10256	6.7	0.01470	2.5	0.38	94.1	2.3	99.1	6.3	222.2	142.6	94.1	2.3
0501B-36	714	3235	2.3	0.05125	10.2	0.00758	1.9	0.19	48.7	0.9	50.7	5.0	150.0	234.4	48.7	0.9

0501B-37	177	1534	5.2	0.08513	9.4	0.01271	3.4	0.36	81.4	2.8	83.0	7.5	127.9	207.1	81.4	2.8
0501B-38	362	3368	1.6	0.11369	6.2	0.01892	2.3	0.36	108.2	2.4	109.3	6.5	134.2	136.5	108.2	2.4
0501B-39	147	421	1.6	0.10058	63.3	0.00903	21.6	0.34	58.0	12.5	97.3	58.8	1215.6	1299.3	58.0	12.5
0501B-40	309	1801	1.3	0.05826	8.3	0.00962	3.5	0.42	61.7	2.2	57.5	4.6	-114.2	185.4	61.7	2.2
0501B-41	469	2149	2.1	0.12637	23.5	0.01383	4.0	0.17	88.6	3.6	120.8	26.8	814.1	490.1	88.6	3.6
0501B-42	707	4318	6.5	0.05890	8.9	0.00882	3.0	0.34	56.6	1.7	58.1	5.0	119.7	197.4	56.6	1.7
0501B-43	376	2636	1.6	0.12117	10.2	0.01610	2.1	0.21	103.0	2.2	116.1	11.2	394.8	223.4	103.0	2.2
0501B-44	118	671	2.1	0.04103	58.6	0.00860	8.5	0.15	55.2	4.7	40.8	23.4	-739.4	1752.7	55.2	4.7
0501B-45	120	1384	1.7	0.13422	25.6	0.01883	4.0	0.15	120.3	4.7	127.9	30.8	271.5	587.7	120.3	4.7
0501B-46	207	272	0.7	0.17349	29.4	0.00902	14.1	0.48	57.9	8.2	162.4	44.2	2221.6	455.0	57.9	8.2
0501B-47	162	3114	2.4	0.17023	10.8	0.02449	1.6	0.15	156.0	2.5	159.6	15.9	214.4	247.4	156.0	2.5
0501B-48	279	917	1.6	0.12973	42.1	0.01145	11.8	0.28	73.4	8.6	123.9	49.1	1249.3	824.7	73.4	8.6
0501B-49	127	890	2.4	0.06903	40.5	0.00887	15.7	0.39	56.9	8.9	67.8	26.6	469.1	854.9	56.9	8.9
0501B-50	417	3963	5.4	0.09525	14.7	0.01422	4.8	0.33	91.0	4.3	92.4	13.0	128.4	328.3	91.0	4.3
0501B-51	74	1310	2.9	0.16047	11.7	0.02455	5.1	0.44	156.4	7.9	151.1	16.5	69.3	251.1	156.4	7.9
0501B-52	122	26972	1.3	4.80972	1.6	0.32051	1.2	0.74	1792.2	18.1	1786.6	13.1	1780.0	19.0	1780.0	19.0
0501B-53	573	5333	1.7	0.10248	12.2	0.01486	2.2	0.18	95.1	2.0	99.1	11.5	195.9	280.4	95.1	2.0
0501B-54	325	13721	2.6	0.48233	2.7	0.06426	2.5	0.93	401.5	9.7	405.5	9.0	435.2	22.7	401.5	9.7
0501B-55	194	1526	1.8	0.08381	7.1	0.01287	3.4	0.47	82.4	2.8	81.7	5.6	61.0	149.5	82.4	2.8
0501B-56	187	1364	2.4	0.10089	21.0	0.01487	5.2	0.25	95.1	4.9	97.4	19.5	153.3	481.3	95.1	4.9
0501B-57	330	2242	2.5	0.06561	9.0	0.01058	3.1	0.35	67.7	2.1	64.5	5.6	-52.4	205.1	67.7	2.1
0501B-58	180	2206	1.0	0.16791	14.9	0.02460	5.2	0.35	156.7	8.0	157.6	21.8	171.7	327.8	156.7	8.0
0501B-59	522	6282	1.2	0.13632	6.0	0.02116	4.0	0.66	135.0	5.3	129.8	7.4	34.7	108.6	135.0	5.3
0501B-60	149	1196	2.3	0.09208	17.5	0.01492	3.9	0.22	95.4	3.7	89.4	15.0	-68.3	419.8	95.4	3.7
0501B-61	165	310	1.0	0.22089	13.6	0.01089	6.2	0.45	69.8	4.3	202.5	25.0	2311.6	208.7	69.8	4.3
0501B-62	564	4866	2.6	0.08244	6.2	0.01259	4.2	0.67	80.7	3.3	80.4	4.8	73.0	110.2	80.7	3.3
0501B-63	473	754	1.8	0.11663	23.9	0.00952	7.7	0.32	61.1	4.7	112.0	25.3	1401.6	438.3	61.1	4.7
0501B-64	111	480	1.0	0.21459	80.8	0.00809	9.8	0.01	52.0	5.1	197.4	#NUM!	2762.2	1179.0	52.0	5.1
0501B-65	244	2011	2.0	0.10886	9.8	0.01503	4.8	0.49	96.2	4.6	104.9	9.7	307.9	193.9	96.2	4.6
0501B-66	276	896	1.6	0.06324	25.4	0.00856	5.8	0.23	54.9	3.2	62.3	15.3	354.4	565.9	54.9	3.2
0501B-67	155	638	2.3	0.08294	16.2	0.00946	4.8	0.30	60.7	2.9	80.9	12.6	728.4	329.4	60.7	2.9
0501B-68	285	1058	2.0	0.04636	17.2	0.00621	5.1	0.30	52.7	2.7	46.0	7.7	-292.1	420.9	52.7	2.7
0501B-69	437	170	4.7	1.03223	37.1	0.02361	30.0	0.81	151.7	45.0	720.0	193.7	3542.9	1617.9	151.7	45.0
0501B-70	652	3534	4.1	0.09502	5.1	0.01403	2.7	0.53	89.8	2.4	92.2	4.5	153.3	102.5	89.8	2.4
0501B-71	418	3287	2.4	0.09425	7.1	0.01439	4.0	0.57	92.1	3.7	91.5	6.2	75.1	137.4	92.1	3.7
0501B-72	268	1850	2.6	0.05085	9.6	0.00870	3.0	0.31	55.9	1.6	50.4	4.7	-204.4	228.5	55.9	1.6
0501B-73	550	4209	1.9	0.10032	9.8	0.01476	3.1	0.31	94.4	2.9	97.1	9.1	162.4	218.2	94.4	2.9
0501B-74	226	1311	2.7	0.08989	18.1	0.01114	4.4	0.25	71.4	3.2	87.4	15.1	549.8	385.1	71.4	3.2
0501B-75	947	2615	1.4	0.13760	13.8	0.01803	4.1	0.30	102.5	4.2	130.9	17.0	682.3	283.2	102.5	4.2
0504A-1	844	8238	1.0	0.08446	5.7	0.01269	2.3	0.40	81.3	1.8	82.3	4.5	113.5	124.3	81.3	1.8
0504A-2	212	3733	3.5	0.07608	14.8	0.01171	5.5	0.37	75.1	4.1	74.4	10.6	54.4	329.5	75.1	4.1
0504A-3	121	2485	2.1	0.22349	26.4	0.03111	12.4	0.47	197.5	24.1	204.8	49.0	290.2	538.9	197.5	24.1
0504A-4	131	1962	1.2	0.06573	20.2	0.01024	5.8	0.29	65.7	3.8	64.6	12.6	26.2	467.8	65.7	3.8
0504A-6	132	1987	1.3	0.06518	32.8	0.01015	6.7	0.20	65.1	4.3	64.1	20.4	26.7	786.5	65.1	4.3
0504A-5	289	4547	2.1	0.09905	8.5	0.01431	2.0	0.23	91.6	1.8	95.9	7.8	203.6	191.5	91.6	1.8
0504A-7	423	7301	3.8	0.52774	6.9	0.06747	2.2	0.31	420.9	8.8	430.3	24.1	481.0	144.1	420.9	8.8
0504A-8	117	3515	2.3	0.11155	7.7	0.01753	3.8	0.50	112.1	4.2	107.4	7.8	5.1	160.5	112.1	4.2
0504A-9	150	7240	3.6	0.20116	5.9	0.03062	3.0	0.52	194.4	5.8	186.1	10.0	82.1	119.3	194.4	5.8
0504A-10	330	4856	1.3	0.07897	11.9	0.01218	6.4	0.54	78.0	5.0	77.2	8.9	50.7	239.9	78.0	5.0
0504A-11	4096	7591	2.2	0.20593	9.8	0.02617	7.9	0.81	166.5	13.0	190.1	17.1	494.2	128.4	166.5	13.0
0504A-12	544	5696	3.9	0.09554	6.6	0.01324	2.8	0.42	84.8	2.3	92.7	5.8	300.6	136.4	84.8	2.3
0504A-13	272	3169	2.8	0.05890	12.7	0.00672	3.5	0.27	56.0	1.9	58.1	7.2	147.1	287.9	56.0	1.9
0504A-14	340	3806	1.4	0.06506	6.1	0.00832	2.8	0.46	59.8	1.7	64.0	3.8	222.8	125.8	59.8	1.7
0504A-15	210	4954	2.1	0.13136	12.3	0.01639	2.6	0.21	104.8	2.7	125.3	14.5	534.2	264.9	104.8	2.7
0504A-16	180	1643	2.1	0.11564	9.7	0.01568	4.6	0.47	100.3	4.6	111.1	10.2	349.1	194.1	100.3	4.6
0504A-17	192	3555	2.6	0.08767	35.8	0.01183	18.0	0.50	75.8	13.5	85.3	29.3	360.1	714.6	75.8	13.5
0504A-18	148	1182	2.0	0.05447	23.5	0.00840	7.5	0.32	53.9	4.0	53.9	12.3	52.1	536.2	53.9	4.0
0504A-19	221	1258	2.7	0.06623	19.0	0.00880	3.4	0.18	56.5	1.9	65.1	12.0	394.3	421.6	56.5	1.9
0504A-20	184	2193	1.9	0.08209	22.5	0.01283	3.7	0.16	82.2	3.0	80.1	17.3	18.9	538.6	82.2	3.0
0504A-21	307	4936	2.0	0.07518	8.8	0.01183	2.4	0.27	75.8	1.8	73.6	6.2	2.4	204.0	75.8	1.8
0504A-22	146	1329	2.0	0.06924	21.7	0.00915	8.2	0.38	58.7	4.8	68.0	14.3	407.4	453.1	58.7	4.8
0504A-23	340	3155	3.1	0.06096	11.9	0.00930	4.1	0.35	59.7	2.5	60.1	6.9	76.2	265.8	59.7	2.5
0504A-24	418	4946	4.7	0.05287	14.2	0.00829	3.8	0.27	53.2	2.0	52.3	7.2	11.9	330.5	53.2	2.0
0504A-25	623	15997	2.7	0.19057	5.2	0.02909	2.0	0.38	184.8	3.6	177.1	8.5	75.4	114.8	184.8	3.6
0504B-1	194	4908	1.9	0.10966	15.3	0.01467	5.4	0.35	93.9	5.0	105.7	15.3	380.1	323.1	93.9	5.0
0504B-2	148	6380	1.8	0.11819	10.3	0.01789	6.6	0.64	114.3	7.4	113.4	11.0	94.8	187.7	114.3	7.4
0504B-3	153	9725	1.8	0.15430	10.2	0.02419	3.7	0.37	154.1	5.7	145.7	13.8	11.4	228.1	154.1	5.7
0504B-4	117	3407	2.0	0.07098	16.1	0.01110	4.7	0.29	71.2	3.3	69.6	10.8	17.0	371.8	71.2	3.3
0504B-5	190	613	2.0	1.31508	48.8	0.04032	37.4	0.77	254.8	93.6	852.4	289.0	3097.0	513.5	254.8	93.6
0504B-6	225	9022	2.0	0.16471	5.4	0.02420	3.4	0.63	154.1	5.2	154.8	7.7	165.4	97.4	154.1	5.2
0504B-7	445	13235	3.3	0.08619	5.6	0.01336	3.5	0.63	85.5	3.0	84.0	4.5	39.2	103.6	85.5	3.0
0504B-8	82	2139	2.0	0.07279	28.5	0.01135	7.4	0.26	72.7	5.4	71.3	19.6	25.3	671.3	72.7	5.4
0504B-9	257	3375	3.2	0.09661	15.7	0.01517	10.5	0.67	97.1	10.1	93.6	14.0	6.8	281.3	97.1	10.1
0504B-10	328	647	1.0	0.56015	35.2	0.01927	24.7	0.70	123.1	30.1	451.6	129.1	2911.7	415.0	123.1	30.1

0504B-11	242	963	1.3	0.08109	26.9	0.01251	10.8	0.40	80.1	8.6	79.2	20.5	50.3	595.8	80.1	8.6
0504B-12	79	1723	2.3	0.09116	14.3	0.01405	4.2	0.29	89.9	3.8	88.6	12.1	52.1	326.5	89.9	3.8
0504B-13	172	2749	2.3	0.06774	12.7	0.00875	5.2	0.41	62.5	3.2	66.5	8.2	213.1	268.6	62.5	3.2
0504B-14	288	6941	3.2	0.09298	6.2	0.01449	3.7	0.59	92.7	3.4	90.3	5.4	26.1	120.3	92.7	3.4
0504B-15	173	3491	3.0	0.10554	15.8	0.01421	5.2	0.33	90.9	4.7	101.9	15.3	366.2	338.7	90.9	4.7
0504B-16	218	2184	1.7	0.05843	18.9	0.00797	8.0	0.42	51.2	4.1	57.7	10.6	335.1	390.3	51.2	4.1
0504B-17	131	3166	1.9	0.11212	11.9	0.01613	7.1	0.60	103.2	7.3	107.9	12.2	213.9	221.8	103.2	7.3
0504B-18	245	6173	2.1	0.16823	8.2	0.02318	2.8	0.35	147.7	4.2	157.9	12.0	313.2	175.5	147.7	4.2
0504B-19	572	6784	17.6	0.10697	12.0	0.01429	10.6	0.88	91.5	9.7	103.2	11.8	382.7	127.3	91.5	9.7
0504B-20	231	2473	1.7	0.05612	12.4	0.00815	5.9	0.48	52.3	3.1	55.4	6.7	192.6	254.1	52.3	3.1
0504B-21	317	3114	0.9	0.08278	38.5	0.00995	8.0	0.21	63.8	5.1	80.8	29.9	615.2	841.6	63.8	5.1
0504B-22	157	8023	1.9	0.20730	5.4	0.03103	1.8	0.34	197.0	3.5	191.3	9.4	121.0	120.0	197.0	3.5
0504B-23	345	3615	1.9	0.06716	13.9	0.00932	4.1	0.30	59.8	2.5	66.0	8.9	297.9	303.7	59.8	2.5
0504B-24	201	9269	2.2	0.15825	5.6	0.02429	1.9	0.34	154.7	3.0	149.2	7.8	62.0	125.6	154.7	3.0
0504B-25	262	8326	1.7	0.14349	7.4	0.02079	4.5	0.61	132.6	6.0	136.1	9.4	198.0	136.1	132.6	6.0

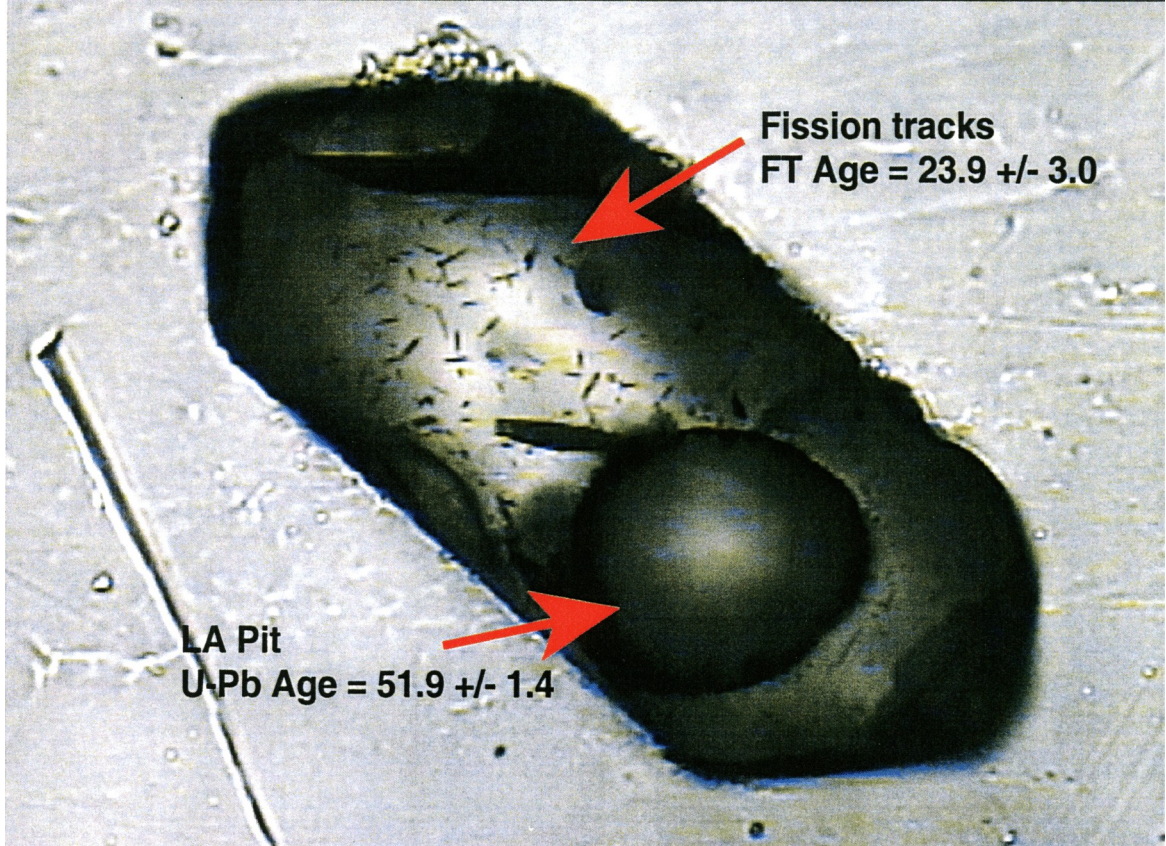


Figure 20. Detrital zircon fission-track grain that was dated by the DZFT method and then by the LA-ICPMS method.

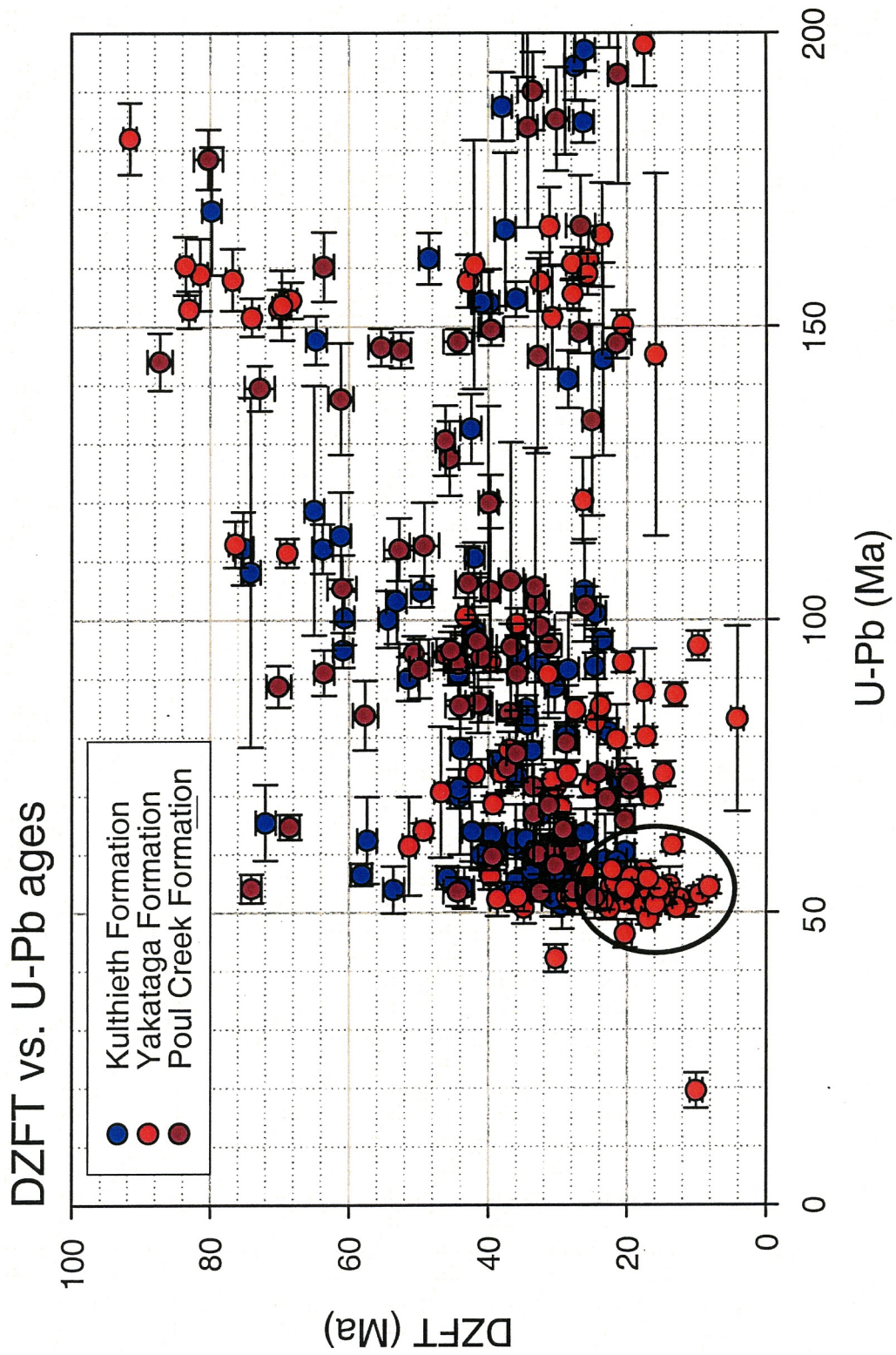


Figure 21. Plot of all double-dated samples showing U/Pb (Ma) versus DZFT (Ma).

Kulthieth 30 Ma DZFT vs. U-Pb

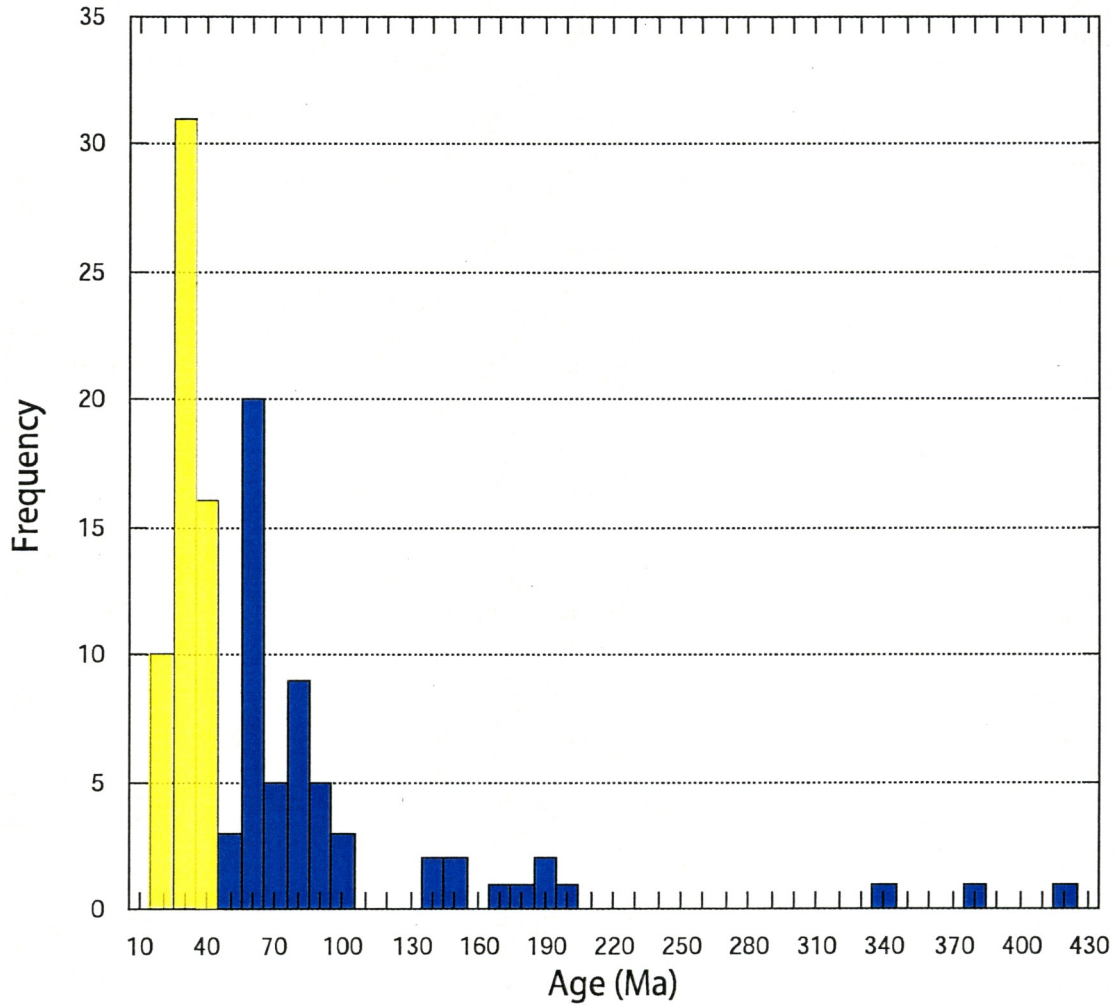
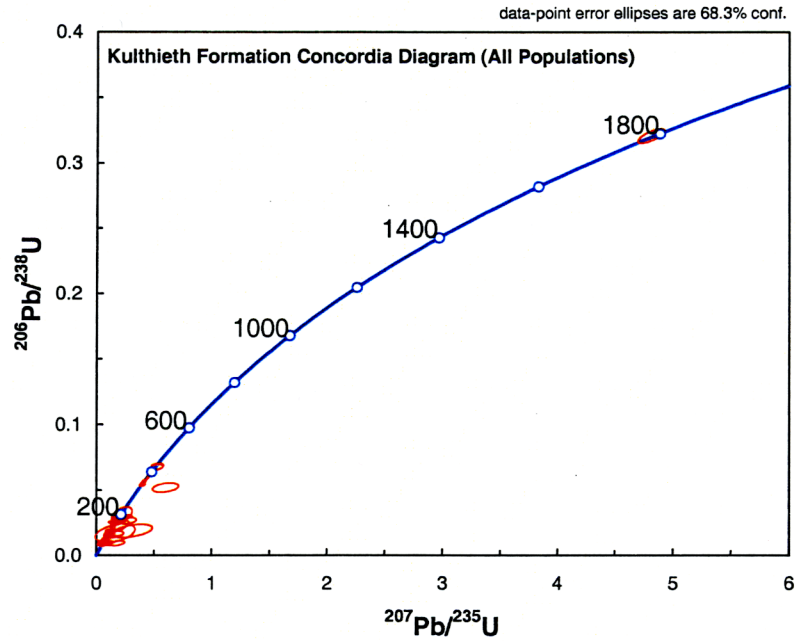


Figure 22. Histogram comparing the ~30 Ma DZFT dated grain-age population versus their equivalent U/Pb determined age. No single grain shares an identical age for both systems.

[A]



[B]

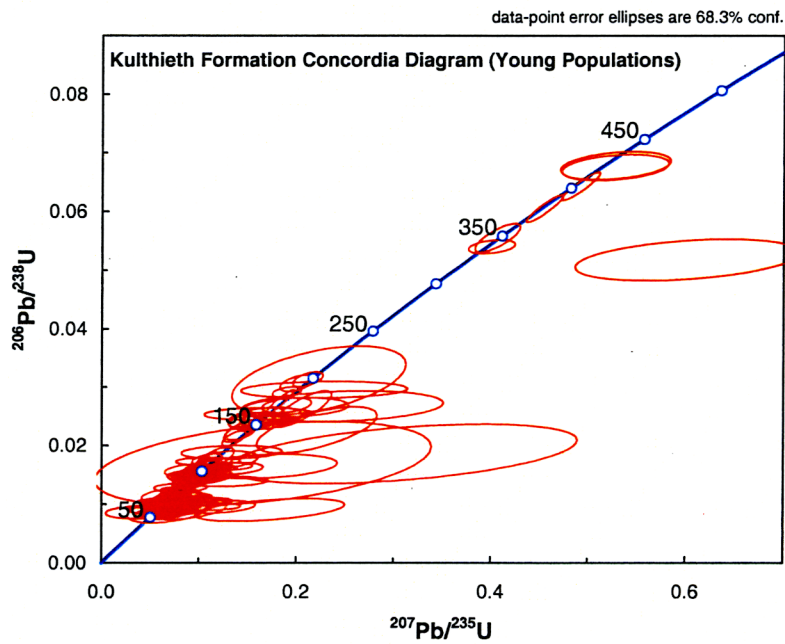
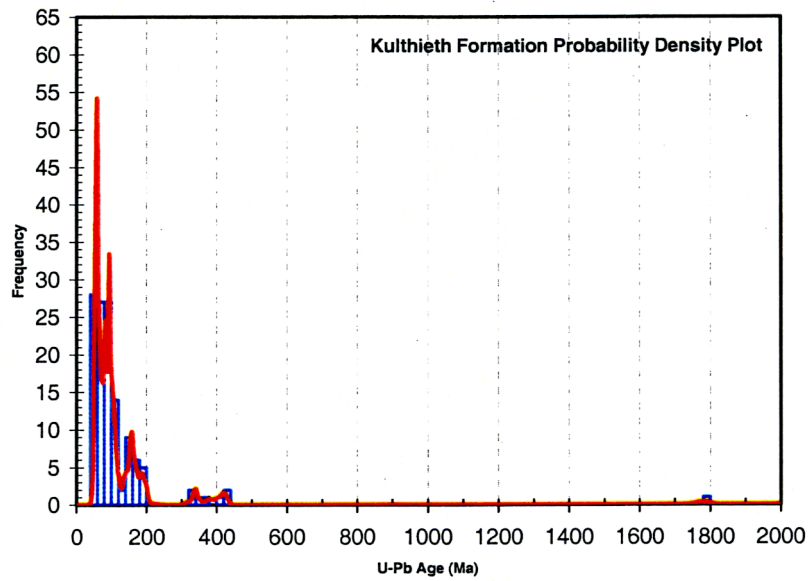


Figure 23 [A], [B]. Concordia diagrams for samples analyzed from the Kulthieth Formation. Diagram [A] Shows all determined U/Pb crystallization ages (Ma) and Diagram [B] Larger-scale version showing a close-up of younger determined age populations. Plots were generated using the Isoplot software (Ludwig, 1980; 2001; 2003).

[A]



[B]

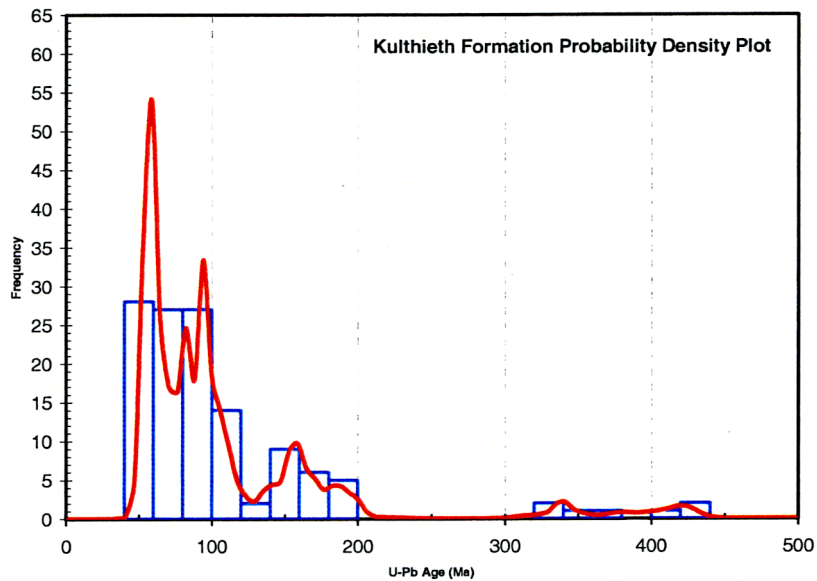


Figure 24 [A], [B]. Histogram probability plots for the Kulthieth Formation with U/Pb age (Ma) plotted against frequency of determinations in each age range. Diagram [A] All ages determined and Diagram [B] Larger-scale view of younger age populations. Plots were generated using the Isoplot program (Ludwig, 1980; 2003).

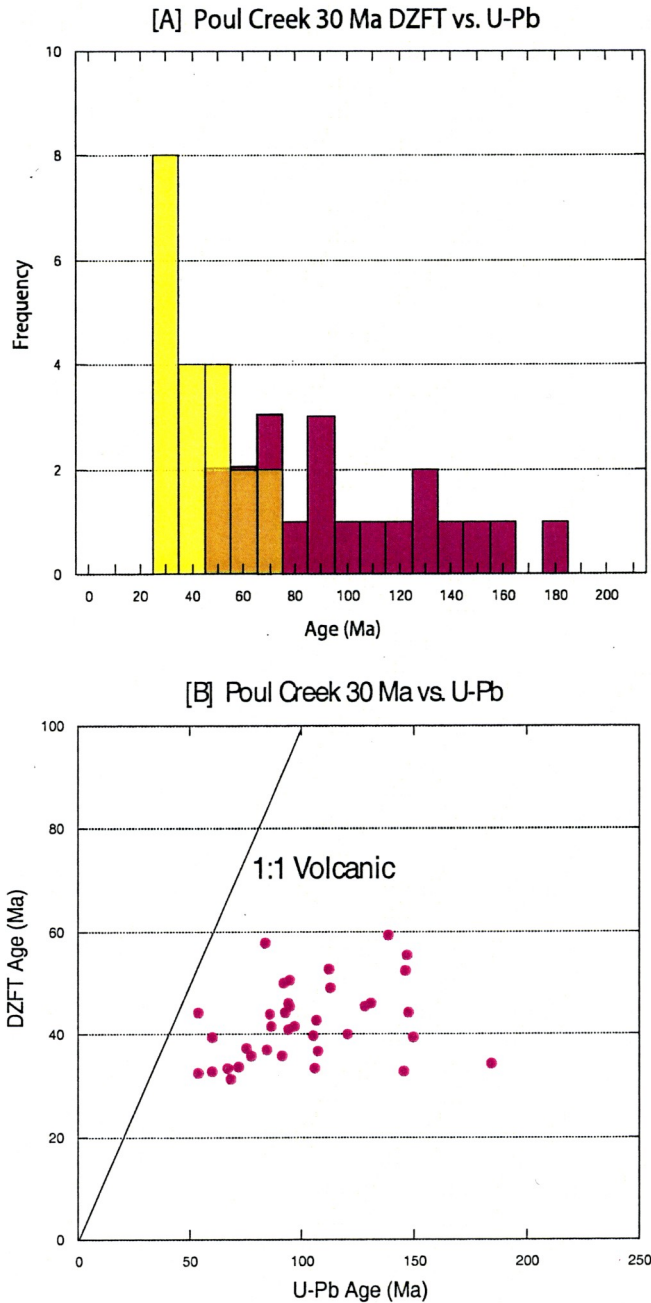
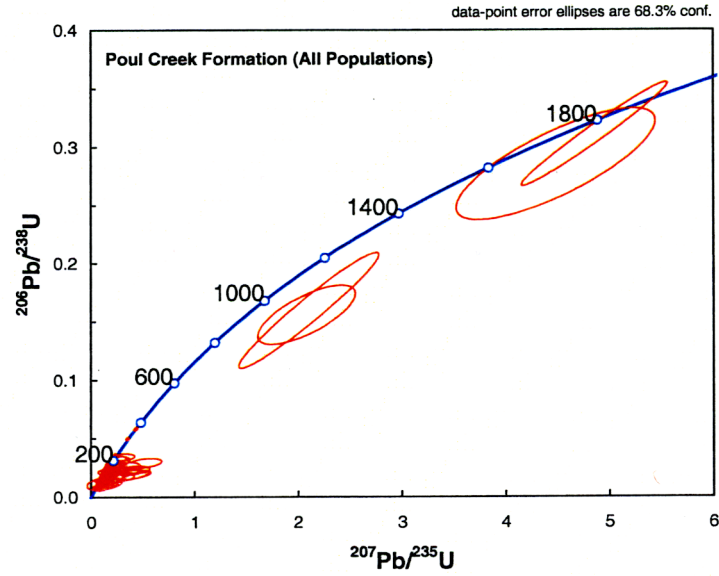


Figure 25. [A] Histogram comparing the ~30 Ma DZFT dated grain-age population versus their equivalent U/Pb determined age. No single grain shares an identical age for both systems. [B] Scatter plot of U/Pb (Ma) versus DZFT (Ma) determined ages for single grains. If a single grain had an identical age for both systems, the grain would plot of the 1:1 regression line.

[A]



[B]

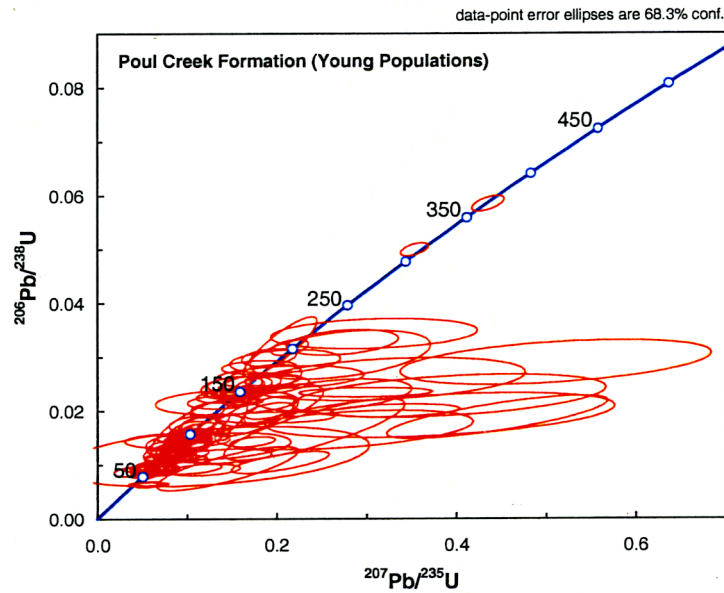
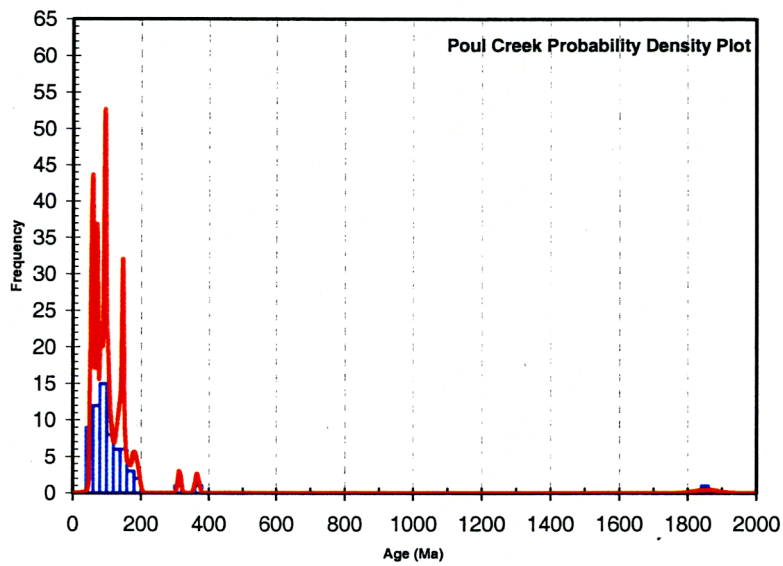


Figure 26 [A], [B]. Concordia diagrams for samples analyzed from the Poul Creek Formation. Diagram [A] Shows all determined U/Pb crystallization ages (Ma) and Diagram [B] Larger-scale version showing a close-up of younger age populations. Plots were generated using the Isoplot software (Ludwig, 1980; 2001; 2003).

[A]



[B]

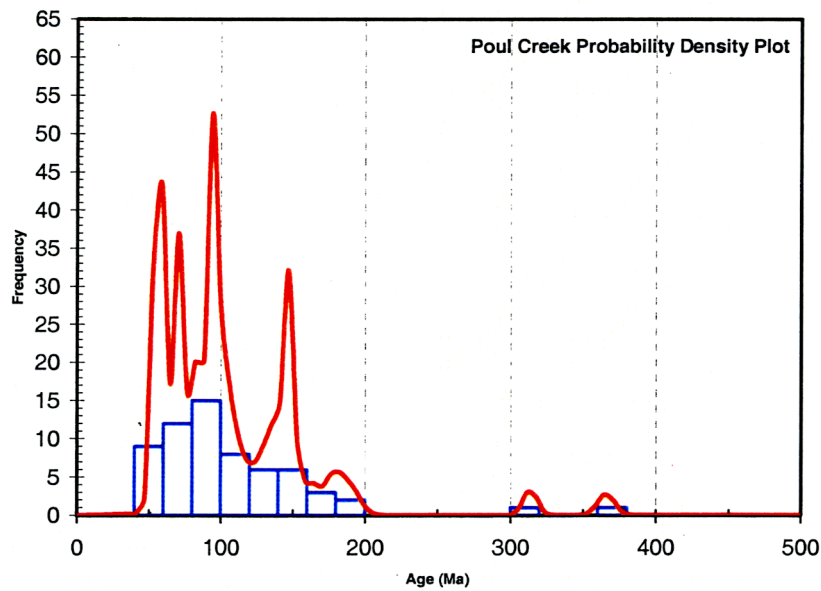


Figure 27 [A], [B]. Histogram probability plots for the Poul Creek Formation with U/Pb age (Ma) plotted against frequency of determinations in each age range. Diagram [A] All ages determined and Diagram [B] Larger-scale view of younger age populations. Plots were generated using the Isoplot program (Ludwig, 1980; 2003).

Yakataga Formation

150 total analyses for the Yakataga Formation were performed on 100 DZFT dated grains from samples 05-10 and 05-11 and 50 random grains from sample 05-11 (Figure 21; Figure 28 [A], [B]). Analyses were normalized and data were plotted on both Concordia diagrams and histogram plots using the Isoplot program (Table 4; Figure 29 [A], [B]; Figure 30 [A], [B]) (Ludwig, 2001; 2003). A significant peak was determined by the number of ages in a distribution equaling three or more. This is because Pb loss leading to isotopic disturbance in zircon grains can still yield analytically concordant U/Pb crystallization ages (Stacey and Kramers, 1975). For the Yakataga Formation three main age populations were determined: ~52 Ma, ~71 Ma and ~155 Ma. A comparison of the DZFT determined cooling ages versus the U/Pb crystallization ages for each grain analyzed can be found in Table 5. All highly discordant ages due to Pb loss or high common Pb content were excluded from the concordia diagrams and are underlined in Table 4. A single analysis resulted in a grain with an U/Pb crystallization age of ~19.6 Ma and a DZFT cooling sum age of ~20 Ma (Table 5). In addition, four single-grain analyses resulted in older crystallization ages of ~311 Ma, ~434 Ma, ~1660 Ma, and ~1940 Ma.

Sedimentary Petrography

Data are plotted as mean value percentages and presented on arkosic petrofacies ternary diagrams in terms of monocrystalline quartz (Q_m), polycrystalline quartz (Q_p),

Table 5. U-Pb (zircon) geochronologic grain age analyses by Laser-Ablation Multicollector ICP Mass Spectrometry versus Detrital Zircon Fission-Track grain-ages

Analysis	U (ppm)	Error (20%)	U/Th	Best age (Ma)	±	DZFT AGE	Error (-)	+	U (ppm)	Error (2S+)
<i>Yakataga Formation</i>										
0510A-1	104	21	3.0	431.6	8.3	69.4	1	1	237	71
0510A-2	274	55	4.3	52.4	1.6	15.7	1	1	397	83
0510A-3	279	56	3.4	92.7	1.7	20.6	1	1	473	127
0510A-4	289	58	6.3	56.1	1.6	26.3	1	1	447	124
0510A-5	612	122	3.5	51.8	1.3	20.4	1	1	577	129
0510A-6	708	142	1.8	51.2	2.0	11.4	1	1	640	137
0510A-7	325	65	2.7	100.6	3.2	43.3	1	1	619	154
0510A-8	218	44	2.1	54.5	2.0	22.4	1	1	270	68
0510A-9	444	89	4.0	53.3	1.1	19.4	1	1	549	126
0510A-10	424	85	3.8	52.9	2.0	16.2	1	1	506	100
0510A-11	94	19	1.4	158.9	6.1	81.4	1	1	145	52
0510A-12	357	71	2.0	151.6	8.9	30.8	1	1	468	91
0510A-13	116	23	1.5	73.9	3.5	38.2	1	1	142	55
0510A-14	300	60	1.8	56.2	2.3	39.7	1	1	368	95
0510A-15	96	19	2.0	167.0	6.7	31.2	1	1	312	103
0510A-16	312	62	2.5	92.8	1.7	39.7	1	1	363	111
0510A-17	156	31	2.1	157.7	4.5	42.9	1	1	312	103
0510A-18	657	131	3.1	53.0	1.4	9.5	1	1	793	121
0510A-19	41	8	2.6	87.7	7.3	17.6	1	1	159	55
0510A-20	181	36	2.3	42.2	2.4	30.3	1	1	277	82
0510A-21	188	38	1.5	111.4	2.5	68.9	1	1	329	106
0510A-22	166	33	2.3	153.1	3.2	70.0	1	1	295	100
0510A-23	598	120	3.1	54.3	1.2	8.2	1	1	621	125
0510A-24	112	22	2.7	79.6	5.9	21.5	1	1	367	80
0510A-25	607	121	2.1	57.0	2.9	26.0	1	1	570	129
0510B-1	291	58	2.2	55.0	1.6	21.7	1	1	484	101
0510B-2	763	153	2.4	52.3	1.4	12.5	1	1	597	122
0510B-3	676	135	2.6	67.9	1.9	29.5	1	1	561	118
0510B-4	518	104	3.6	52.3	2.9	38.7	1	1	443	137
0510B-5	494	99	8.8	50.6	1.9	22.6	1	1	347	82
0510B-6	180	36	1.8	90.7	7.5	31.4	1	1	259	79
0510B-7	219	44	5.9	52.7	2.0	28.7	1	1	290	64
0510B-8	243	49	5.7	54.7	3.1	13.9	1	1	371	92
0510B-9	344	69	2.1	52.0	2.2	18.1	1	1	352	82
0510B-10	789	158	1.8	64.0	1.3	49.3	1	1	577	181
0510B-22	135	27	2.2	112.9	4.0	76.3	1	1	181	66
0510B-23	279	56	2.1	80.1	1.5	17.3	1	1	448	99
0510B-24	130	26	1.7	182.0	6.2	91.6	1	1	90	46
0510B-25	124	25	1.9	151.6	3.2	73.9	1	1	164	59
0510B-11a	82	16	2.9	120.2	4.6	39.7	1	1	194	81
0510B-12a	649	130	4.5	50.8	1.2	12.9	1	1	612	133
0510B-13a	377	75	5.2	52.7	1.3	14.5	1	1	405	84
0510B-14a	168	34	1.7	157.6	5.0	32.5	1	1	300	72
0510B-15a	463	93	3.6	53.3	1.6	14.6	1	1	587	102
0510B-16a	547	109	2.5	57.0	1.7	17.6	1	1	582	102
0510B-17a	86	17	2.3	158.0	5.3	76.7	1	1	295	100
0510B-18a	90	18	2.9	198.1	7.1	17.5	1	1	386	98
0510B-19a	220	44	4.0	52.3	2.7	27.6	1	1	304	101
0510B-20a	232	46	2.0	46.4	2.4	20.3	1	1	249	85
0511A-1	553	111	2.8	51.9	1.4	23.5	0.9	1	453	114
0511A-2	530	106	5.2	57.3	1.2	22.2	0.9	1	530	124
0511A-3	614	123	2.9	50.8	2.7	34.9	0.9	1	577	117
0511A-4	1128	226	4.3	69.8	1.4	16.6	0.9	1	707	144
0511A-5	174	35	2.3	143.4	3.4	115.1	0.9	1	106	47
0511A-6	379	76	2.5	71.6	4.5	30.3	0.9	1	456	140
0511A-7	298	60	1.9	72.7	1.7	30.8	0.9	1	424	121
0511A-8	782	156	2.2	50.7	0.9	16.9	0.9	1	679	141
0511A-9	424	85	2.8	87.2	2.0	13.1	0.9	1	497	112
0511A-10	760	152	3.6	55.9	2.7	19.5	0.9	1	647	167
0511A-11	589	118	3.2	71.8	2.0	25.4	0.9	1	687	155
0511A-12	1223	245	4.5	73.6	2.2	14.7	0.9	1	788	198
0511A-13	755	151	3.2	52.3	1.1	15.2	0.9	1	598	104
0511A-14	2653	531	1.4	61.6	1.2	13.5	0.9	1	535	98
0511A-15	824	165	2.8	82.5	1.0	24.6	0.9	1	764	164
0511A-16	201	40	1.9	153.0	3.2	83.0	0.9	1	267	81
0511A-17	251	50	1.5	161.4	4.5	25.6	0.9	1	361	102
0511A-18	1339	268	1.9	51.3	0.9	17.7	0.9	1	728	147
0511A-19	543	109	4.1	209.9	17.4	35.0	0.9	1	518	134
0511A-20	623	125	3.8	53.9	1.5	20.2	0.9	1	665	140

0511A-21	446	89	3.8	73.8	2.2	28.6	0.9	1	919	231
0511A-22	395	79	3.4	99.3	2.6	35.9	0.9	1	622	135
0511A-23	1513	303	3.0	84.6	2.1	27.5	0.9	1	637	127
0511A-24	584	117	2.6	61.4	8.4	51.4	0.9	1	398	107
0511A-25	504	101	1.7	95.5	2.5	9.8	0.9	1	594	119
0511B-1	391	78	3.0	70.6	11.2	46.8	0.9	1	331	119
0511B-2	239	48	2.6	68.6	1.4	39.3	0.9	1	391	106
0511B-3	207	41	2.1	160.7	2.8	27.9	0.9	1	220	79
0511B-4	552	110	2.7	83.1	15.9	4.2	0.9	1	701	134
0511B-5	161	32	3.4	160.4	4.9	83.5	0.9	1	219	73
0511B-6	786	157	3.5	145.2	30.9	15.9	0.9	1	591	123
0511B-7	1636	327	2.2	48.9	1.0	17.0	0.9	1	835	147
0511B-8	560	112	2.0	158.9	3.5	25.7	0.9	1	629	119
0511B-9	281	56	2.6	52.7	2.5	35.8	0.9	1	366	79
0511B-10	1238	248	3.5	85.2	2.3	23.8	0.9	1	529	98
0511B-11	248	50	2.3	73.8	2.4	41.9	0.9	1	240	72
0511B-13	1426	285	7.2	53.6	0.7	16.8	0.9	1	1018	164
0511B-14	133	27	2.2	154.5	3.1	68.3	0.9	1	171	69
0511B-15	181	36	1.6	153.6	5.9	69.6	0.9	1	237	68
0511B-16	1290	258	5.9	120.3	7.3	26.4	0.9	1	541	126
0511B-17	993	199	4.7	51.3	1.1	16.0	0.9	1	610	105
0511B-18	130	26	4.4	77.8	3.0	37.0	0.9	1	302	84
0511B-19	386	77	1.2	19.6	3.0	10.1	0.9	1	640	138
0511B-20	278	56	2.4	150.3	2.5	20.6	0.9	1	408	101
0511B-21	509	102	13.1	54.2	1.4	15.4	0.9	1	683	124
0511B-22	316	63	3.1	165.6	8.8	23.6	0.9	1	256	77
0511B-23	312	62	3.8	55.7	1.8	17.0	0.9	1	337	77
0511B-24	1394	279	3.8	160.5	21.2	42.0	0.9	1	306	94
0511B-25	145	29	2.0	155.5	2.5	27.8	0.9	1	290	71

Poul Creek Formation

0507A-1	83	17	1.7	138.0	5.3	59.3	1.8	1.9	165	60
0507A-2	310	62	1.9	84.1	1.4	37.0	1.8	1.9	401	98
0507A-3	178	36	1.1	185.3	8.8	30.2	1.8	1.9	427	153
0507A-5	162	32	2.3	149.5	2.7	39.6	1.8	1.9	289	90
0507A-6	214	43	1.5	137.7	9.5	61.2	1.8	1.9	207	70
0507A-7	125	25	1.7	98.6	3.6	70.1	1.8	1.9	224	73
0507A-8	218	44	1.8	59.9	2.5	30.0	1.8	1.9	434	134
0507A-9	268	54	2.2	53.8	1.8	27.7	1.8	1.9	578	147
0507A-10	74	15	2.3	83.7	5.9	57.7	1.8	1.9	116	50
0507A-11	130	26	3.1	146.5	3.2	55.4	1.8	1.9	190	56
0507A-12	92	18	2.1	144.1	4.9	87.2	1.8	1.9	132	54
0507A-14	178	36	1.4	106.7	23.6	36.8	1.8	1.9	294	104
0507A-15	329	66	1.3	52.4	3.5	24.7	1.8	1.9	386	145
0507A-16	589	118	1.6	73.7	2.7	20.4	1.8	1.9	331	79
0507A-17	293	59	3.6	95.6	2.0	31.3	1.8	1.9	567	184
0507A-18	175	35	2.2	313.7	4.9	26.1	1.8	1.9	461	114
0507A-19	157	31	1.0	94.1	2.7	46.2	1.8	1.9	294	79
0507A-20	74	15	3.6	106.3	6.3	42.9	1.8	1.9	321	78
0507A-21	94	19	1.5	85.9	5.1	41.5	1.8	1.9	303	92
0507A-22	138	28	2.1	79.0	3.4	28.8	1.8	1.9	339	106
0507A-23	116	23	2.9	71.0	2.6	19.6	1.8	1.9	372	102
0507A-24	124	25	1.9	60.1	3.5	29.7	1.8	1.9	212	66
0507A-25	110	22	1.8	102.9	2.8	33.1	1.8	1.9	297	81
0507B-2	248	50	1.6	102.3	3.3	26.0	2.1	2.2	332	125
0507B-3	113	23	4.0	95.4	3.9	36.7	2.1	2.2	254	69
0507B-4	107	21	2.0	167.1	8.6	26.7	2.1	2.2	305	92
0507B-5	128	26	2.2	112.6	7.4	49.2	2.1	2.2	314	77
0507B-6	290	58	2.0	365.9	5.9	28.9	2.1	2.2	332	89
0507B-7	260	52	3.1	92.4	1.4	44.3	2.1	2.2	136	66
0507B-8	297	59	1.9	93.6	1.8	41.0	2.1	2.2	356	93
0507B-9	225	45	3.0	59.3	2.8	32.6	2.1	2.2	270	105
0507B-10	474	95	2.0	94.7	3.3	45.4	2.1	2.2	405	130
0507B-11	240	48	2.3	98.8	2.5	32.6	2.1	2.2	343	88
0507B-12	117	23	2.0	178.5	5.1	80.2	2.1	2.2	143	51
0507B-13	236	47	2.2	147.4	2.2	44.4	2.1	2.2	201	74
0507B-14	371	74	4.1	59.6	2.3	39.4	2.1	2.2	406	123
0507B-15	332	66	1.4	112.0	5.3	52.8	2.1	2.2	187	56
0507B-16	349	70	1.4	147.1	2.6	21.5	2.1	2.2	339	97
0507B-17	237	47	1.5	139.5	3.9	72.8	2.1	2.2	83	65
0507B-18	121	24	1.5	96.3	4.5	41.6	2.1	2.2	178	65
0507B-19	503	101	2.3	74.8	3.9	37.3	2.1	2.2	224	61
0507B-20	146	29	3.7	85.4	4.0	44.1	2.1	2.2	133	47
0507B-21	109	22	2.2	53.5	2.5	44.4	2.1	2.2	134	50

0507B-22	105	21	2.0	190.1	6.6	33.6	2.1	2.2	291	90
0507B-23	122	24	1.8	60.3	2.7	31.0	2.1	2.2	168	61
0507B-24	162	32	2.2	105.4	5.6	61.0	2.1	2.2	173	69
0507B-25	188	38	1.8	94.3	3.0	50.7	2.1	2.2	191	79
0513B-1	194	39	1.4	160.2	5.9	63.6	1.4	1.4	164	83
0513B-3	306	61	1.3	1854.3	33.7	42.4	1.4	1.4	414	135
0513B-4	234	47	1.2	53.5	1.7	32.5	1.4	1.4	284	91
0513B-5	513	103	3.4	69.4	1.6	23.0	1.4	1.4	601	155
0513B-6	565	113	3.5	134.0	16.3	25.1	1.4	1.4	602	147
0513B-9	353	71	2.7	127.6	6.4	45.6	1.4	1.4	403	133
0513B-11	906	181	1.1	71.5	1.3	33.6	1.4	1.4	523	152
0513B-13	351	70	2.4	60.0	1.9	32.9	1.4	1.4	407	110
0513B-17	274	55	1.8	90.8	6.3	35.9	1.4	1.4	361	93
0513B-19	279	56	2.1	65.8	2.3	20.3	1.4	1.4	349	84
0513B-20	155	31	2.6	104.9	15.2	39.7	1.4	1.4	262	96
0513B-21	316	63	2.3	73.8	23.2	24.3	1.4	1.4	473	119
0513B-22	313	63	1.7	130.6	6.0	46.2	1.4	1.4	297	102
0513B-23	162	32	1.8	60.3	4.7	28.0	1.4	1.4	240	84
0513B-25	461	92	1.6	72.0	2.3	19.6	1.4	1.4	550	140
0513B-26	397	79	5.4	149.1	3.6	26.9	1.4	1.4	611	148
0513B-27	215	43	1.3	58.1	4.5	30.4	1.4	1.4	299	72
0513B-31a	326	65	2.6	66.8	8.5	33.5	1.4	1.4	300	77
0513B-29a	244	49	1.8	119.9	16.6	40.0	1.4	1.4	698	203
0513B-34	382	76	5.1	144.9	16.6	32.9	1.4	1.4	427	123
0513B-35	145	29	3.1	207.2	9.7	22.6	1.4	1.4	211	78
0513B-36	571	114	1.3	77.2	4.9	36.0	1.4	1.4	366	94
0513B-37	525	105	8.3	105.6	23.7	33.3	1.4	1.4	378	106
0513B-38	140	28	2.1	91.6	5.0	49.9	1.4	1.4	240	84
0513B-40	433	87	3.3	68.3	3.0	31.3	1.4	1.4	556	157
0513B-41	511	102	1.4	91.0	3.9	63.6	1.4	1.4	368	97
0513B-42	188	38	1.1	933.4	93.4	56.6	1.4	1.4	157	73
0513B-43	415	83	2.4	64.7	2.2	68.5	1.4	1.4	167	69
0513B-44	129	26	2.0	183.9	17.1	34.3	1.4	1.4	145	90
0513B-45	311	62	2.4	54.1	2.4	74.0	1.4	1.4	273	80
0513B-46	113	23	3.7	202.1	22.9	28.9	1.4	1.4	124	59
0513B-48	168	34	2.1	146.0	3.0	52.5	1.4	1.4	196	75
0513B-49	783	153	3.3	192.9	18.7	21.3	1.4	1.4	630	159
0513B-50	611	122	3.8	64.1	2.7	29.2	1.4	1.4	676	174

Kulthieth Formation

0501A-1	579	116	1.9	61.6	1.4	44.2	1.4	1.5	505	164
0501A-2	179	36	3.0	156.3	4.6	46.3	1.4	1.5	388	124
0501A-3	213	43	3.7	56.3	2.8	30.0	1.4	1.5	359	107
0501A-4	100	20	1.8	161.8	4.3	48.5	1.4	1.5	212	75
0501A-5	233	47	2.1	63.3	1.9	39.5	1.4	1.5	219	76
0501A-6	473	95	1.8	92.1	2.2	24.7	1.4	1.5	408	128
0501A-7	100	20	2.0	98.1	4.1	42.0	1.4	1.5	159	53
0501A-9	275	55	2.0	60.5	2.9	34.6	1.4	1.5	279	105
0501A-10	619	124	2.6	141.0	4.9	28.5	1.4	1.5	404	97
0501A-11	92	18	2.7	63.6	4.1	26.0	1.4	1.5	148	58
0501A-12	197	39	3.8	110.5	2.7	42.0	1.4	1.5	229	95
0501A-13	152	30	2.4	422.9	9.5	66.6	1.4	1.5	259	83
0501A-14	760	152	2.1	60.4	1.3	20.3	1.4	1.5	682	157
0501A-15	602	120	5.9	101.1	2.8	24.5	1.4	1.5	548	149
0501A-16	477	95	2.8	77.7	5.5	33.7	1.4	1.5	266	69
0501A-17	308	62	1.8	96.5	1.6	23.6	1.4	1.5	336	88
0501A-18	343	69	2.6	61.6	1.5	36.4	1.4	1.5	534	132
0501A-19	63	13	1.7	65.4	6.5	72.0	1.4	1.5	73	43
0501A-20	199	40	3.1	112.2	6.2	75.2	1.4	1.5	199	88
0501A-21	107	21	2.4	100.1	4.9	54.4	1.4	1.5	215	82
0501A-22	880	176	8.8	69.8	9.9	44.1	1.4	1.5	199	88
0501A-23	293	59	1.7	55.5	2.2	26.6	1.4	1.5	216	70
0501A-24	214	43	2.0	55.5	2.4	32.6	1.4	1.5	353	90
0501A-25	299	60	2.7	73.3	1.8	35.8	1.4	1.5	398	126
0501B-1	300	60	6.8	144.4	16.5	23.5	1.4	1.5	525	138
0501B-2	478	96	1.5	378.5	9.5	34.0	1.4	1.5	481	139
0501B-3	152	30	2.0	104.9	8.7	26.2	1.4	1.5	534	121
0501B-4	204	41	2.8	62.3	7.4	57.4	1.4	1.5	183	65
0501B-5	413	83	2.7	55.5	3.7	36.0	1.4	1.5	334	95
0501B-6	255	51	2.4	187.4	5.9	38.0	1.4	1.5	309	85
0501B-7	183	37	2.2	338.5	4.7	35.3	1.4	1.5	254	82
0501B-8	293	59	1.5	66.6	3.2	32.6	1.4	1.5	200	60
0501B-9	381	76	2.0	55.2	1.9	33.1	1.4	1.5	481	100
0501B-10	194	39	2.0	54.2	3.5	43.5	1.4	1.5	143	57

0501B-11	279	56	2.2	61.3	3.0	31.2	1.4	1.5	430	132
0501B-12	105	21	1.8	58.9	7.9	23.2	1.4	1.5	194	72
0501B-13	1343	269	1.3	62.6	5.9	36.1	1.4	1.5	240	80
0501B-14	367	73	1.7	118.7	21.3	65.0	1.4	1.5	160	79
0501B-15	310	62	1.8	79.7	2.0	28.7	1.4	1.5	380	123
0501B-16	174	35	1.9	94.8	3.0	60.9	1.4	1.5	260	102
0501B-17	186	37	1.6	94.2	3.1	35.9	1.4	1.5	280	106
0501B-18	186	37	1.3	88.5	4.4	30.5	1.4	1.5	352	106
0501B-19	450	90	2.3	56.0	2.1	27.7	1.4	1.5	374	100
0501B-20	84	17	1.9	108.1	29.8	74.1	1.4	1.5	93	49
0501B-21	157	31	2.2	169.7	10.9	79.7	1.4	1.5	174	95
0501B-22	158	32	2.1	58.1	2.6	39.9	1.4	1.5	191	58
0501B-23	259	52	2.3	80.9	2.2	22.7	1.4	1.5	348	76
0501B-24	191	38	2.6	324.9	14.3	41.8	1.4	1.5	194	72
0501B-25	298	60	2.7	57.1	2.0	33.7	1.4	1.5	383	94
0504A-1	844	169	1.0	81.3	1.8	30.9	1.5	1.6	488	127
0504A-2	212	42	3.5	75.1	4.1	22.3	1.5	1.6	302	84
0504A-3	121	24	2.1	197.5	24.1	50.3	1.5	1.6	366	140
0504A-4	131	26	1.2	65.7	3.8	27.9	1.5	1.6	289	69
0504A-6	132	26	1.3	65.1	4.3	36.2	1.5	1.6	417	130
0504A-5	289	58	2.1	91.6	1.8	44.0	1.5	1.6	350	107
0504A-7	423	85	3.8	420.9	8.8	26.9	1.5	1.6	407	129
0504A-8	117	23	2.3	112.1	4.2	63.8	1.5	1.6	183	85
0504A-9	150	30	3.6	194.4	5.8	27.5	1.5	1.6	588	139
0504A-10	330	66	1.3	78.0	5.0	44.0	1.5	1.6	295	109
0504A-11	4096	819	2.2	166.5	13.0	37.6	1.5	1.6	468	194
0504A-12	544	109	3.9	84.8	2.3	34.6	1.5	1.6	813	231
0504A-13	272	54	2.8	56.0	1.9	45.9	1.5	1.6	302	84
0504A-14	340	68	1.4	59.8	1.7	38.9	1.5	1.6	244	81
0504A-15	210	42	2.1	104.8	2.7	49.6	1.5	1.6	284	85
0504A-16	180	36	2.1	100.3	4.6	60.7	1.5	1.6	234	97
0504A-18	148	30	2.0	53.9	4.0	53.6	1.5	1.6	187	78
0504A-19	221	44	2.7	56.5	1.9	58.2	1.5	1.6	244	99
0504A-20	184	37	1.9	82.2	3.0	34.4	1.5	1.6	244	99
0504A-21	307	81	2.0	75.8	1.8	38.6	1.5	1.6	390	113
0504A-22	146	29	2.0	58.7	4.8	21.5	1.5	1.6	282	97
0504A-23	340	68	3.1	59.7	2.5	27.6	1.5	1.6	366	140
0504A-24	418	84	4.7	53.2	2.0	37.3	1.5	1.6	427	108
0504A-25	623	125	2.7	184.8	3.6	26.3	1.5	1.6	393	104
0504B-1	194	39	1.9	93.9	5.0	44.8	1.5	1.6	286	124
0504B-2	148	30	1.8	114.3	7.4	61.2	1.5	1.6	164	73
0504B-3	153	31	1.8	154.1	5.7	39.9	1.5	1.6	311	101
0504B-4	117	23	2.0	71.2	3.3	44.2	1.5	1.6	170	68
0504B-6	225	45	2.0	154.1	5.2	41.0	1.5	1.6	409	149
0504B-7	445	89	3.3	85.5	3.0	41.0	1.5	1.6	436	110
0504B-8	82	16	2.0	72.7	5.4	21.1	1.5	1.6	439	134
0504B-9	257	51	3.2	97.1	10.1	42.0	1.5	1.6	345	112
0504B-11	242	48	1.3	80.1	8.6	28.8	1.5	1.6	320	94
0504B-12	79	16	2.3	89.9	3.8	51.5	1.5	1.6	184	71
0504B-13	172	34	2.3	62.5	3.2	34.6	1.5	1.6	327	115
0504B-14	288	58	3.2	92.7	3.4	32.8	1.5	1.6	450	122
0504B-15	173	35	3.0	90.9	4.7	44.3	1.5	1.6	401	115
0504B-16	218	44	1.7	51.2	4.1	29.4	1.5	1.6	238	81
0504B-17	131	26	1.9	103.2	7.3	53.2	1.5	1.6	245	89
0504B-18	245	49	2.1	147.7	4.2	64.7	1.5	1.6	168	52
0504B-19	572	114	17.6	91.5	9.7	28.5	1.5	1.6	294	70
0504B-20	231	46	1.7	52.3	3.1	30.8	1.5	1.6	286	108
0504B-21	317	63	0.9	63.8	5.1	42.3	1.5	1.6	350	91
0504B-22	157	31	1.9	197.0	3.5	26.1	1.5	1.6	279	87
0504B-23	345	69	1.9	59.8	2.5	41.0	1.5	1.6	378	124
0504B-24	201	40	2.2	154.7	3.0	36.0	1.5	1.6	466	124
0504B-25	262	52	1.7	132.6	6.0	42.5	1.5	1.6	266	104

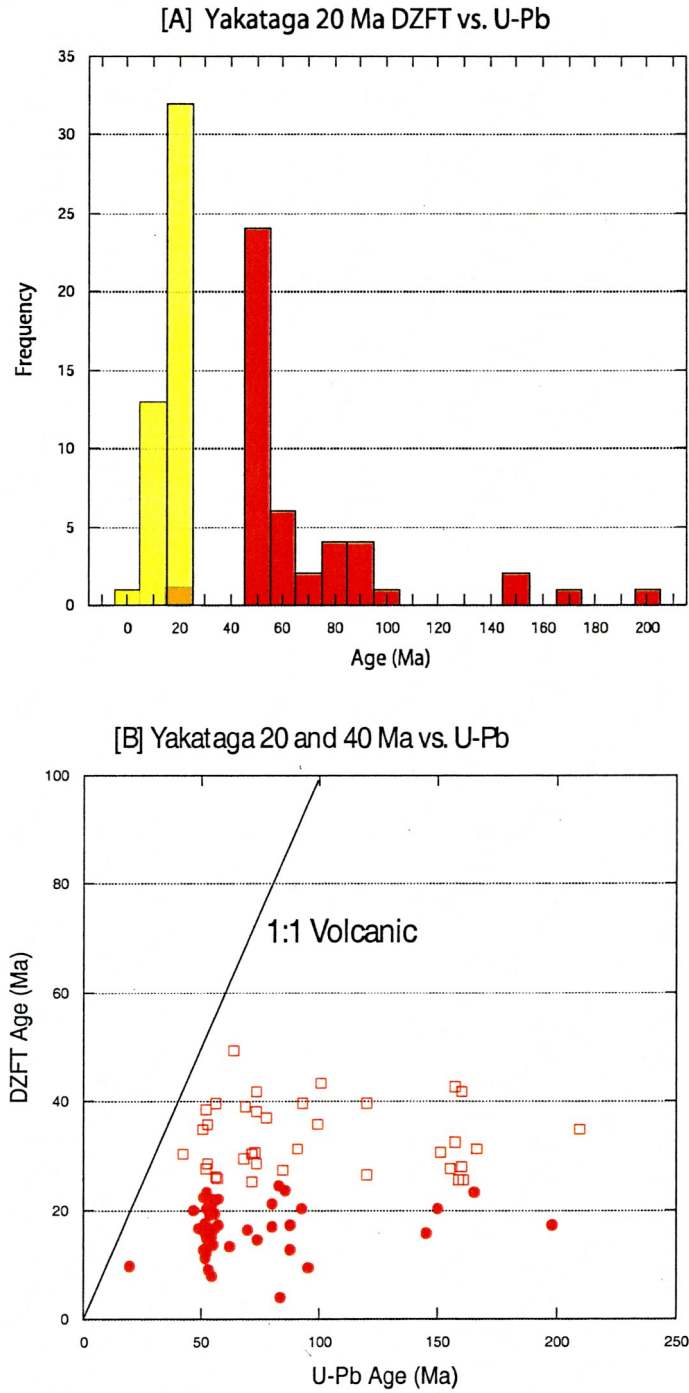
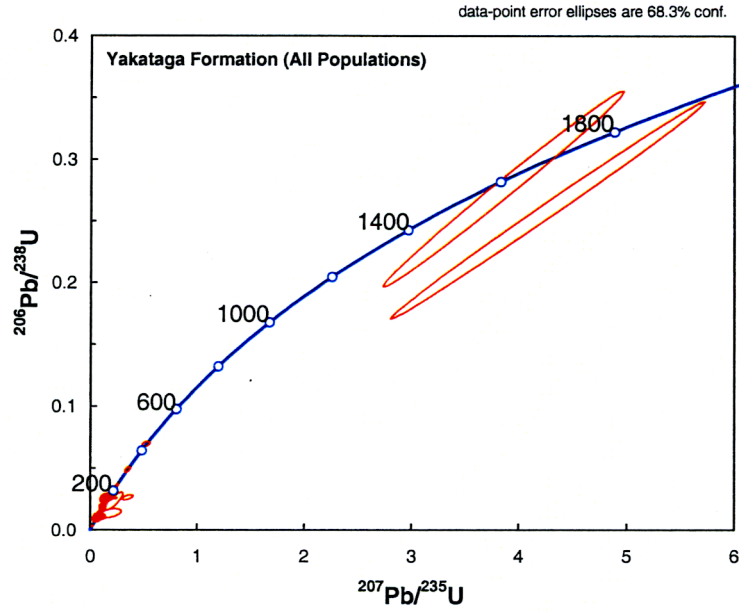


Figure 28. [A] Histogram comparing the ~20 Ma DZFT dated grain-age population versus their equivalent U/Pb determined age. No single grain shares an identical age for both systems. [B] Scatter plot of U/Pb (Ma) versus DZFT (Ma) determined ages for single grains. If a single grain had an identical age for both systems, the grain would plot of the 1:1 regression line.

[A]



[B]

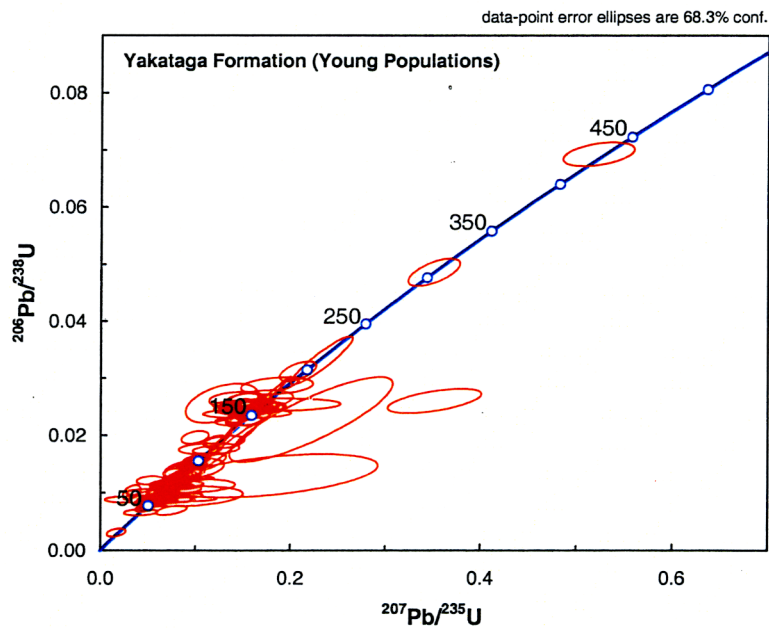


Figure 29 [A], [B]. Concordia diagrams for samples analyzed from the Yakataga Formation.

Diagram [A] Shows all determined U/Pb crystallization ages (Ma) and Diagram [B] Larger-scale version showing a close-up of younger age populations. Plots were generated using the Isoplot software (Ludwig, 1980; 2001; 2003).

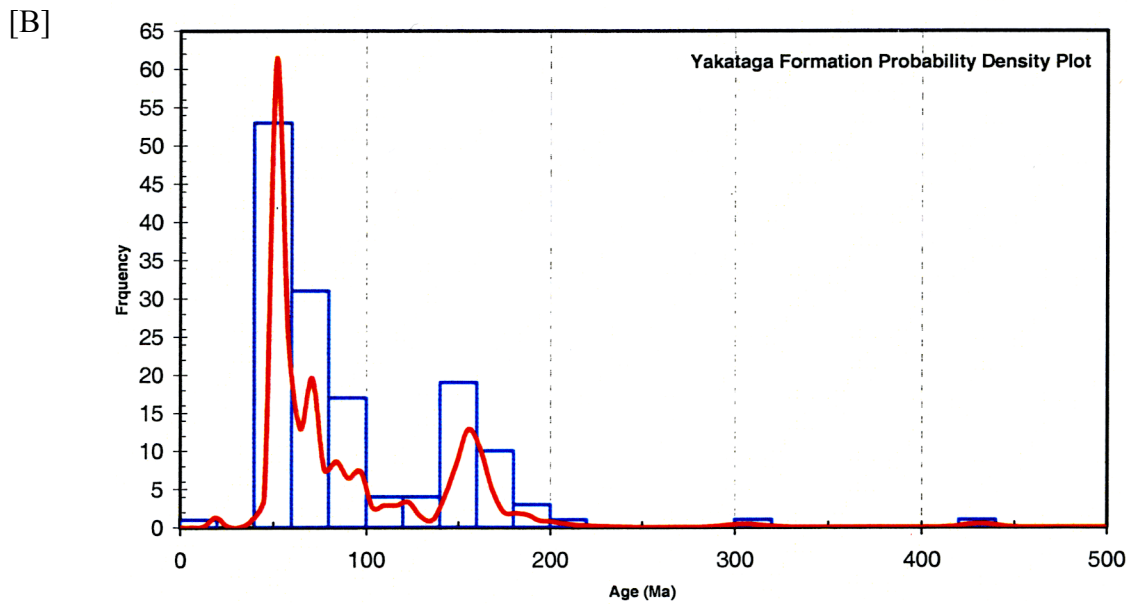
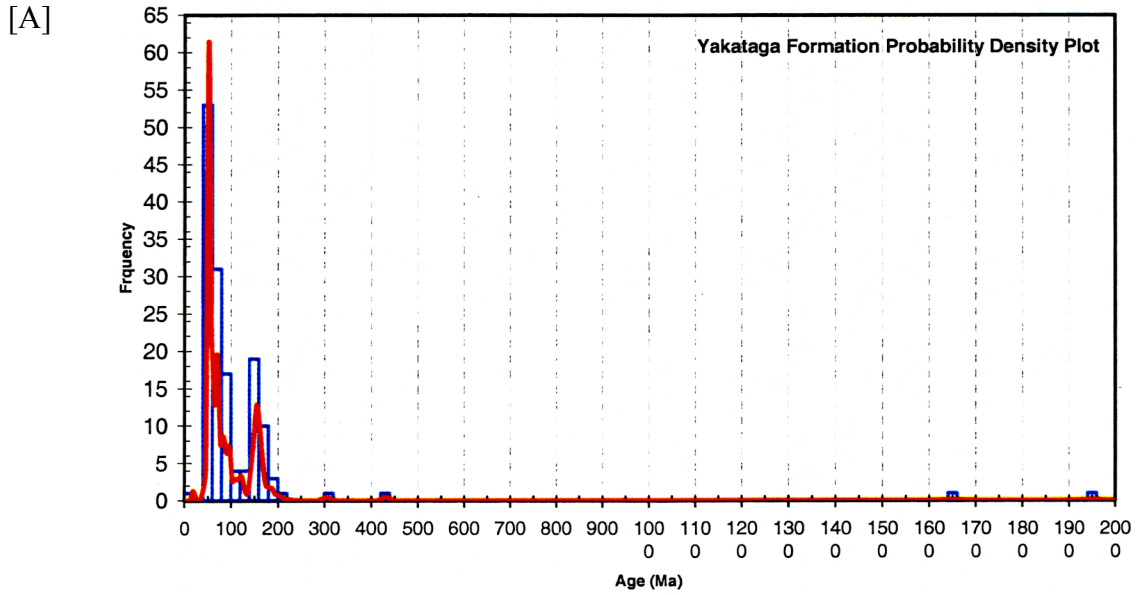


Figure 30 [A], [B]. Histogram probability plots for the Yakataga Formation with U/Pb age (Ma) plotted against frequency of determinations in each age range. Diagram [A] All ages determined and Diagram [B] Larger-scale view of younger age populations. Plots were generated using the Isoplot program (Ludwig, 1980; 2003).

feldspar (F), volcanic-lithic fragments (L_v), sedimentary-lithic fragments (L_s), metamorphic-lithic fragments (L_m), and total lithic fragments ($L_t = L + Q_p$) (Table 6; Figure 31 [A], [B]; Figure 32 [A], [B]) (Folk, 1974).

Kulthieth Formation

The Kulthieth Formation is an arkosic-rich sandstone with a QFL ratio of 38-48-14% (Table 6) (see Folk, 1974). The Kulthieth Formation is low in lithics with very few volcanic grains (Figure 33 [A], [B]). Accessory minerals include epidote, sphene, titanite, apatite, and zircon. Monocrystalline quartz and polycrystalline quartz were divided and a Q_mFL_t and $Q_pL_{vm}L_{sm}$ diagrams were constructed. Results show that the Kulthieth Formation is rich in quartz varieties, feldspars, and has considerable epidote.

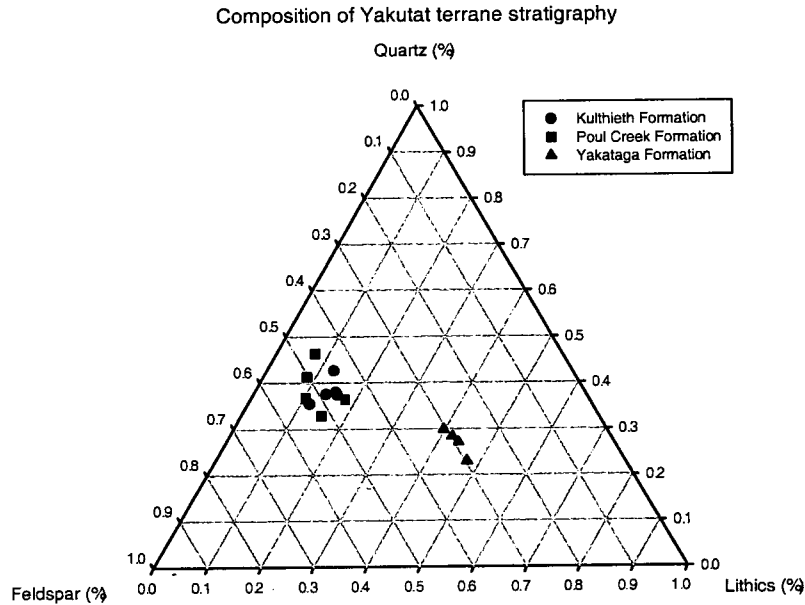
Poul Creek Formation

Sandstones in the Poul Creek Formation are arkosic and have a QFL ratio of 39-50-12%. The formation is rich in feldspars, especially K-feldspar, and low in lithics almost identical in composition to the underlying Kulthieth Formation (Table 6). Metamorphic and sedimentary lithics are locally altered but not enough to overprint the original mineral present. There were significant amounts of glauconite in every thin section analyzed (Figure 34 [A], [B]). Accessory minerals include epidote, sphene, titanite, actinolite, apatite, and zircon. Mica is abundant in the form of biotite and chlorite with a few grains of muscovite present.

Table 6. Summary of sedimentary petrographic analysis.

Formation	Sample	Q	Q %	Qm	Qm %	Qt	Qund	Qund	*Qp	F	F %	L	L %	Lt	Lt %	QFL #				
Yakataga	05-09	31	0.22963	31	0.19	63	27	4	32	40	0.30	64	0.47	91	0.56	135				
Yakataga	05-10	39	0.27083	39	0.23	60	35	4	21	42	0.29	63	0.44	92	0.53	144				
Yakataga	05-11	43	0.29861	43	0.24	56	41	2	13	44	0.31	57	0.40	92	0.51	144				
Yakataga	05-12	46	0.28395	46	0.25	68	46	0	22	48	0.30	68	0.42	92	0.49	162				
Poul Creek	05-13	55	0.41353	55	0.26	71	53	2	16	67	0.50	11	0.08	89	0.42	133				
Poul Creek	05-15	43	0.36752	43	0.22	68	43	0	25	62	0.53	12	0.10	90	0.46	117				
Poul Creek	05-16	51	0.36429	51	0.25	69	50	1	18	64	0.46	25	0.18	90	0.44	140				
Poul Creek	05-07	51	0.46364	51	0.27	81	49	2	30	51	0.46	8	0.07	89	0.47	110				
Poul Creek	05-08	48	0.32877	48	0.22	78	47	1	30	76	0.52	22	0.15	90	0.42	146				
Kulthieth	05-01	44	0.37607	44	0.24	74	35	9	30	57	0.49	16	0.14	84	0.45	117				
Kulthieth	05-03	43	0.35537	43	0.22	71	42	1	28	64	0.53	14	0.12	91	0.46	121				
Kulthieth	05-04	45	0.375	45	0.24	74	38	7	29	56	0.47	19	0.16	88	0.47	120				
Kulthieth	05-06	61	0.42657	61	0.29	84	54	7	23	64	0.45	18	0.13	89	0.42	143				
Kulthieth	05-17	40	0.38095	40	0.24	70	40	0	30	49	0.47	16	0.15	80	0.47	105				
Yakataga	05-09	33	0.83	0.34	0.59	142	37	26	63	44	42	30	64	41	64.1	22	34.4	1	1.6	
Yakataga	05-10	36	0.86	0.35	0.63	142	38	27	63	44	41	29	63	41	65.1	22	34.9	0	0.0	
Yakataga	05-11	37	0.84	0.23	0.68	139	38	27	57	41	44	32	57	44	77.2	13	22.8	0	0.0	
Yakataga	05-12	36	0.75	0.22	0.56	159	38	24	68	43	53	33	68	53	77.9	15	22.1	0	0.0	
Poul Creek	05-13	48	0.72	0.36	0.49	50	35	70	8	16	7	14	11	4	36.4	4	36.4	3	27.3	
Poul Creek	05-15	46	0.74	0.17	0.53	56	36	64	10	18	10	18	12	8	66.7	2	16.7	2	16.7	
Poul Creek	05-16	44	0.69	0.24	0.52	78	36	46	23	29	19	24	25	17	68.0	6	24.0	2	8.0	
Poul Creek	05-07	48	0.94	0.38	0.43	45	35	78	5	11	5	11	8	2	25.0	3	37.5	3	37.5	
Poul Creek	05-08	45	0.59	0.36	0.46	70	36	51	20	29	14	20	22	12	54.5	8	36.4	2	9.1	
Kulthieth	05-01	42	0.74	0.25	0.41	50	30	60	8	16	12	24	16	4	25.0	4	25.0	4	50.0	
Kulthieth	05-03	41	0.64	0.07	0.52	63	37	59	13	21	13	21	14	12	85.7	1	7.1	1	7.1	
Kulthieth	05-04	51	0.91	0.37	0.46	55	34	62	12	22	9	16	5	31.3	7	43.8	4	25.0	4	25.0
Kulthieth	05-06	64	1.00	0.39	0.42	61	35	57	15	25	11	18	8	8	44.4	7	38.9	3	16.7	
Kulthieth	05-17	48	0.98	0.06	0.37	45	26	58	4	9	15	33	16	3	18.8	1	6.3	12	75.0	

[A]



[B]

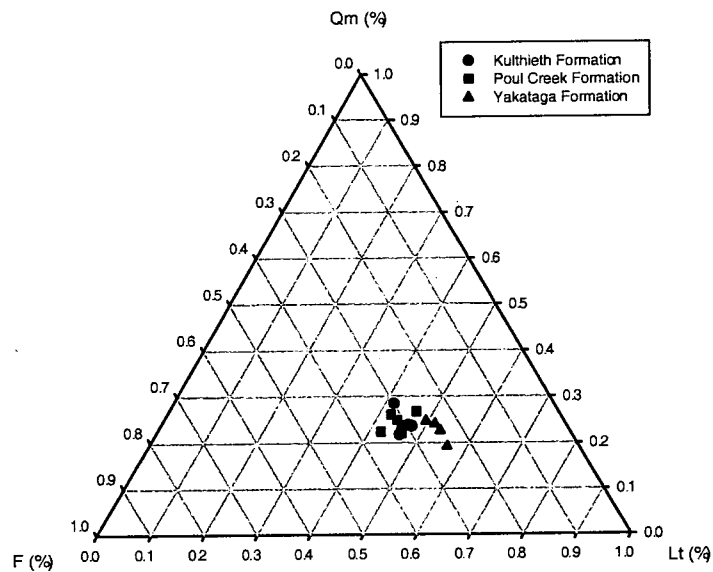
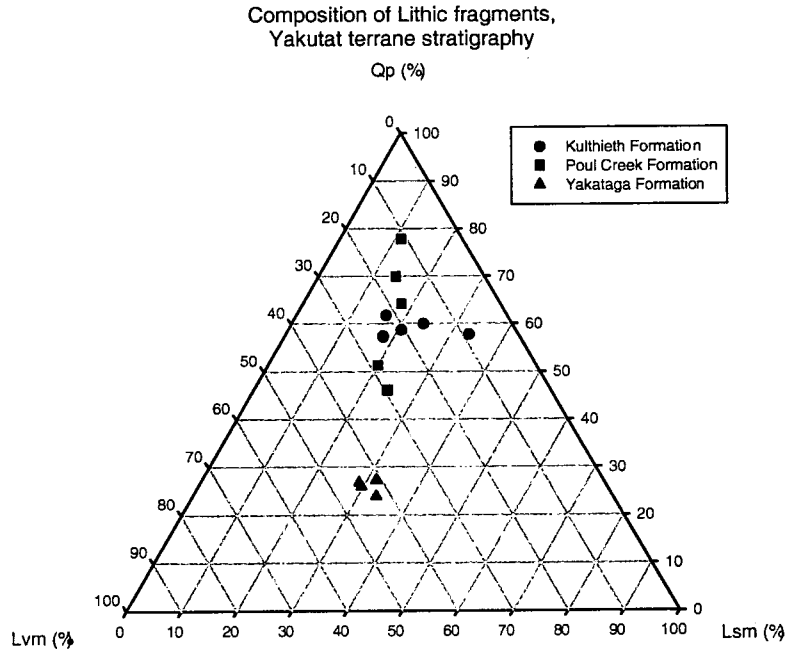


Figure 31 [A], [B]. Compositional characteristics of the Kulthieth, the Poul Creek, and the Yakataga Formations, southern Alaska. Diagram [A] QFL – Quartz (monocrystalline and polycrystalline quartz), feldspar and lithic grains; [B] Q_mFL_t – monocrytalline quartz, feldspar and total lithic fragments (includes polycrystalline quartz). The Kulthieth and Poul Creek Formations are characterized as arkosic sandstones and the Yakataga Formation as a lithoarenite sandstone (Folk, 1974).

[A]



[B]

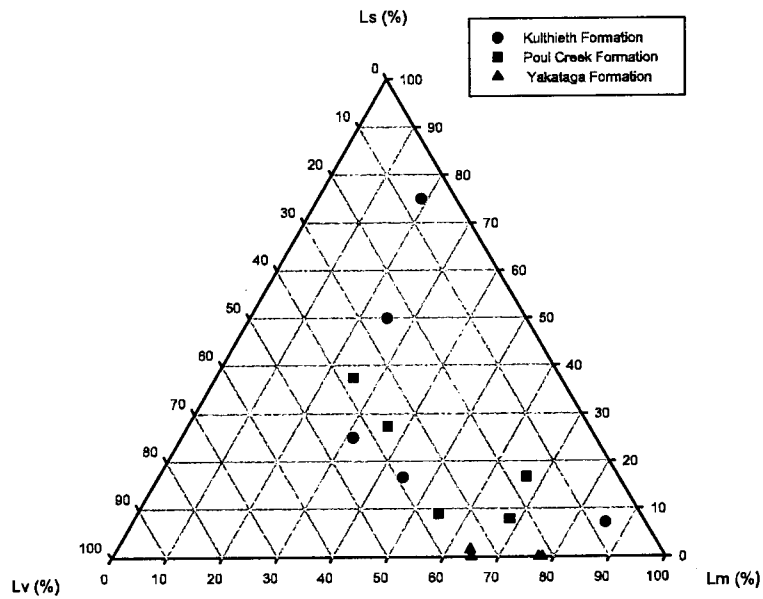
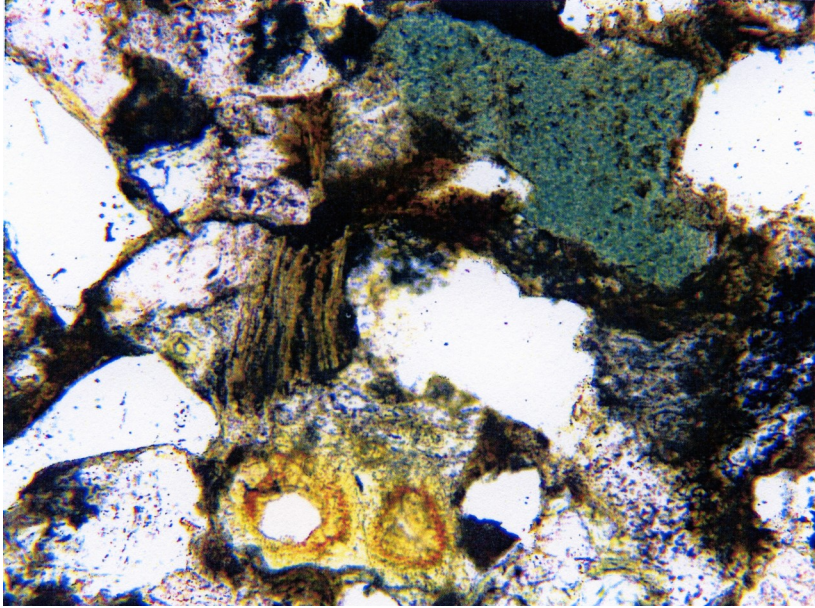
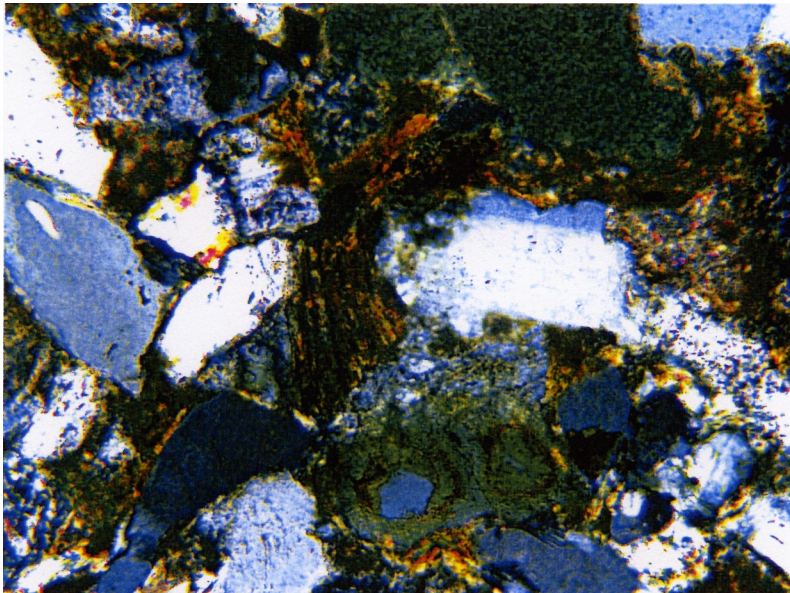


Figure 32 [A], [B]. Compositional characteristics of the Kulthieth, the Poul Creek, and the Yakataga Formations, southern Alaska. Diagram [A] $Q_p L_{vm} L_{sm}$ – Polycrystalline quartz, Volcanic and metavolcanic lithic fragments, and Sedimentary and metasedimentary lithic fragments; Diagram [B] $L_s L_v L_m$ – Sedimentary lithic, Volcanic lithic, and Metamorphic lithic.

[A]



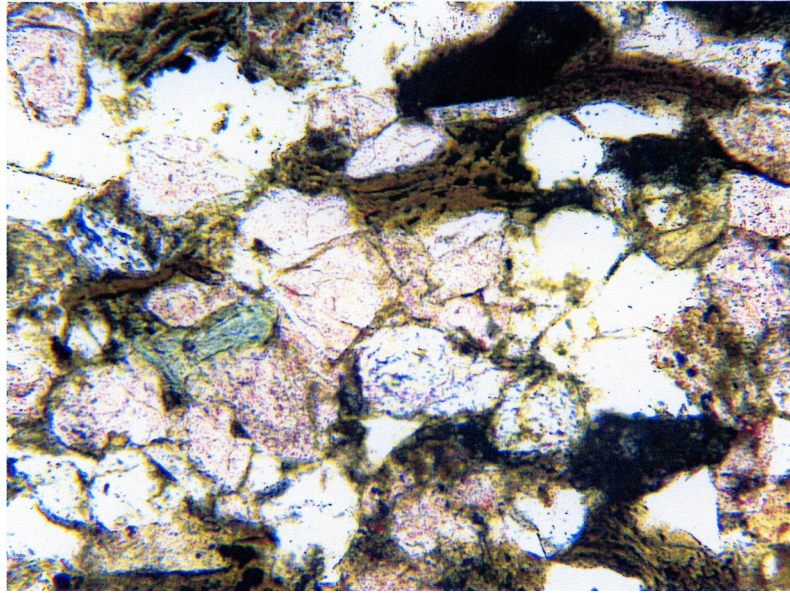
[B]



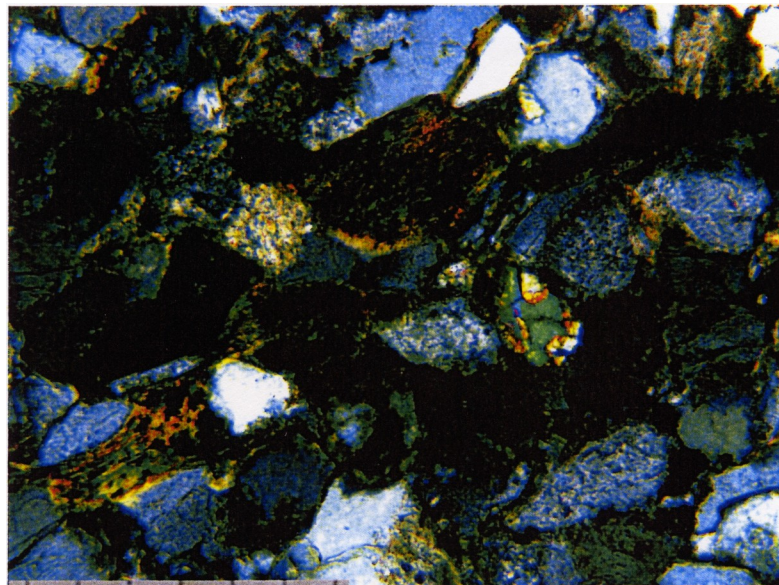
0.01mm at 125x (1 mark = 10 microns)

Figure 33 [A], [B]. Photomicrograph of an arkosic sandstone from the Kulthieth Formation. Diagram [A] was taken in plane light and Diagram [B] in cross-polarized light. Note the abundance of Ca, Na and K-feldspar with biotite and undulatory and polycrystalline quartz fragments. The thin section also contains glauconite fragments identified in plane polars by the green-colored, glassy-structure characteristics.

[A]



[B]



0.01mm at 125x (1 mark = 10 microns)

Figure 34 [A], [B]. Photomicrograph of an arkosic sandstone from the Poul Creek Formation. Diagram [A] was taken in plane light and Diagram [B] in cross-polarized light. Note the abundance of Ca, Na and K-feldspar with biotite and undulatory and polycrystalline quartz fragments. The thin section also contains abundant epidote characterized by 3rd order birefringence colors in cross-polarized light.

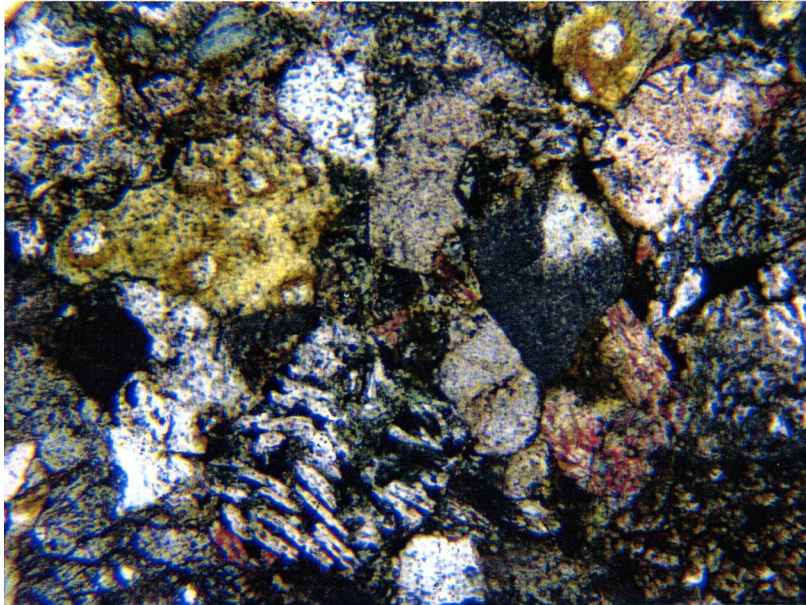
Yakataga Formation

The Yakataga Formation sandstones are lithoarenites with a QFL ratio of 22-24-35%. The QFL ratio is different than underlying Poul Creek and Kulthieth Formations because the unit clearly has more lithics (broken down into $L_vL_sL_m$ and $Q_pL_{vm}L_{sm}$ ternary diagrams) (Table 6). In some thin sections, severe alteration of volcanic grains is seen, commonly to the point of rendering the section unrecognizable. Some volcanic grains are basalt or mafic. Mica includes muscovite, biotite and chlorite with muscovite being the dominant grain types. A common mineral assemblage includes quartz-feldspar-garnet-muscovite, indicating possible amphibolite facies metamorphic rocks in the source (Figure 35 [A], [B]). Minor actinolite and hornblende are also identified.

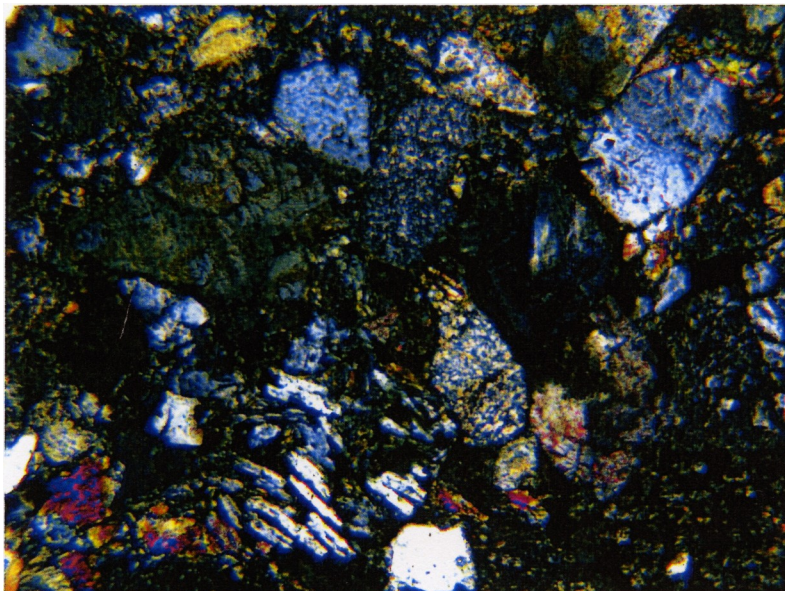
Vitrinite Reflectance

Samples 05-01, 05-03, and 05-04 from the Kulthieth Formation, and sample 05-07 from the Poul Creek Formation were analyzed for vitrinite reflectance on isolated kerogen to determine the degree of heating these samples experienced. Sample 05-01 (taken from Donald Ridge) was an orange-brown color with poor preservation and a Total Alteration Index (TAI) of 2+ (slight alteration) based on 20 total readings. The source material consisted of 88% amorphinite debris, 10% woody plant debris, and 2% coaly fragments and contained an abundant amount of palynomorphs. It was determined to be a nearshore palynofacies with a 3% OM Fluorescing and a measured R_o (%) of 0.56%.

[A]



[B]



0.01mm at 125x (1 mark = 10 microns)

Figure 35 [A], [B]. Photomicrograph of a lithoarenite sandstone from the Yakataga Formation. Diagram [A] was taken in plane light and Diagram [B] in cross-polarized light. Note the abundance of polycrystalline quartz fragments and volcanic lithic fragments. The thin section contains a lathwork volcanic grain characterized by interstitial growth patterns of individual fragments within the grain.

Sample 05-03 was collected from the Kulthieth Formation north of Donald Ridge, was orange-brown in color, and had a TAI of 2+ (slight alteration) based on 3 readings. The sample consisted of 93% amorphinite debris, 5% woody plant debris, 2% coaly fragments and has a typical amount of palynomorphs. The preservation of the sample was poor and was determined to represent a nearshore palynofacies. The % OM Fluorescing was zero and the measured R_o value (%) was 0.66% (Table 7).

Sample 05-04 was collected from the Kulthieth Formation in the Northern Robinson Mountains, was orange-brown in color, and has a TAI of 2+ (slight alteration) based on 7 readings. The percent source material consisted of 100% coaly fragments with common palynomorphs, poor preservation, and represented a continental palynofacies. The % OM Fluorescing was zero and the measured R_o (%) was 0.71% (Table 7).

Sample 05-07 was collected from the Poul Creek Formation in the Northern Robinson Mountains at an elevation of 4533 feet and lies stratigraphically above the Kulthieth Formation. The Total Organic Carbon (TOC) of this sample was 0.18 with a TAI of 2+ (slight alteration) based on 17 readings. The sample was orange-brown and the source material consisted of 5% amorphinite debris and 95% coaly fragments with no palynomorphs seen. Preservation was poor, the % OM Fluorescing was zero with a measured R_o (%) of 0.64 and was determined to represent a continental palynofacies (Table 7).

Table 7. Dispersed Organic Matter Thermal Alteration, Kerogen Type and Total Compositional Analysis

Union College

HGS ID	Well Name	Depth (ft.)		Source Quality				% Source Material						Preservation			Recovery				Palynofacies			Vitrinite					
		1	2	TOC	S2	Hydrogen Index (HI)	Tmax (°C)	Color	TAI	Amorphinite Debris	Finely Dissem. OM	Herb. Plant Debris (VH.)	Woody Plant Debris	Coaly Fragments	Algal Debris	Palyomorphs	Good	Fair	Poor	Very Poor	Barren	MARINE	NEARSHORE	CONTINENTAL	LACUSTRINE	UNKNOWN	% OM Fluorescing	Measured Ro(%)	No. of Readings
06-3473-135864	AL05-01							OB	2+	88		10	2	A	X							X					3	0.56	20
06-3473-135865	AL05-03							OB	2+	93		5	2	C	X							X					0	0.66	3
06-3473-135866	AL05-04							OB	2+			100		C	X							X				0	0.71	7	
06-3473-135867	AL05-07			0.18				OB	2+	5		95		N	X							X				0	0.64	17	

*Tmax data not reliable due to poor S2 peak

tr = trace

Color Abbreviations:

- GLY Green-Light Yellow
- Y Yellow
- YO Yellow-Orange
- OB Orange-Brown
- LB Light Brown
- B Brown
- DBDG Dark Brown-Dark Gray
- DGBL Dark Gray-Black
- BLK Black

TAI Scale:

- 1=Unaltered
- 1+ or 1.5
- 2=Slight alteration
- 2+ or 2.5
- 3=Moderate alteration
- 3+ or 3.5
- 4=Strong alteration
- 4+ or 4.5
- 5=Severe alteration

Palyomorph Key

- A=Abundant
- C=Common
- R=Rare
- N=Not seen

INTERPRETATION

Kulthieth and Poul Creek Formations

Sandstones of the Kulthieth and Poul Creek Formations are rich in K-feldspar and quartz and are virtually identical in terms of sedimentary petrography, DZFT ages, and U/Pb ages of detrital zircon. These overall findings suggest that the Kulthieth and Poul Creek Formations received sediment from a similar source. Deposition of the Poul Creek and Kulthieth Formations spanned the Late Eocene to Early Miocene suggesting that the primary source terrain was long-lived and provided sediment with uniform characteristics for this entire interval.

DZFT and U/Pb age populations are almost identical in the Kulthieth and Poul Creek Formations. The Paleocene to Cretaceous DZFT peak ranges from ~58-96 Ma in the Kulthieth Formation and ~55-67 Ma in the Poul Creek Formation. The Eocene DZFT peak, which comprises about 50% of all grains analyzed, ranges from ~38-45 Ma in the Kulthieth Formation and ~33-42 Ma in the Poul Creek Formation (Table 3). U/Pb age populations for the grains that make the DZFT Eocene peak in both the Kulthieth and the Poul Creek Formations are ~59 Ma, ~71 Ma, ~94 Ma, and ~147-159 Ma (Figure 20). The similarity in both cooling age populations and crystallization ages implies a long-lived source terrane that shed >50% of the zircons analyzed onto the Yakutat terrane in the Tertiary (Figure 36; Figure 37).

Comparison of U/Pb ages for DZFT dated vs. Non-DZFT dated zircon grains

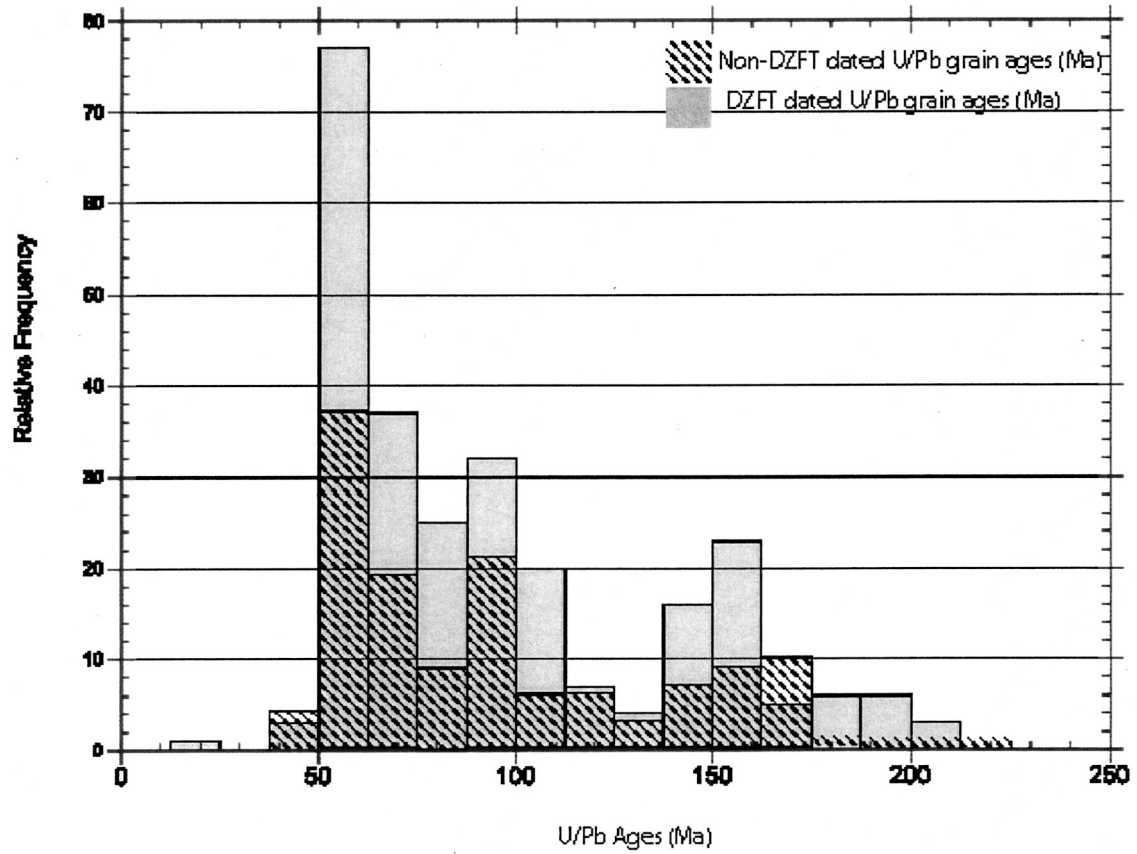


Figure 36. Comparison of U/Pb age distribution of grains that were dated by the DZFT system versus grains that were selected randomly for U/Pb analysis.

U/Pb grain-age distribution comparison

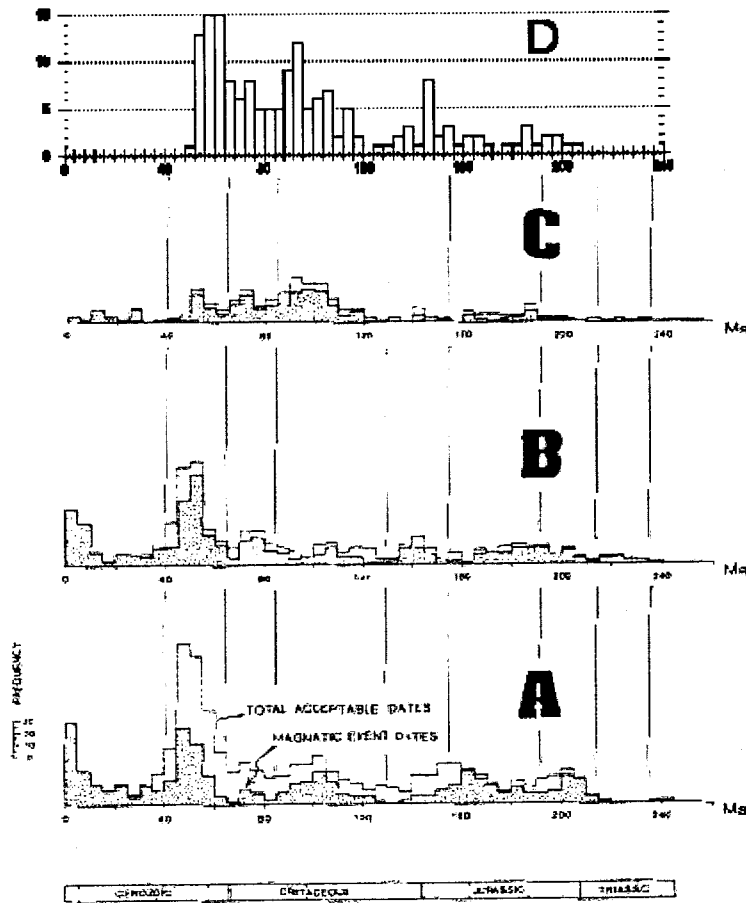


Figure 37. U/Pb distribution represented in the Kulthieth and Poul Creek samples of the Yakutat terrane versus the U/Pb age distribution represented in the northern Coast Plutonic Complex (CPC) (modified from Armstrong, 1988). [A] Represents the U/Pb distribution typical of the southern portion of the CPC; [B] Represents the middle portion of the CPC; [C] Represents the northern portion of the CPC located close to the southeastern Alaska panhandle; [D] Represents the U/Pb data represented in the stratigraphy of the Yakutat terrane.

Analysis of the Miocene DZFT population in the Kulthieth and Poul Creek Formations shows much greater variation. The Miocene peak ranges from ~22-31 Ma in the Kulthieth Formation (12-80% of the grains) and ~24-29 Ma in the Poul Creek Formation (36-40% of the grains). These peaks are generally similar in age in each unit, but the percentage varies widely from 18-80%. Therefore these peaks are generally minor and variable in the percentage of zircon grains that represent them.

The Miocene DZFT ages represent an important proxy for the depositional age of the Kulthieth and Poul Creek Formations provided these young ages represent source rock cooling and not in situ resetting. For the Poul Creek Formation this is an important caveat because a tongue of the Cenotaph Volcanics occurs in the Poul Creek Formation to the west (but not in the study area), and therefore is a reason to carefully consider its thermal history. The non marine Cenotaph volcanics and marine equivalent Topsy Formation are located from Fairweather Glacier to Topsy Creek to Icy Point and are mainly abundant around the Lituya Bay area (MacKevett, Brew, Hawley, Huff and Smith, 1971). The volcanics are believed to be postearly Oligocene to premiddle Miocene in age and range in thickness from ~1,200 to 4,400 feet (MacKevett, Brew, Hawley, Huff and Smith, 1971).

Our best clue comes from vitrinite reflectance studies which generally show the unit in the study area remained below temperatures required for annealing. Based on vitrinite reflectance analysis it is unlikely that temperatures were in excess of ~160°C for both the Kulthieth and the Poul Creek Formations. A map outlining vitrinite reflectance values for the stratigraphy throughout the Northern Robinson Mountains suggests thermal maturity for the Kulthieth Formation ranges anywhere from $R_o = 0.37-3.41\%$ translating

to a temperature range of ~44-275°C (Johnsson, Pawlewicz, Harris and Valin, 1992; Johnsson and Howell, 1996). These upper values are well within the range to reset fission-tracks in zircon. However, vitrinite reflectance on three samples used for both DZFT and U/Pb analysis yield much lower values for in situ organic material of $R_o = 0.49-0.80\%$ (~40-160°C) (Palmer, 1983; Johnsson and Howell, 1996). According to these new vitrinite reflectance results, the stratigraphic unit in the study area did not experience enough heating to reset the zircon fission-track system, even partially. A single indigenous vitrinite reflectance population in sample 05-04, yielded a value of $R_o = 0.80-1.00\%$ or ~150-200°C. For very radiation-damaged grains these conditions would be sufficient to reset fission-tracks (Bernet and Garver, 2005). Radiation-damaged grains have a lower annealing temperature, so it is possible to reset damaged grains as low as ~180-200°C (Garver et al., 2005). If radiation-damaged grains were reset, these reset grains should have the oldest U/Pb-determined ages, generally >100 Ma, because only very old grains with typical uranium concentration would have accumulated sufficient alpha-damage (see discussion in Garver et al., 2005). However, because the U/Pb ages are generally less than ~50-97 Ma it would be unlikely that these grains from this single sample are reset in situ because they only would have ~20-70 million years to accumulate damage.

For the Poul Creek Formation, the DZFT Miocene cooling age population (~24-29 Ma) is within the fossil age range of the unit (minimum age of Pliocene). These young cooled grains of the Miocene peak have the same U/Pb age distribution as those that represent the Eocene peak in both formations (i. e. crystallization at ~59 Ma, ~71 Ma, ~94 Ma, and ~147-159 Ma). U/Pb age comparison shows that the source terrain has a

long-lived Early Cretaceous to Paleocene crystallization age geochronological signal. The Miocene peak does not represent a volcanic source, but they could represent older rocks heated by young volcanics.

Therefore, possible sources of the Miocene DZFT population has one of two characteristics: 1) a variable, rapidly exhuming young source terrain; or 2) sub-volcanic or hypabyssal intrusions, which reset near-surface rocks that had a wide range of crystallization ages. The former (rapid exhumed source) is not obvious from the literature, but it may be represented by local rapidly exhumed rock along the Queen Charlotte-Fairweather fault system. Plenty of source rocks exist for the later near surface volcanic resetting because deposition of the Poul Creek Formation coincides with isolated plutonism and volcanism near the present coastline from Washington to Alaska. The important point is that the lack of volcanic grains within the young Miocene peak rules out a volcanic-dominated source for deposition of the Kulthieth and Poul Creek Formations.

Analysis of the Eocene populations (~58-96 Ma in the Kulthieth Formation, ~55-67 Ma in the Poul Creek Formation) and Oligocene (~38-45 Ma in the Kulthieth Formation, ~33-42 Ma in the Poul Creek Formation) peak age populations helps reveal details of the source terrain. By comparing the DZFT and U/Pb age results for the Oligocene peak (>50% of zircon grains represented) the Kulthieth and Poul Creek Formations are almost identical. U/Pb ages of the same grains analyzed by the DZFT method yield concordant age populations of ~59 Ma, ~71 Ma, ~94 Ma, and ~147-159 Ma. These U/Pb ages are all older (most much older) than all single grain DZFT determinations suggesting that these populations are not volcanic but are exhumed rock.

The Eocene fission-track populations represent a range of U/Pb crystallization ages mainly between 50-100 Ma (see Figure 21), and therefore it is likely that this source has an Eocene-cooled sequence of Cretaceous plutons.

If deposition of the Kulthieth and the Poul Creek Formations is within the bounds of the fossil age constraints, lag-time (cooling to deposition) can be established for peak ages. Assuming several key parameters, exhumation rates can be estimated for the Kulthieth and Poul Creek Formations. These assumptions include: 1) a geothermal gradient of 25°C/km; 2) a ZFT closure temperature of 240°C; and 3) that the Miocene peak age range is a proxy for depositional age. These parameters provide estimated exhumation rates (for the Eocene peak) of 350-1250 m/my for the Kulthieth Formation and 400-1250 m/my for the Poul Creek Formation, with a mean exhumation rate ~750 m/my. Therefore, the potential source terrain must have been exhumed moderately rapidly in the Eocene to Oligocene.

Yakataga Formation

Sedimentary petrography on the Yakataga Formation suggests that intermixing of one or more sediment sources resulted in the rapid deposition and accumulation of >5000 meters of strata (Plafker, 1987; Eyles and Lagoe, 1990; Harbor and Warburton, 1993). The Q_{FL} and Q_pFL_t ratios are similar to the Poul Creek and Kulthieth Formations (Figure 31 [A], [B]). However, the Yakataga Formation is more lithic rich, and a big difference is revealed when total lithics are divided into $L_vL_sL_m$ and $L_{vm}L_{sm}L_t$ ternary diagrams (Figure 32 [A], [B]). These diagrams show a largely metamorphic and volcanic sediment

source signal unlike that of the Poul Creek and Kulthieth Formations. This lithic source recorded in the Yakataga Formation is likely greenschist to amphibolite facies metamorphic rocks based on accessory mineral assemblages such as garnet, chlorite, actinolite and muscovite (Figure 35 [A], [B]).

All Yakataga Formation samples have multiple age populations. Three populations include: Middle Miocene (Peak 1) ~15-17 Ma (~40%); Peak 2 at ~21-30 Ma (only one sample); Oligocene (Peak 3) at ~30-35 Ma (~30-50%); and a minor older Eocene population (Peak 4) between 68-77 Ma (11-30%). The older Oligocene and Eocene age populations (Peak 2, Peak 3 and Peak 4) are statistically identical to DZFT cooling ages in the underlying Poul Creek and Kulthieth Formations. However, the young Middle Miocene population (Peak 1) is unique and distinctive to the Yakataga Formation. So, at this point it is useful to consider separately the older peaks (Peak 2, 3, and 4) in relation to those in the Kulthieth and Poul Creek Formations and the young peak which is unique to the Yakataga Formation.

U/Pb crystallization ages were compared to DZFT cooling ages for specific grain age populations to determine if the source(s) of the older Peak 2, Peak 3 and Peak 4 were influenced strongly by either volcanic or plutonic activity. U/Pb-LA-ICPMS determined ages range from Cretaceous to Early Tertiary ages suggesting the original source of sediment to the Yakataga Formation is similar if not identical to that of the Poul Creek and Kulthieth Formations. Results also show that U/Pb crystallization ages do not yield similar DZFT cooling ages for specific grains analyzed and therefore these ages do not represent deposition of a volcanic source.

The young Middle Miocene DZFT population (~20 Ma) occurs only in the Yakataga Formation. U/Pb ages on the same grains used for DZFT analysis indicate the original crystallization ages range from the Cretaceous to the Early Tertiary with a distinct population of ages from 50-55 Ma (Figure 38). The Cretaceous to Early Tertiary U/Pb crystallization age populations represent an exhumed source terrain, not a volcanic source. The large population of U/Pb crystallization ages of ~50-55 Ma most likely represents a provenance source associated with the superimposed Sanak-Baranof Plutonic Belt located from the Kodiak Islands to the southeastern Alaska panhandle. This belt has numerous plutons within the current location of the Yakutat terrane that were emplaced at ~50 Ma (Bradley et al., 2003; Madsen et al., 2006).

Of the 150 grains double-dated for the Yakataga Formation, only a single grain with a similar Early Tertiary DZFT (9.8 Ma $-6.1/+15.2$) and U/Pb age (~19 Ma ± 3.0) (both within 2 sigma) may represent derivation from a volcanic source. Because distinctive clasts in the Yakataga Formation can be linked to the adjacent Chugach-Prince William composite terrane, it is likely that much or most of this unit is derived from the collisional belt (Plafker, 1987; Nokleberg et al., 2005). Therefore, this ~20 Ma peak suggests deposition associated with the erosion of the Chugach terrane. If this is the case, this result indicates that much or most of the Chugach rocks within the Chugach terrane have been thermally reset in the Tertiary. This resetting was most likely driven by early Tertiary plutonism and metamorphism within the Chugach terrane (Armstrong, 1988; Cook, Crawford, Omar and Crawford, 1991; Plafker, 1994).

U/Pb age comparison of the Late Miocene DZFT determined population
in the Yakataga Formation vs. all U/Pb ages for the Kulthieth and Poul Creek Formations

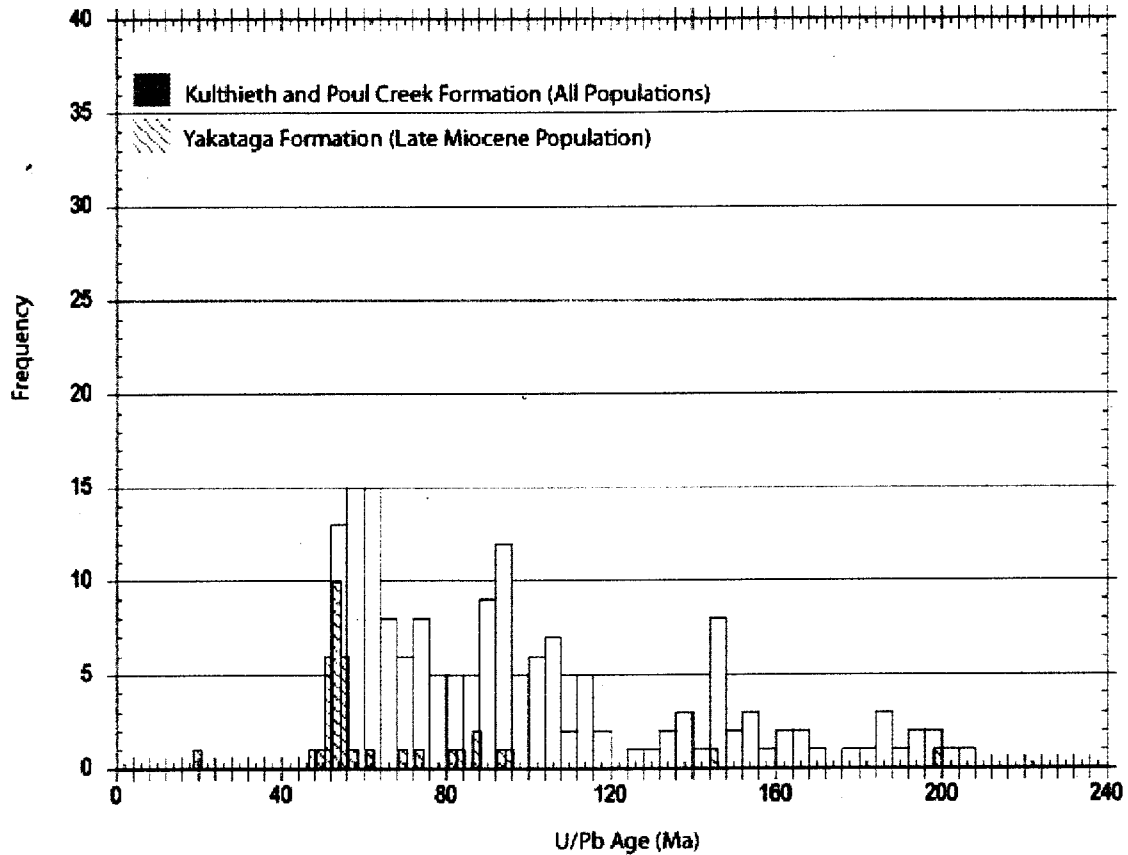


Figure 38. Histogram diagram comparing all U/Pb age determinations in the Kulthieth and Poul Creek Formations to the U/Pb grain age distribution for the DZFT determined Late Miocene population in the Yakataga Formation. The Kulthieth and Poul Creek Formations have a long-lived continuous crystallization record whereas in comparison the Yakataga Formation Late Miocene population has a distinct distribution from ~50-53 Ma.

REGIONAL CONSIDERATIONS

There are two mutually exclusive models for the translation of the Yakutat terrane from the Late Eocene to the Recent. One hypothesis, here the southern option, suggests that the Yakutat terrane originated somewhere off the coast of northern California to Washington and experienced continuous displacement from ~45 Ma to the Recent (Bruns, 1983). The other hypothesis, here the northern option, suggests a more conservative short-traveled displacement from the Late Eocene to the present (Figure 39) (Plafker, 1994). Both models agree that the Yakutat terrane collided with Cretaceous to Early Tertiary accretionary complex of the Chugach-Prince William composite terrane that formed the southern part of the Alaskan continental framework from the Pliocene to the present. The crucial difference between these models is the translation history of the Yakutat block.

The southern far-traveled hypothesis assumes that the Yakutat originated at or near the Farallon-Pacific boundary and moved on the Pacific plate since the Eocene (Bruns, 1983). The northern option assumes some continuity of the block with the Chugach-Prince William composite terrane, and allows only reasonable reconstruction southward on faults with known displacement (i. e. 225km of Queen Charlotte-Fairweather Fault (see discussion in Plafker et al., 1994) (Figure 40).

Double-dating of detrital zircon grains from the stratigraphic units of the Yakutat terrane provides some fundamental conclusions about possible source terrains and terrane movement. Two important conclusions can be made. 1) U/Pb versus DZFT ages virtually everywhere in the stratigraphy show that the terrane was never adjacent to a significant

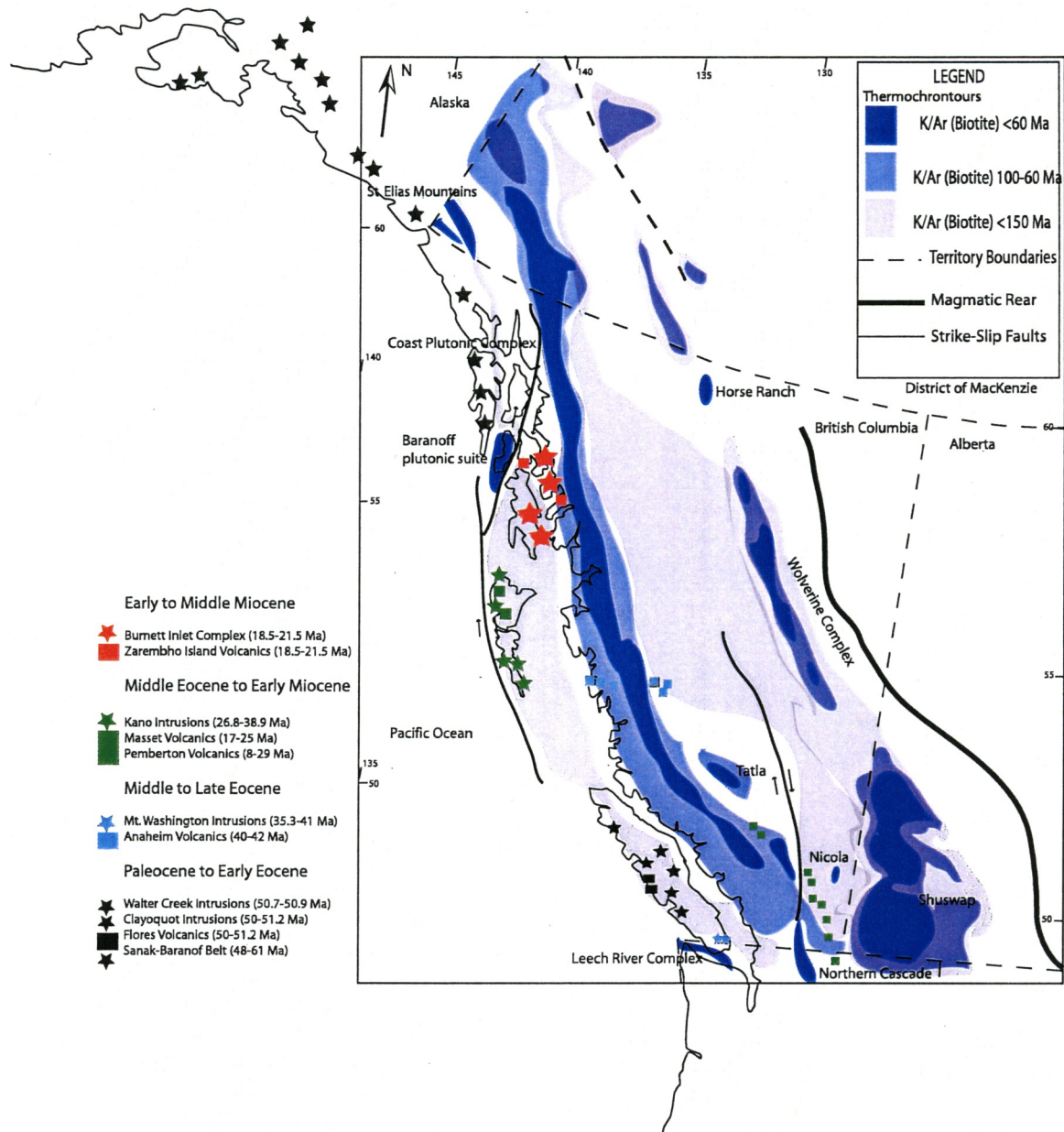
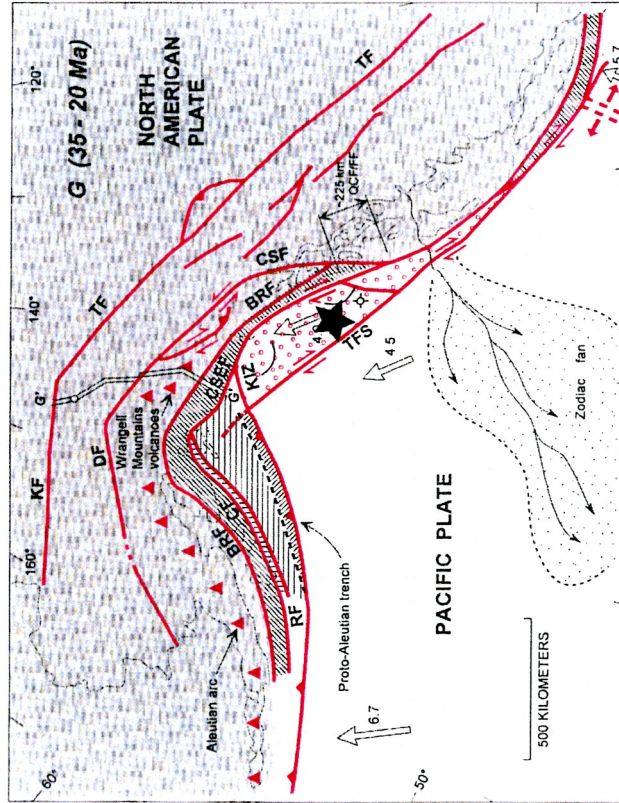


Figure 39. Map of British Columbia outlining locations of major tectonic and plutonic events and thermochronotour distribution associated with the evolution of the Coast Plutonic Complex (modified from Madsen, Thorkelson, Friedman and Marshall 2006; Armstrong, 1988).

Northern In Situ Translation Model (Plafker et al., 1994)



Southern Long-Transport Translation Model (Bruns, 1994)

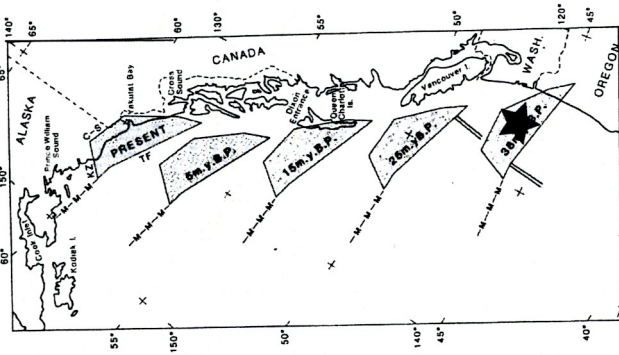


Figure 40. Two opposing models for Yakutat terrane translation. The black star represents the approximate location of samples collected in this study. The northern *in situ* model suggests little to no translation and would be represented by a long-lived, continuous, uniform provenance signal throughout time (Plafker et al., 1994). The southern long-transport model would be represented by a more complex provenance signal because of the continuous motion required for the terrane to be translated to southeastern Alaska (Bruns, 1983). This signal would include DZFT cooling age populations of ~40 Ma (Cascade Arc) and ~48 Ma (Challis volcanics) and would contain numerous volcanic grains.

volcanic source terrain; 2) much or most of the stratigraphy (Kulthieth and Poul Creek Formations) have a very similar provenance that indicates a uniform source fed the basin over a long interval of time. If the Yakutat terrane originated off the coast of northern California or Washington, then the stratigraphy should have captured sediment shed off of the Cascade Arc and the southern Coast Plutonic Complex (CPC) on the early part of its journey (Eocene-Oligocene) (Figure 37; Figure 39). The Cascade Arc consists of two sectors all of which has been built since about 40 Ma. To the south of Mt. Rainier in Washington, they are almost entirely volcanic rocks and volcanoclastic sediment (i. e. Madsen et al., 2006). To the north, from Mt. Rainier to Garibaldi in southern British Columbia, it consists of abundant Tertiary volcanics and plutons on a pre-Tertiary basement (Madsen et al., 2006). In either case this area can be ruled out as a potential source for the Yakutat terrane due to the lack of volcanic signal in the Yakutat stratigraphy. A large volume of Eocene volcanic rocks exist behind the Cascade Arc and these clearly imprint a cooling age signal on sediments that by-pass the arc and make it to offshore basins (Brandon and Vance, 1992; Garver and Brandon, 1994). The British Columbia Ranges, largely composed of the Coast Plutonic Complex, has a very distinct cooling age signal that changes from south to north (i. e. Parrish, 1983). In general the southern CPC has ZFT cooling age of 40 Ma, moderate rates of implied exhumation and a clear and distinct volcanic signal associated with the superimposed Cascade Arc.

The northern CPC (north of Prince Rupert) has moderate to high rates of exhumation and a distinct lack of volcanic rock (Parrish, 1983; Madsen et al., 2006). In part, this signal is recorded by a large population of DZFT-dated zircon grains in the Tofino Basin that flanks the southern CPC (~40-20 Ma) (Garver and Brandon, 1994). In

these strata, clearly derived from the southern to middle CPC, there is a major moving population of ~60-40 Ma. In the Yakutat terrane, the major peak is 40 Ma or less, which must represent a different source. Also lacking from the DZFT populations in either the Kulthieth or the Poul Creek Formations is a significant peak-age population of ~48 Ma, distinctive to the Omenica Belt and Idaho Batholith of interior belts of British Columbia and Washington (Brandon and Vance, 1992).

What is striking about the U/Pb and DZFT data for the Kulthieth and the Poul Creek Formations is the similarity to the U/Pb magmatic signal recorded in the northern CPC (as summarized by Armstrong, 1988). By combining all of the U/Pb determined crystallization ages for the Kulthieth and Poul Creek Formations and comparing them to the compilation discussed by Armstrong (1988), a direct comparison of U/Pb magmatic events recorded in the stratigraphy of the Yakutat terrane and the CPC can be visually represented (Figure 38). What is significant about this comparison is the continuous long-lived, meta-plutonic signal provided by the source terrain from ~50-220 Ma (Armstrong, 1988). The DZFT cooling age populations that correspond to Eocene to Cretaceous populations of U/Pb dated grains and episodes of magmatism within the CPC are represented by the Paleocene-Eocene populations within the Kulthieth and Poul Creek Formations (~97-47 Ma). This comparison would favor a more northerly option for the source of the pre-Pliocene Yakutat stratigraphy because the northern CPC has higher exhumation rates and lacks the distinctive signal characteristic of Cascade volcanism.

Double-dating of zircon grains provides a powerful method of discriminating provenance. The DZFT cooling age of ~36 Ma in the Kulthieth and Poul Creek Formations must have had relatively fast exhumation rates (~750 m/my) and minimal

lag-time (~10 Ma). Therefore the source terrain for the Miocene DZFT peak age populations must be a rapidly exhumed, arkosic-rich source with cooling ages ~35-36 Ma and emplacement ages of ~65-220 Ma (Hollister, 1982). Multiple plutonic suites have been identified as experiencing cooling episodes within this range, most of which are located in and around the Kuiu-Etolin Belt of southeastern Alaska (Smith and Diggles, 1981; Armstrong and Ward, 1991; Karl, Haeussler, and McCafferty, 1999; Lindline, Crawford, Crawford, and Omar, 2000; Lindline, Crawford, and Crawford, 2004; Crawford, Crawford and Lindline, 2005).

A comparison of U/Pb-determined ages of the Yakataga Formation to those of the magmatic record of the CPC provides two obvious conclusions (Figure 38). One is that the U/Pb age of the Miocene (young-peak) population first appears in this unit. The other is that the U/Pb ages for younger DZFT cooled grains (c. 20 Ma) was almost exclusively crystallized (U/Pb) at ~51 Ma. This result indicates that the Yakataga Formation tapped into a completely new source terrain for the younger population. This source terrain must have a crystallization age of ~51 Ma and a cooling age distribution of ~15-20 Ma. This is perhaps the most distinctive provenance clue the sequence has yielded.

Two major plutonic episodes are recorded in the Chugach-Prince William composite terranes (Bradley et al., 2003). This terrane is intruded by the Sanak-Baranof Plutonic Belt. This belt has plutonic phases that are Paleocene to Early Eocene (60-50) and Late Eocene. The first phase of plutonism ranges in age from ~61-50 Ma progressively from west to east, and the young ages of ~50 Ma are on Baranof Island in southeastern Alaska (Cowan, 1982). The distribution of Oligocene to Late Early Miocene plutons (c. 35 Ma) is highly variable and not continuous. These plutons are not within the

U/Pb determined crystallization ages or the DZFT cooling ages for the young peak (Late Miocene) represented within the Yakataga Formation and therefore a likely source would not include the local areas where these rocks occur.

If these data favor a northern option and refute a southern option for the Yakutat terrane, there are several interesting predictions that can be made (Figure 40). One is that the submarine fans in the Gulf of Alaska may provide important clues about the nature of sediment shed to the offshore region. The northern option also suggests that some specific rock units probably were eroded and shed material onto the Yakutat terrane. It would be fruitful to look at the exact nature of these adjacent terranes in the northern option.

CONCLUSIONS

The double-dating of zircon grains by the DZFT and U/Pb techniques is a powerful tool in evaluating provenance. The sediment provenance and zircon geochronology from the Yakutat terrane shows that most sediment was derived from a Tertiary cooled, Cretaceous to Early Tertiary metaplutonic complex most likely the northern Coast Plutonic Complex and adjacent terranes. The Miocene DZFT population within the Kulthieth and Poul Creek Formations records a rapidly cooled source terrain (~750 m/my) with a U/Pb grain age distribution of ~50-220 Ma, which likely recorded the time of crystallization and cooling of the Kuiu-Etoilin Belt of southeastern Alaska. The Late Miocene DZFT population in the Yakataga Formation records deposition from a source terrain that has crystallization ages of 50-53 Ma and cooling ages of ~16-20 Ma.

The Late Miocene population was likely deposited by the erosion of the Chugach accretionary complex and superimposed Sanak-Baranof Plutonic Belt (~50 Ma in the St. Elias area). The lack of volcanic grains in all the units favors the northern *in situ* option for Yakutat terrane translation and does not support a more southern option for the origin of the Yakutat terrane (i.e. Bruns, 1983).

These overall conclusions narrow the search for the specific source area to the Yakutat terrane stratigraphy. Future studies may look for specific unique source rocks in the indicated source region.

REFERENCES CITED

- Ainsfield, V. J., 1972, The stratigraphy and sedimentology of the Lyre Formation, northwestern Olympic Peninsula, Washington (Ph. D. thesis), Seattle, University of Washington, 130 p.
- Anderson, R. G., and Reichenbach, I., 1991, U-Pb and K-Ar framework for the Middle to Late Jurassic [172-158 Ma] and Tertiary [46-27 Ma] plutons in Queen Charlotte Islands, British Columbia *in* Woodsworth, G. J., ed., Evolution and hydrocarbon potential of the Queen Charlotte Basin, British Columbia, Ottawa, Ontario, Geological Survey of Canada Special Paper 90-10, p. 59-87.
- Anderson, R. G., 1988, An Overview of some Mesozoic and Tertiary plutonic suites and their associated mineralization in the northern Canadian Cordillera *in* R. P. Taylor, and D. F. Strong, eds., Recent Advances in the Geology of Granite-related Mineral Deposits, Canadian Institute of Mining and Metallurgy, Special Volume 39, p. 96-113.
- Armstrong, R. L., and Ward, P., 1991, Evolving Geographic Patterns and Cenozoic Magmatism in the North American Cordillera: The Temporal and Spatial Association of Magmatism and Metamorphic Core Complexes, *Journal of Geophysical Research*, v. 96, n. B6, p. 13,201-13,224.
- Armstrong, R. L., 1988, Mesozoic and early Cenozoic magmatic evolution of the Canadian Cordillera, *Geological Society of America Special Paper* 218, p. 55-91.

- Armstrong, R. L., Taubeneck, W. H., and Hales, P. O., 1977, Rb-Sr and K-Ar geochronometry of Mesozoic granitic rocks and their Sr isotopic composition Oregon, Washington, and Idaho, *Geological Society of American Bulletin*, v. 88, p. 397-411.
- Basu, A. W., Young, W. W., Suttner, L. J., James, W. C., and Mack, G. H., 1975, Re-evaluation of the use of undulatory extinction and polycrystallinity in detrital quartz for provenance interpretation, *Journal of Sedimentary Petrology*, v. 45, p. 873-882.
- Bayer, K. C., Mattick, R. E., Plafker, G., and Bruns, T. R., 1978, Refraction studies between Icy Bay and Kayak Island, eastern Gulf of Alaska, *Journal of Research of the U. S. Geological Survey*, v. 6, n. 5, p. 625-636.
- Bernet, M., and Garver, J. I., 2005, Fission-track analysis of detrital zircon, *in* Reiners, P. W., and Ehlers, T. A., eds., *Low-Temperature thermochronology: Reviews in Mineralogy and Geochemistry*, Virginia, The Mineralogical Society of America Geochemical Society, p. 205-234.
- Bernet, M., Brandon, M. T., Garver, J. I., and Molitor, B., 2004a, Downstream changes of Alpine zircon fission-track ages in the Rhone and Rhine Rivers, *Journal of Sedimentary Research*, v. 74, p. 82-94.
- Bernet, M., Brandon, M. T., Garver, J. I., and Molitor, B., 2004b, Fundamentals of detrital zircon fission-track analysis for provenance and exhumation studies with examples from the Southern Alps, *in* Bernet, Matthias, and Spiegel, Cornelia, 2004, *Detrital Thermochronology: Provenance Analysis, Exhumation, and*

- Landscape Evolution of Mountain Belts, The Geological Society of America
Special Paper 378, Boulder, Colorado, The Geological Society of America, p. 25-36.
- Bernet, M., Zattin, M., Garver, J. I., Brandon, M. T., and Vance, J. A., 2001, Steady-state exhumation of the European Alps, *Geology*, v. 29, p. 35-38.
- Blatt, H., and Christie, J. M., 1963, Undulatory extinction in quartz of igneous and metamorphic rocks and its significance in provenance studies of sedimentary rocks, *Journal of Sedimentary Petrology*, v. 33, p. 559-579.
- Bostick, N. H., 1979, Microscopic measurement of the level of catagenesis of solid organic matter in sedimentary rocks to aid exploration for petroleum and to determine former burial temperatures – a review., *in* Scholle, P. A., and Schluger, P. R., eds., *Aspects of diagenesis: SEPM Special Publication 26*, p. 17-43.
- Bradley, D., Klusky, T., Haeussler, P., Goldfarb, R., Miller, M., Dumoulin, J., Nelson, S. W., and Karl, S., 2003, Geologic signature of early Tertiary ridge subduction in Alaska, *in* Sisson, V. B., Roeske, S. M., and Pavlis, T. L., eds., *Geology of a transpressional orogen developed during ridge-trench interaction along the North Pacific margin*, Geological Society of America Special Paper 371, p. 1- 31.
- Brandon, M. T., Roden-Tice, M. K., and Garver, J. I., 1998, Late Cenozoic exhumation of the Cascadia accretionary wedge in the Olympic Mountains, northwest Washington State, *Geological Society of America Bulletin*, v. 110, p. 985-1009.

- Brandon, M. T., 1996, Probability Density Plot for Fission-track Grain-age samples, *Radiation Measurements*, v. 26, n. 5, p. 663-676.
- Brandon, M. T., 1992, Decomposition of Fission-track Grain-age Distributions, *American Journal of Science*, v. 292, p. 535-564.
- Brandon, M. T., and Vance, J. A., 1992, Tectonic evolution of the Cenozoic Olympic subduction complex, Washington State, as deduced from fission-track ages for detrital zircons, *American Journal of Science*, v. 292, n. 8, p. 565-636.
- Brandon, M. T., 1989b, Origin of igneous rocks associated with mélanges of the Pacific Rim Complex, western Vancouver Island, Canada, *Tectonics*, v. 8, p. 1,115-1,136.
- Bruhn, R. L., Pavlis, T. L., Plafker, G., and Serpa, L., 2004, Deformation during terrane accretion in the St. Elias orogen, Alaska, *GSA Bulletin*, v. 116, p. 771-787.
- Bruns, T. R., 1983, Model for the origin of the Yakutat block, an accreting terrane in the northern Gulf of Alaska, *Geology*, v. 11, p. 718-721.
- Bruns, T. R., and Schwab, W. C., 1983, Structure maps and seismic stratigraphy of the Yakataga segment of the continental margin, northern Gulf of Alaska, U. S. Geological Survey Miscellaneous Field Studies Map, scale 1: 250,000.
- Burnham A. K., and Sweeney, J. J., 1989, A chemical kinetic model of vitrinite maturation and reflectance, *Geochimica et Cosmochimica Acta*, v. 53, p. 2,649-2,657.

- Carter, A., and Moss, S. J., 1999, Combined detrital-zircon fission-track and U-Pb dating: a new approach to understanding hinterland evolution, *Geology*, v. 27, p. 235-238.
- Conolly, J. R., 1965, The occurrence of polycrystallinity and undulatory extinction in quartz in sandstones, *Journal of Sedimentary Petrology*, v. 35, p. 116-135.
- Cook, R. D., Crawford, M. L., Omar, G. I., and Crawford, W. A., 1991, Magmatism and deformation, southern Revillagigedo Island, southeastern Alaska, *Geological Society of America Bulletin*, v. 103, p. 829-841.
- Cook, A. C., and Sherwood, N. R., 1991, Classification of oil shales, coals, and other organic-rich rocks, *Organic Geochemistry*, v. 17, p. 211-222.
- Cook, A. C., and Murchison, D. G., 1977, The accuracy of refractive and absorptive indices derived from reflectance measurements on low-refracting materials, *Journal of Microscopy*, v. 109, pt. 1, p. 29-40.
- Cowan, D. S., 1982, Geological evidence for post-40 m. y. B. P. large-scale northwestward displacement of part of southeastern Alaska, *Geology*, v. 10, p. 309-313.
- Crawford, M. L., Crawford, W. A., and Lindline, J., 2005, 105 Million years of igneous activity, Wrangell, Alaska, to Prince Rupert, British Columbia, *Canadian Journal of Earth Science*, v. 42, p. 1097-1116.
- Crawford, M. L., Crawford, W. A., and Gehrels, G. E., 2000, Terrane assembly and structural relationships in the eastern Prince Rupert quadrangle, British Columbia, *in* Stowell, H. H., and McClelland, W. C., eds., *Tectonics of the Coast Mountains*,

southern Alaska and British Columbia, Geological Society of America Special Paper 343, p. 1-21.

Crawford, M. L., and Crawford, W. A., 1991, Magma emplacement in a convergent tectonic orogen, southern Revillagigedo Island, southeastern Alaska, *Canadian Journal of Earth Science*, v. 28, p. 929-938.

Criss, R. E., and Champion, D. E., 1984, Magnetic properties of granitic rocks from the southern half of the Idaho Batholith: influences of hydrothermal alteration and implications for aeromagnetic interpretation, *Journal of Geophysical Research*, v. 89, p. 7061-7076.

Criss, R. E., and Taylor, H. P., Jr., 1983, An ^{18}O - ^{16}O and D/H study of Tertiary hydrothermal systems in the southern half of the Idaho Batholith, *Geological Society of America Bulletin*, v. 94, p. 640-663.

Davis, D. W., Williams, I. S., and Krogh, T. E., 2003, Historical Development of Zircon Geochronology in J. M. Hancher, and P. W. O. Hoskin (eds), *Reviews in Mineralogy and Geochemistry: Zircon*, Mineralogical Society of America and Geochemical Society, v. 53, p. 145-181.

Davis, D. W., and Krogh, T. E., 2000, Preferential dissolution of ^{234}U and radiogenic Pb from alpha-recoil-damaged lattice sites in zircon: implications for thermal histories and Pb isotopic fractionation in the near surface environment, *Chemical Geology*, v. 172, p. 41-58.

- Dean, M. T., and Turner, N., 1995, Conodont Colour Alteration Index (CAI) values for the Carboniferous of Scotland, Transactions of the Royal Society of Edinburgh, Earth Sciences, v. 85, p. 211-220.
- DeChant, J., 1989, Sedimentary petrology, depositional environment and paleogeographic significance of the upper Eocene Hoko River Formation, northern Olympic Peninsula, Washington (M. S.), Bellingham, Western Washington University, 170 p.
- Dempster, A. J., 1935, Isotopic composition of uranium, Nature, v. 136, p. 180.
- Dickinson, W. R., 1988, Provenance and sediment dispersal in relation to paleotectonics and paleogeography of sedimentary basins, *in* Kleinspehn, K., and Paola, C., eds., New perspectives in basin analysis, New York, Springer-Verlag, p. 3-25.
- Ehlers, T. A., and Farley, K. A., 2003, Apatite (U-Th)/He thermochronometry: methods and applications to problems in tectonics and surface processes, Earth and Planetary Science Letters, v. 206, n.1-2, p. 1-14.
- Eyles, C. H., and Lagoe, M. B., 1990, Sedimentation patterns and facies geometries on a temperate glacially-influenced continental shelf: the Yakataga Formation, Middleton Island, Alaska, *in* Dowdeswell, J. A., and Scourse, J. D., eds., 1990, Glacimarine Environments: Processes and Sediments, Geological Society Special Publication No 53, p. 363-386.
- Fairchild, L. H., and Cowan, D. S., Structure, petrology, and tectonic history of the Leech River Complex northwest Victoria, Vancouver Island, 1982, Canadian Journal of Earth Sciences, v. 28, p. 1,285-1,300.

- Fleischer, R. L., 2004, Fission tracks in solids-production mechanisms and natural origins, *Journal of Materials Science*, v. 39, p. 3901-3911.
- Fleischer, R. L., Price, P. B., and Walker, R. M., 1975, *Nuclear Tracks in Solids: Principles and Techniques*, Berkeley, University of California Press, p. 605.
- Fleischer, R. L., Price, P. B., and Walker, R. M., 1965, The Ion Spike Mechanism for Formation of Charged Particle Tracks in Solids, *Journal of Applied Physics*, 1965a, v. 36, p. 3645-3652.
- Fletcher, H. J., and Freymueller, J. T., 1999, New GPA constraints on the Motion of the Yakutat Block, *Geophysical Research Letters*, v. 26, n. 19, p. 3,029-3,032.
- Fitzgerald, P. G., Sorkhabi, R. B., Redfield, T. F., and Stump, Edmund, 1995, Uplift and denudation of the central Alaska Range: A case study in the use of apatite fission track thermochronology to determine absolute uplift parameters, *Journal of Geophysical Research*, v. 100, p. 20, 175-20, 191.
- Folk, R. L., 1974, *Petrology of Sedimentary Rocks*, Hemphill Publishing Company, Austin, Texas, p. 182.
- Frisbie, A. J., 1995, A Fission-Track Study of Detrital Zircons From Pacific Northwest River Sediments, B. S. Thesis, Union College, Schenectady, N. Y., p.72.
- Galbraith, R. F., 1998, The Trouble with "Probability Density" Plots of Fission Track Ages, *Radiation Measurements*, v. 29, n. 2, p. 125-131.
- Galbraith, R. F., and Laslett, G. M., 1997, Statistical modeling of thermal annealing of fission tracks in zircon, *Chemical Geology*, v. 140, p. 123-135.

- Galbraith, R. F., and Green, P. F., 1990, Estimating the component ages in a finite mixture, *Nuclear Tracks and Radiation Measurements*, v. 17, p. 197-206.
- Garver, J. I., Reiners, P. W., Walker, J. I., Ramage, J. M., and Perry, S. E., 2005, Implications for timing of Andean uplift from thermal resetting of radiation-damaged zircon in the Cordillera Huayhuash, Northern Peru, *Journal of Geology*, v. 113, p. 117-138.
- Garver, J. I., 2003, Etching zircon age standards for fission-track analysis, *Radiation Measurements*, v. 37, p. 47-53.
- Garver, John I., and Kamp, Peter J. J., 2002, Integration of zircon color and zircon fission-track zonation patterns in orogenic belts: application to the Southern Alps, New Zealand, *Tectonophysics*, v. 349, p. 203-219.
- Garver, J. I., Soloviev, A. V., Bullen, M. E., and Brandon, M. T., 2000, Towards a more complete record of magmatism and exhumation in continental arcs, using detrital zircon fission-track thermochronology, *Physical Chemical Earth (A)*, v. 25, n. 6-7, p. 565-570.
- Garver, J. I., Brandon, M. T., Roden-Tice, M., and Kamp P. J. J., 1999, Exhumation of orogenic highlands determined by detrital fission-track thermochronology, *in* Ring, U., Brandon, M. T., Lister, G. S., and Willet, S. D., eds., 1999, v. 154, p. 283-304.
- Garver, J. I., and Brandon, M. T., 1994a, Fission-track ages of detrital zircon from mid-Cretaceous sediments of the Methow-Tyughton basin, southern Canadian Cordillera, *Tectonics*, v. 13, n. 2, p. 401-420.

- Garver, J. I., and Brandon, M. T., 1994b, Erosional denudation of the British Columbia Coast Ranges as determined from fission-track ages of detrital zircon from the Tofino basin, Olympic Peninsula, Washington, Geological Society of America Bulletin, v. 106, p. 1398-1412.
- Gehrels, G. E., 2004, unpublished data, University of Arizona Laserchron Lab website, <http://www.geo.arizona.edu/alc/>, Tucson, Arizona.
- Gehrels, G. E., 2001, Geology of the Chatham Sound region, Southeast Alaska and coastal British Columbia, Canadian Journal of Earth Sciences, v. 38, n. 11, p. 1,579-1,599.
- Gehrels, G. E., 2000, Reconnaissance geology and U-Pb geochronology of the west flank of the Coast Mountains between Juneau and Skagway, southeastern Alaska, *in* Stowell, H. H., and McClelland, W. C., eds., Tectonics of the Coast Mountains, southern Alaska and British Columbia, Geological Society of America Special Paper 343, p. 213-233.
- Gehrels, G. E., Dickinson, W. R., Ross, G. M., Stewart, J. H., and Howell, D. G., 1995, Detrital zircon reference for Cambrian to Triassic miogeoclinal strata of western North America, Geology, v. 23, p. 831-834.
- Gulick, S., and Jaeger, J., 2003, The Interplay of Collisional Tectonics and Late Cenozoic Glacial Climate in Alaska and the Northeastern Pacific Ocean: Science Plan, p. 1-78.

- Haeussler, P. J., Gehrels, G. E., and Karl, S. M., *in prep.*, Constraints on the Age and Provenance of the Chugach Accretionary Complex from detrital zircons in the Sitka Graywacke near Sitka, Alaska.
- Harbor, J., and Warburton, J., 1993, Relative rates of glacial and nonglacial erosion in alpine environments, *Arctic and Alpine Research*, v. 25, n. 1, p. 1-7.
- Heller, P. L., Tabor, R. W., O'Neil, J. R., Pevear, D. R., Shafiquillah, M., and Winslow, N. S., 1992, Isotopic provenance of Paleogene sandstones from the accretionary core of the Olympic Mountains, Washington, *Geological Society of America Bulletin*, v. 104, p. 140-153.
- Hollister, L. S., 1982, Metamorphic evidence for rapid (2 mm/yr) uplift of a portion of the Central Gneiss Complex, Coast Mountains, B. C., *Canadian Mineralogist*, v. 20, p. 319-332.
- Hurford, A. J., and Green, P. F., 1983, The zeta age calibration of fission-track dating, *Isotope Geoscience*, v. 1, p. 285-317.
- Hyndman, D. W., 1983, The Idaho Batholith and associated plutons, Idaho and western Montana, *Geological Society of America Memoir* 159, p. 213-240.
- Johnsson, M. J., and Howell, D. G., 1996, Generalized thermal maturity map of Alaska, U. S. Geological Survey Miscellaneous Geologic Investigations Map, scale 1: 2,500,000.

- Johnsson, M. J., Pawlewicz, M. J., Harris, A. G., and Valin, Z. C., 1992, Vitrinite reflectance and conodont color alteration index data from Alaska; data to accompany the thermal maturity map of Alaska, U. S. Geological Survey Open File-Report 92-409, U. S. Geological Survey.
- Johnston, S. A., 2005, Geologic Structure and Exhumation Accompanying Yakutat Terrane Collision, Southern Alaska, M. S. Thesis, Oregon State University, p. 49.
- Kapp, P. A., and Gehrels, G. E., 1998, Detrital zircon constraints on the tectonic evolution of the Gravina Belt, Southeastern Alaska, *Canadian Journal of Earth Sciences*, v. 35, n. 3, p. 253-268.
- Karl, S. M., Haeussler, P. J., and McCafferty, A. E., 1999, Reconnaissance Geologic Map of the Duncan Canal/Zarembo Island Area, Southeastern Alaska, U.S.G.S. Open-File Report 99-168, p. 1-30.
- Khorasani, G. K., and Michelsen, J. K., 1994, The effects of overpressure, lithology, chemistry, and heating rate on vitrinite reflectance evolution, and its relationship with oil generation, *APEA Journal*, v. 34, pt. 1, p. 418-434.
- Krogh, T. E., 1973, A low contamination method for hydrothermal decomposition of zircon and extraction of U and Pb for isotopic age determinations, *Geochimica Cosmochimica Acta*, v. 37, p. 631-635.
- Lagoë, M. B., and Zellers, S. D., 1996, Depositional and microfaunal response to Pliocene climate change and tectonics in the eastern Gulf of Alaska, *Marine Micropaleontology*, v. 27, n. 1-4, p. 121-140.

- Lagoë, M. B., Eyles, C. H., Eyles, N., and Hale C., 1993, Timing of late Cenozoic tidewater glaciation in the far North Pacific, Geological Society of America Bulletin, v. 105, p. 1542-1560.
- Lagoë, M. B., 1983, Oligocene through Pliocene foraminifera from the Yakataga Reef section, Gulf of Alaska Tertiary Province, Alaska, Micropaleontology, v. 29, n. 2, p. 202-222.
- Lewis, P. D., Dietrich, J. R., and Rohr, K. M. M., 1991, Triassic to Neogene evolution of the Queen Charlotte region, Canadian Journal of Earth Sciences, v. 28, p. 854-869.
- Lindline, J., Crawford, W. A., and Crawford, M. L., 2004, A bimodal volcanic-plutonic system: the Zarembo Island extrusive suite and the Burnett Inlet intrusive complex, Canadian Journal of Earth Science, v. 41, p. 355-375.
- Lindline, J., Crawford, W. A., Crawford, M. L., and Omar, G. I., 2000, Post-Accretion Magmatism within the Kuiu-Etolin Igneous Belt, Southeastern Alaska, The Canadian Mineralogist, v. 38, p. 951-974.
- Ludwig, K. R., 2003, User's manual for Isoplot 3.0: a geochronological toolkit for Microsoft Excel, Berkeley California, Berkeley Geochronology Center Special Publication 4, p. 71.
- Ludwig, K. R., 2001, Eliminating mass-fractionation effects on U-Pb isochron ages without double spiking, Geochimica Cosmochimica Acta, v. 65, p. 3139-3145.

- Ludwig, K. R., 1998b, Using the ISOPLOT/Ex version 1.00b-a geochronological toolkit for Microsoft Excel, Berkeley Geochronology Center Special Publications 1, p. 43.
- Ludwig, K. R., 1998a, On the treatment and concordant uranium-lead ages, *Geochimica Cosmochimica Acta*, v. 62, p. 665-676,
- Ludwig, K. R., 1980, Calculation of uncertainties of U-Pb isotopic data, *Earth and Planetary Science Letters*, v. 46, p. 221-232.
- MacKevett, E. M., Brew, D. A., Hawley, C. C., Huff, L. C., and Smith, J. G., 1971, Mineral Resources of Glacier Bay National Monument, Alaska, Geological Survey Professional Paper 632, p. 96.
- Madsen, J. K., Thorkelson, D. J., Friedman, R. M., and Marshall, D. D., 2006, Cenozoic to Recent plate configurations in the Pacific Basin: Ridge subduction and slab window magmatism in western North America, *Geosphere*, v. 2, n. 1, p. 11-34.
- Marcott, K., 1984, Sedimentary petrography, depositional environment and tectonic setting of the Adwell Formation, northern Olympic Peninsula, Washington (M.S.), Bellingham, Western Washington University, 78 p.
- Martin, G. C., Lithostratigraphy, 1993, *in* Risely, D. E., ed., Geologic Report for the Gulf of Alaska Planning Area, Anchorage, Alaska, Mineral Management Service, p. 63-98.

- Meigs, A., and Sauber, J., 2000, Southern Alaska as an example of the long-term consequences of mountain building under the influence of glaciers, *Quaternary Science Reviews*, v. 19, p. 1543-1562.
- Miller, D. J., 1971, Geologic Map of the Yakataga district, Gulf of Alaska Tertiary Province, Alaska, U. S. Geological Survey Miscellaneous Investigations Map Series, Map I-610, scale 1:125,000.
- Miller, D. J., 1957, Geology of the southeastern part of the Robinson Mountains, Yakataga District, Alaska, U. S. Geological Survey Oil and Gas Investigations Map OM 187, scale 1:63, 360.
- Montgomery, D. R., 2002, Valley formation by fluvial and glacial erosion, *Geology*, v. 30, n. 11, p. 65.
- Naeser, N. D., Zeitler, P. K., Naeser, C. W., and Cervený, P. F., 1987, Provenance Studies By Fission-Track Dating of Zircon-Etching and Counting Procedures, *Nuclear Tracks and Radiation Measurements*, v. 13, n. 2-3, p. 121-126.
- Naeser, B. S., 1979, Fission-track dating and geologic annealing of fission-tracks, *in* E. Jager and J. C. Hunziker (eds), *Lectures in Isotope Geology*, Springer-Verlag, Heidelberg, p. 154-169.
- National Science Foundation, 2003, The Interplay of Collisional Tectonics and Late Cenozoic Glacial Climate in Alaska and the Northeastern Pacific Ocean, Continental Dynamics Program Workshop, May 5-6, p. 77.

- Nokleberg, W. J., Bundtzen, T. K., Eremin, R. A., Ratkin, V. V., Dawson, K. M., Shpikerman, V. I., Goryachev, N. A., Byalobzhesky, S. G., Frolov, Y. F., Khanchuk, A. I., Koch, R. D., Monger, J. W. H., Pozdeev, Rozenblum, I. S., Rodionov, S. M., Parfenov, L. M., Scotese, C. R., and Sidorov, A. A., 2005, Metallogensis and Tectonics of the Russian Far East, Alaska, and the Canadian Cordillera, U. S. Geological Survey, Professional Paper 1697, p. 397.
- Oberli, F., Bachmann, O., Meier, M., and Dungan, M. A., 2002, The Fish Canyon tuff: Ar-Ar versus U-Pb age discrepancy reassessed, Abstract 12th Annual V. M. Goldschmidt Conference, Davos, Switzerland, August 18-23, *Geochimica, Cosmochimica Acta Special Suppl.*, p. A565.
- O'Sullivan, Paul B., and Currie, Lisel D., 1996, Thermotectonic history of Mt. Logan, Yukon Territory, Canada: implications of multiple episodes of middle to late Cenozoic denudation, *Earth and Planetary Science Letters*, v. 144, p. 251-261.
- O'Sullivan, Paul B., Plafker, George, and Murphy, John M., 1995, Apatite Fission-Track Thermotectonic History of Crystalline Rocks in the Northern Saint Elias Mountains, Alaska, *Geologic Studies in Alaska by the U. S. Geological Survey*, p. 283-292.
- Palmer, A. R., 1983, The Decade of North American Geology 1983 Geologic Time Scale, *Geology*, v. 11, p. 503-504.

Parrish, R. R., 1983, Cenozoic Thermal Evolution and Tectonics of the Coast Mountains of British Columbia 1. Fission Track Dating, Apparent Uplift Rates, and Patterns of Uplift, *Tectonics*, v. 2, n. 6, p. 601-631.

Pavlis, Terry L., Picornell, Carlos, Serpa, Laura, Bruhn, Ronald L., and Plafker, George, 2004, Tectonic processes during oblique collision: Insights from the St. Elias orogen, northern North American Cordillera, *Tectonics*, v. 23, p. TC3001.

Plafker, G., Moore, J. C., and Winkler, G. R., 1994, Geology of the southern Alaska margin *in* Plafker, George, and Berg, H. C., eds., *The Geology of Alaska*, v. G-1, *The Geology of North America*, Boulder, Colorado, Geological Society of America, p. 389-449.

Plafker, George, Naeser, Charles W., Zimmerman, Robert A., Lull, John S., and Hudson, Travis, 1991, Cenozoic Uplift History of the Mount McKinley Area in the Central Alaska Range Based on Fission-Track Dating, *in* Bradley, D. C., and Dusel-Bacon, Cynthia, eds., *Geologic studies in Alaska by the U. S. Geological Survey, 1991: U. S. Geological Survey Bulletin 2041*, p. 202-212.

Plafker, George, 1987, Regional geology and petroleum potential of the northern Gulf of Alaska continental margin, *in* Scholl, D. W., Grantz, A., and Vedder, J. G., eds., *Geology and resource potential of the continental margin of western North America and adjacent ocean basins- Beaufort Sea to Baja California: Earth Science Series: Houston, Texas, Circum-Pacific Council for Energy and Mineral Resources*, p. 229-268.

- Plafker, George, Winkler, Gary R., Coonrad, Warren L., and Claypool, George, 1980, Preliminary report on the geology of the continental slope adjacent to OCS Lease Sale 55, Eastern Gulf of Alaska: Petroleum Resource Implications, U. S. Geological Survey Open-File Report 80-1089, p. 1-72.
- Powell, R. D., and Cooper, J. M., 2002, A glacial sequence stratigraphic model for temperate, glaciated continental shelves, Geological Society of America Special Publication 203, p. 215-244.
- Rahl, J. M., Reiners, P. W., Campbell, I. H., Nicolescu, S., and Allen, C. M., 2003, Combined single-grain (U-Th)/He and U/Pb dating of detrital zircons from the Navajo Sandstone, Utah, *Geology*, v. 31, n. 9., p. 761-764.
- Reiners, P. W., Spell, T. L., Nicolescu, S., and Zanetti, K. A., 2003, Zircon (U-Th)/He thermochronometry: He diffusion and intercalibration with $^{40}\text{Ar}/^{39}\text{Ar}$ dating, *Geochimica et Cosmochimica Acta*, v. 16.
- Reiners, P. W., Farley, K. A., and Hickey, H. J., 2002, He diffusion and (U-Th)/He thermochronometry of zircon: initial results from Fish Canyon Tuff and Gold Butte, *Tectonophysics*, v. 349, p. 297-308.
- Sauber, J., McClusky, S., and King, R., 1997, Relation of ongoing deformation rates to the subduction zone process in southern Alaska, *Geophysical Research Letters*, v. 24, p. 2853-2856.

- Shackleton, N. J., Hall, M. A., and Pate, D., 1995, Pliocene stable isotope stratigraphy of Site 846, *in* Pisias, N. G., Janacek, L. A., Palmer-Julson, A., and Van Andel, T. H., eds., *Proceedings of the Ocean Drilling Program, Scientific Results, Leg 138*, p. 337-355.
- Sheaf, M. A., Serpa, L., and Pavlis, T., 2003, Exhumation in the St. Elias Mountains, Alaska, *Tectonophysics*, v. 367, p. 1-11.
- Shouldice, D. H., 1971, Geology of the Western Canadian Continental Shelf, *Bulletin of Canadian Petroleum Geology*, v. 19, n. 2, p. 405-436.
- Smith, J. G., and Diggles, M. F., 1981, Potassium-argon determinations in the Ketchikan and Prince Rupert quadrangles, southeastern Alaska, U. S. Department of the Interior Geological Report, Open-file Report 78-73N, p. 1-16.
- Snavely, P. D., Jr., Niem, A. R., MacLeod, N. S., Pearl, J. E., and Rau, W. W., 1980, Makah Formation – A Deep-Marginal-Basin Sequence of Late Eocene and Oligocene Age in the Northwestern Olympic Peninsula, Washington, *Geological Survey Professional Paper 1162-B*, p. 28.
- Spotila, J. A., Buscher, J. T., Meigs, A. J., and Reiners, P. W., 2004, Long-term glacial erosion of active mountain belts: Example of the Chugach-St. Elias Range, Alaska, *Geology*, v. 32, p. 501-504.
- Stacey, J. S., and Kramers, J. D., 1975, Approximation of terrestrial lead isotope evolution by a two-stage model, *Earth and Planetary Science Letters*, v. 26, n. 2, p. 207-221.

- Stevenson, A. J., and Embley, R., 1987, Deep-Sea Fan Bodies, Terrigenous Turbidite Sedimentation, and Petroleum Geology, Gulf of Alaska *in* Scholl, D. W., Grantz, A., and Vedder, J. G., eds., Geology and resource potential of the continental margin of western North America and adjacent ocean basins- Beaufort Sea to Baja California: Earth Science Series: Houston, Texas, Circum-Pacific Council for Energy and Mineral Resources, p. 503-522.
- Stevenson, A. J., Scholl, D. J., and Vallier, T. L., 1983, Tectonic and geologic implications of the Zodiac fan, Aleutian Abyssal Plain, northeast Pacific, Geological Society of America Bulletin, v. 94, p. 259-273.
- Stewart, R. J., 1976, Turbidites of the Aleutian Abyssal Plain: Mineralogy, provenance, and constraints for Cenozoic motion of the Pacific plate, Geological Society of America Bulletin, v. 87, p. 793-808.
- Sweeney, J. J., and Burnham, A. K., 1990, Evaluation of a simple model of vitrinite reflectance based on kinetics, AAPG Bulletin, v. 74, p. 1,559-1,570.
- Sweetkind, D. S., and Blackwell, D. D., 1989, Fission-track evidence of the Cenozoic thermal history of the Idaho batholith, Tectonophysics, v. 157, p. 241-250.
- Taylor, H. P., Jr., and Magaritz, M., 1978, Oxygen and hydrogen isotope studies of the Cordilleran batholiths of western North America *in* Robinson, B. W., ed., Stable Isotopes in the Earth Sciences (Rafter Volume), New Zealand Department of Science Industrial Research Bulletin, v. 220, p. 151-173.

- Tiffin, D. L., Cameron, B. E. B., and Murray, J. W., 1972, Tectonic and Depositional History of the Continental Margin Off Vancouver Island, British Columbia, Canadian Journal of Earth Sciences, v. 9, p. 280.
- Tilton, G. R., and Aldrich, C. T., 1955, The reliability of zircons as age indicators: Transaction-American Geophysical Union, v. 36/3, p. 531.
- Wahrhaftig, C., Bartsch-Winkler, S., and Stricker, G. D., 1994, Coal in Alaska, *in* Plafker, G., and Berg, H. C., eds., The Geology of Alaska, Boulder, Geological Society of America, p. 937-978.
- Wetherill, G. W., 1956a, Discordant uranium-lead ages, International Transcontinental American Geophysical Union, v. 37, p. 320-326.
- White, J. M., Ager, T. A., Adam, D. P., Leopold, E. B., Liu, G., Jette, H., and Schweger, C. E., 1997, 18-million year record of vegetation and climate change in northwestern Canada and Alaska: Tectonic and global climatic correlates, Palaeogeography Palaeoclimatology Palaeoecology, v. 130, n. 1-4, p. 293-306.
- Yorath, C. J., 1987, Petroleum geology of the Canadian Pacific continental margin *in* Scholl, D. W., Grantz, A., and Vedder, J. G., eds., Geology and resource potential of the continental margin of western North America and adjacent ocean basins-Beaufort Sea to Baja California: Earth Science Series: Houston, Texas, Circum-Pacific Council for Energy and Mineral Resources, p. 283-304.
- Yorath, C. J., and Chase, R. L., 1981, Tectonic history of the Queen Charlotte Islands and adjacent area-A model, Canadian Journal of Earth Sciences, v. 18, p. 1,717-1,739.